

Physical volcanology, sedimentology and geochemistry of the Mid-Cretaceous Chisana Formation, south-central Alaska: implications for models of Wrangellia composite terrane accretion

by

Patrick Manselle

B.S., Eastern Illinois University, 2017

A THESIS

submitted in partial fulfillment of the requirements for the degree

MASTER OF SCIENCE

Department of Geology  
College of Arts and Sciences

KANSAS STATE UNIVERSITY  
Manhattan, Kansas

2019

Approved by:

Major Professor  
Matthew Brueseke

## Abstract

Currently, there are two main models for Mesozoic suturing of the Wrangellia composite terrane in the North American Cordillera. Studies from southeastern Alaska and British Columbia suggest that collision of the Wrangellia composite terrane with the North American craton occurred during the Middle Jurassic, and that early volcanism and sedimentation occurred in post-accretionary transtensional basins that were created by a strike-slip fault system. Another model suggests that accretion in eastern Alaska and the Yukon Territory occurred during the late Jurassic-early Cretaceous; associated volcanism was subduction-related and basin development evolved from an offshore Jurassic intraoceanic arc to a Cretaceous collisional arc setting. South-central Alaska, in the Nutzotin Mts. where the Chisana Formation crops out, is an ideal location for testing models for Wrangellia accretion because it is defined by two major collisional episodes: the Mesozoic collision of the Wrangellia composite terrane, and the ~30Ma to ongoing collision of the Yakutat terrane. The Chisana Formation consists of a succession of volcanic and sedimentary strata that conformably overlie late Jurassic–early Cretaceous marine sedimentary strata of the Nutzotin Mt. Sequence. Geochronologic and geochemical data from upper Chisana lavas document ~121 to 117 Ma arc volcanism, however lavas from the lower parts of the Chisana Formation may be >121 Ma. New stratigraphic analysis indicates that the lavas are >2-km-thick at the Bonanza Creek type section. The lavas are overlain unconformably by fluvial strata of the Beaver Lake Formation, the age of which is uncertain but between 117 – 98 Ma. Our field evidence suggests the Chisana Formation at Bonanza Creek can be divided into a lower subaqueous unit, a middle transitional unit, and an upper subaerial unit. Lateral lithofacies changes between Bonanza Creek and Jacksina Creek show a northwestward transition from a primarily marine environment of deposition/emplacement at Bonanza Creek to an environment

that was primarily subaerial, with minor, shallow marine influences present at Jacksina Creek. Chisana Formation lavas sampled at both locations range from calc-alkaline to tholeiitic basalts to basaltic andesites. Stratigraphically lower lavas are typically more andesitic and become more basaltic and tholeiitic up-section. Trace element geochemistry shows high field strength element (Ti, Nb, Y, Zr) depletions relative to large ion lithophile elements (Rb, K, Ba) as well as hydrous mineral assemblages with calc-alkaline to tholeiitic chemistries, both of which are consistent with an arc origin. Our data imply more significant subaerial eruptions and sedimentation from an oceanic arc constructed upon Wrangellia than previously recognized from this area of the Wrangellia composite terrane. When combined with data from other studies in the area, all results support of an east-dipping, subduction-related island arc model for the origin of the Gravina-Nutzotin belt.

## Table of Contents

List of Figures .....	vi
List of Tables .....	vii
Acknowledgements .....	viii
Dedication .....	x
Chapter 1 - Introduction .....	1
Geologic Setting .....	4
Chapter 2 - Methods .....	13
Chapter 3 - Results .....	16
Sedimentary and Volcanic Lithofacies .....	16
Marine Mudstones and minor fine-grained volcanoclastic sandstone (K <sub>CM</sub> ) .....	17
Volcanoclastic Conglomerate (K <sub>CCGL</sub> ) .....	17
Marine Lavas (K <sub>CLL</sub> ) .....	18
Lahar Breccias (K <sub>CB</sub> ) .....	19
Block and Ash Flow deposit (K <sub>CBAF</sub> ) .....	19
Oxidized Lavas (K <sub>CUL</sub> ) .....	20
Nutzotin Mountain Sequence at Bonanza Creek (K <sub>js</sub> ) .....	20
Nutzotin Mountains Sequence at Jacksina Creek (K <sub>js</sub> ) .....	21
Petrography .....	21
Geochemical classification and bulk rock geochemical characteristics .....	24
Chapter 4 - Discussion .....	48
Stratigraphic Relationships of the Chisana Formation .....	48
Geochemical constraints on Chisana Formation magmatism .....	49
Origin of the Chisana Formation and tectonic implications .....	51
Comparison to other volcanic arcs and other tectonomagmatic environments .....	54
Chapter 5 - Conclusions .....	76
References .....	77
Appendix A - Petrography .....	85
Appendix B - Alteration Photomicrographs .....	96
Appendix C - Geochemical Analyses .....	97



Appendix D - XRF precision and accuracy .....	102
Appendix E - CIPW data .....	103
Appendix F - Alteration Filter from Beswick and Soucie .....	104
Appendix G - Sr/Y Calculations .....	105

## List of Figures

Figure 1-1 Geologic map of south-central Alaska.....	8
Figure 1-2 Geologic Map of study areas.....	9
Figure 1-3 Geologic Map of Bonanza Creek and Beaver Lake study areas.....	11
Figure 1-4 Overview Photographs of study areas.....	12
Figure 3-1: Pictures of Bonanza Creek Study area, lower section.....	27
Figure 3-2 Pictures of Bonanza Creek Study area, lower section.....	28
Figure 3-3 Pictures of Bonanza Creek study area, middle section.....	30
Figure 3-4 Pictures of Bonanza Creek upper section and Jacksina Creek study areas.....	32
Figure 3-5 Picture of Jacksina Creek study area.....	34
Figure 3-6: Bonanza Creek stratigraphic column.....	37
Figure 3-7: Jacksina Creek stratigraphic column.....	39
Figure 3-8: Thin section photographs.....	40
Figure 3-9 Geochemical classification diagrams.....	42
Figure 3-10: Major element diagrams.....	44
Figure 3-11: Trace element diagrams.....	45
Figure 3-12: Chemo-stratigraphic diagrams.....	46
Figure 3-13: Primitive mantle normalized multi-element diagram.....	47
Figure 4-1 Depiction of differences in depositional environments between study areas.....	58
Figure 4-2: Selected geochemical diagrams showing differences between upper and middle sections of the Chisana Formation at Bonanza Creek.....	59
Figure 4-3: Comparison of the Chisana Formation to Cretaceous plutons in the Nutzotin belt...	61
Figure 4-4: Trace element comparison of Chisana Formation to White Mountain plutons.....	63
Figure 4-5 Ternary diagram of tholeiitic basalts from the Chisana Formation.....	64
Figure 4-6: Geochemical comparison of the Chisana Formation to Gravina belt volcanic rocks.....	65
Figure 4-7: Trace element comparison of Chisana Formation to Gravina metabasalts.....	67
Figure 4-8: Geochemical comparison of the Chisana Formation to the Talkeetna arc.....	69
Figure 4-9: Geochemical Comparison of the Chisana Formation to the Wrangell Arc.....	70
Figure 4-10: Geochemical comparison of the Chisana Formation to the modern Honshu arc.....	72

## List of Tables

Table 3-1: Facies Table.....	26
------------------------------	----

## **Acknowledgements**

I could not have created this document without the help, support and guidance of many people. None of this would have been possible if not for funding provided by the Alaskan Geological Society Don Richter Memorial Scholarship as well as NSF funding provided by Dr. Brueseke (EAR-1450689), Dr. Jeff Benowitz (EAR-1450730), and Dr. Jeffrey Trop (EAR-1450687). I would also like to thank Paul and Deana Strunk for their generous scholarship.

Thank you to Dr. Stan Mertzman at Franklin & Marshall college for providing the major and trace element analysis for this study. Thank you to Kirk Ellis and the other pilots at K-Air who flew us around to our remote study areas, sometimes through inclement weather.

I would like to extend my gratitude to Dr. Jeff Benowitz, for graciously allowing us the use of his home and equipment during our study in Alaska. I would also like to thank him for lending us his assistance in the field, providing us with his insight and expertise in both Alaskan hiking and geology. He also has provided me with excellent feedback on many of my presentations related to this project and has helped me to become a better scientific writer in general.

Dr. Jeff Trop, who is a veteran of southern Alaska tectonics and geology, has been an enormous source of information and guidance throughout the entire project. His assistance in interpreting the sedimentary lithofacies at our study areas provided key insights that would have been overlooked if not for him. His constant questions in the field kept me on my toes and thinking about everything we were seeing. He has shown me how important knowing the sedimentology and stratigraphy of an area is to understanding it, and how approaching problems from a multidisciplinary standpoint makes a project much stronger than approaching it from a single perspective. He has been a veritable font of knowledge about the tectonic history of

south-central Alaska and has provided me with numerous publications that have made this project much stronger as a whole. As a member of my committee, his comments on my work have always helped me to better understand the tectonic history of south-central Alaska.

I would like to thank Dr. Pamela Kempton for being very patient with me and my numerous questions (and general comments) regarding my thin sections. I would also like to thank her for her comments on my work, which have not only helped me to increase the level of professionalism in my writing and in my presentations but have helped me to become a better scientist in general.

Matt Brueseke took a chance in choosing me to pursue this project almost two years ago, as he was not sure how able he would be to pursue parts of it. I am very glad he decided to do this in the end, and I owe him a lot. Over the course of this project, Matt has pushed me to work harder than I ever have before. The reason this project turned out as well as it did is mainly due to his constant suggestions to make this comparison, or to make these figures. He has taught me so much about not only my study area, but about academia in general. I would especially like to thank Matt for his saintly level of patience in dealing with my near-constant questioning about both my project and other, sometimes unrelated, topics.

I would like to thank all my friends, especially Kayleigh, Mikaela and Nina, who have been with me since I started this project and are always there to support me.

I would like to thank my family, whose love and support have gotten me to where I am today. Thank you.

Finally, I would also like to thank my undergraduate professor Dr. Craig Chesner, who introduced me to volcanology and igneous petrology. Without his guidance, I would not have found my passion for volcanology and igneous petrology. Thank you.

## **Dedication**

This thesis is dedicated to my parents, Tim and Pam. Both of them went back to school to pursue their master's degrees while also working and raising three children. Their example has inspired me to work hard and to never give up, even when things get difficult or didn't work out the way I expected.

## Chapter 1 - Introduction

Suturing of oceanic crust onto continental crust following subduction is a fundamental process in the growth of Earth's continents (Nokleberg et al., 1989; Abbott and Mooney, 1995; Jahn et al., 2000). Despite being a global tectonic process, suturing remains poorly understood when compared to other processes, such as subduction of oceanic plates and mid-ocean ridge formation. The evolutionary history of the south-central margin of Alaska is ideally suited to study suturing, because it is defined by two major collisional episodes: the Mesozoic collision of the Wrangellia composite terrane (WCT) and the ca. 30 Ma to ongoing collision of the Yakutat terrane (Nokleberg et al., 2000; Trop and Ridgway, 2007). The Wrangellia composite terrane is a subcontinent-sized fragment of crust that consists of the Wrangellia, Peninsular, and Alexander terranes (Plafker and Berg., 1994; Nokleberg et al., 1994). Paleomagnetic studies (Stamatakis et al., 2001) indicate that the WCT was located thousands of kilometers south of its present location during the late Triassic and was translated northward to its current position during the Middle Jurassic-Late Cretaceous (Plafker et al., 1989; Nokleberg et al., 2000; Trop and Ridgway, 2007). The suture zone between the WCT and the former North American paleomargin is defined by sequences of sedimentary basinal strata that have been uplifted and exposed along south-central and south-eastern Alaska (McClelland et al., 1992; Kapp and Gehrels, 1998; Manuszak et al., 2007) These basins are known as the Kahiltna, Nutzotin Mountain, Dezadeash, and Gravina basins (from north to south), and are commonly referred to as the Gravina-Nutzotin belt (Figure 1-1; Plafker and Berg, 1994). Currently, the tectonic setting of the Gravina-Nutzotin belt is a subject of much debate (Berg et al., 1972; McClelland and Mattinson, 2000; Manuszak et al., 2007; Sigloch and Mihalynuk, 2017), due to uncertainty regarding the timing and location of WCT accretion onto the North American paleomargin, as well as the polarity of subduction

associated with WCT accretion. The Gravina-Nutzotin belt sequence is a package of variably deformed Upper Jurassic to Lower Cretaceous metavolcanic and sedimentary rocks that are exposed nearly 750 km along the eastern portion of the Wrangellia and Alexander terranes (Figure 1-1)(Rubin and Saleeby, 1991). Multiple hypotheses for the origin of the Gravina-Nutzotin belt have been suggested, and include back-arc basin (Berg et al., 1972), a sinistral transtensional basin (Gehrels et al., 2009; Yokelson et al., 2015), a rift basin (van der Heyden, 1992; Kapp and Gehrels, 1998), a dextral transtensional basin (McClelland et al., 1992), an intra-arc basin (McClelland and Mattinson, 2000), a retroarc foreland basin (Manuszak et al., 2007), and a forearc basin related to west-dipping subduction (Sigloch and Mihalynuk; Lowey 2018).

The Kahiltna assemblage in the western Alaska Range represents development of a marine basin along the suture zone of the Late Jurassic-Cretaceous accretion of the WCT to the North American paleomargin (Kalbas et al., 2007; Hampton et al., 2010). The Dezadeash basin is a 3000-m-thick sequence of deepwater turbidites in southwestern Yukon that are inferred to have been deposited as a submarine fan in a back-arc basin to the Late Jurassic Chitina arc (Lowey, 2011). The Gravina basin in southeastern Alaska is composed of a western Gravina belt, which consists primarily of volcanic-rich turbidites and mafic to intermediate volcanic rocks, and an eastern Gravina belt, which consists mainly of pelitic schists with metaconglomerate horizons (Yokelson et al., 2015). The western Gravina basin strata are inferred to have been deposited in a back-arc position and were derived from the WCT (Yokelson et al., 2015), whereas the eastern Gravina basin strata are inferred to have been deposited in a forearc basin in respect to the eastern Coast Mountains batholith located on the Yukon composite terrane (Yokelson et al., 2015).



The Nutzotin Mountains basin represents a unique area to study the WCT suture zone because unlike the other basins in the suture zone, thick packages of relatively unmetamorphosed volcanic strata and plutonic bodies are exposed in the Chisana Formation (Richter and Jones, 1976). The Chisana Formation consists of volcanic, plutonic, and sedimentary rocks that were erupted, emplaced, and/or deposited in the Early Cretaceous (Figure 1-1)(Berg et al., 1972; Richter and Jones, 1976; Snyder and Hart, 2007; Graham et al., 2016), which have an estimated composite thickness of ~3 km (Barker, 1994). An over 200 km-long belt of Early Cretaceous plutonic rocks of granodiorite and diorite affinities crop out along the Nutzotin basin (Richter et al., 1975; Snyder and Hart, 2007; Graham et al., 2016), and likely represent the roots of the Chisana arc (Plafker and Berg, 1994; Snyder and Hart, 2007). Prior studies assume Chisana igneous rocks are the product of subduction-related volcanism (Trop and Ridgeway, 2007); however, this is based primarily on the presence of forearc subduction complex deposits to the south of the study area in the Chugach and Wrangell Mountains (Plafker and Berg, 1994; Trop and Ridgeway, 2007) sedimentary and volcanic rocks exposed hundreds of kilometers away from the study area (e.g., Gravina belt (Figure 1-1)) and a set of geochemical and radiogenic isotope data from the scarce amount of erupted lavas and plutons of the Gravina-Nutzotin belt, which consists of only 88 igneous whole-rock geochemical and 20 whole-rock radiogenic isotope samples from the Gravina-Nutzotin belt (30 whole rock and 16 isotope from White Mountain pluton and 28 other whole rock geochemical analyses: only 17 with trace element data) characterizing the entirety of a >3,000 km suture zone (Berg et al., 1972; Richter et al., 1975; Rubin and Saleeby, 1991; McClelland et al., 1992; Barker, 1994; Aleinikoff et al., 2000; Stowell et al., 2000; Short et al., 2005; Snyder and Hart, 2007). Most of the previous studies of the inboard margin of the WCT in the Kahiltna basin from south-central and southwestern Alaska

(Ridgway et al., 2002; Kalbas et al., 2007) and in the Dezadeash, Nutzotin, and Gravina basins of southeastern Alaska (McClelland et al., 1992; Manuszak et al., 2007; Lowey, 2011; Yokelson et al., 2015) have focused on the sedimentary record, as volcanic rocks in the Kahiltna and Dezadeash basins are completely exhumed or were never deposited (Kalbas et al., 2007; Hampton et al., 2010), and volcanic rocks in the Gravina basin are intensely deformed or affected by post-depositional alteration effects (Stowell et al., 2000). Therefore, analysis of the Chisana Formation, which contains volcanic rocks that have undergone less pervasive metamorphism than other igneous rocks of the Gravina-Nutzotin belt, represents a method to evaluate the role of Cretaceous magmatism. Accurate evaluation of the igneous and sedimentary strata of the Chisana Formation will provide a clearer view of Upper Jurassic/Lower Cretaceous tectonics in the area and additional constraints to restrict the possible tectonic setting of Wrangellia accretion.

In order to improve petrologic and geochemical characterizations and lithostratigraphic frameworks, this study presents new major and trace element geochemistry, thin section petrography and field-based lithologic observations from physical volcanological and sedimentary analysis of the Chisana Formation type section at Bonanza Creek, Alaska and outcrops at Jacksina Creek near Nabesna, Alaska. We use these data, in conjunction with prior published and unpublished data from similarly-aged regional rocks, to elucidate the tectonomagmatic setting of Chisana volcanism and demonstrate that it occurred due to subduction.

## **Geologic Setting**

The outboard margin of southern Alaska and western Canada consists of three composite terranes. They are, from northeast to southwest, the Yukon, Wrangellia, and Southern Margin

composite terranes (Figure 1-1). The Yukon composite terrane consists of Paleozoic metamorphic rocks and overlying arc-related rocks (Nokelberg et al., 1994). The Wrangellia composite terrane is located on the outboard margin of the Yukon composite terrane along the Denali fault. The Southern Margin composite terrane is located on the outboard margin of the Wrangellia composite terrane along the Border Ranges fault (Plafker and Berg, 1994). The Southern Margin terrane is a complexly deformed accretionary prism, made up of Upper Triassic to Paleogene oceanic and arc-related volcanic and volcanoclastic rocks (Plafker and Berg, 1994). A >3,000 km suture zone extending along strike from western Alaska to coastal British Columbia separates the WCT from the outboard margin of the Yukon composite terrane (Figure 1-1). The suture zone is characterized by complexly deformed sedimentary, igneous and metamorphic rocks (Trop and Ridgway, 2007; Hampton et al., 2010; Lowey, 2011) attributed to collision processes. The suture zone separating the WCT from inboard terranes consists of Jurassic-Cretaceous sedimentary and igneous rocks that crop out in the Alaska Range/Talkeetna Mountains, Nutzotin Mountains, Dezadeash Range, and coastal southeastern Alaska (Figure 1-1, McClelland et al., 1992; Trop and Ridgway, 2007; Lowey, 2011). Basinal sediments from the Wrangell Mountains basin, located to the south of our study area, expose sediments with ages similar to the Chisana Formation volcanic rocks and are interpreted to represent forearc deposits relative to the Chisana and Chitina arcs (Trop et al., 2002; Trop and Ridgway, 2007). Plutonic rocks of Late Jurassic-Early Cretaceous ages crop out discontinuously along the Nutzotin basin and have been suggested to represent the roots of the volcanic arc complex of the Chisana Formation (Richter et al., 1975; Plafker and Berg, 1994; Aleinikoff et al., 2000; Snyder and Hart 2007).

The Chisana Formation, located along the suture zone separating the WCT from the North American continent, consists of approximately three km of relatively undeformed igneous and sedimentary rocks that conformably overlie Jurassic-Cretaceous sedimentary strata. The Chisana Formation is unlike other suture zone units in the northern Cordillera, because thick packages of relatively unmetamorphosed volcanic strata crop out (Figure 1-1; Figure 1-2; Figure 1-4). Reconnaissance study of the basal 600 m of the Chisana Formation, at its Bonanza Creek type section (Figure 3-7), showed that it consists of submarine lahars, basalt and andesite lavas, tuff, volcanoclastic sedimentary rocks, and marine argillite, greywacke, and conglomerate (Short et al., 2005). Lower Chisana Formation (basal 1100 m) volcanic rocks include aphanitic to porphyritic lavas, volcanic-lithic breccia, crystal-lithic and volcanic-lithic tuff, minor mudstone and volcanoclastic sandstone deposited by effusive and pyroclastic eruptions (Short et al., 2005; this study) The upper 2500 m of the Chisana Formation consists of interlayered basalt lavas, lahars, pyroclastic breccia, tuff and volcanoclastic greywacke and conglomerate (Barker, 1994; this study). Published geochemical data are limited to 19 major-element analyses from the Chisana lavas (Barker, 1994), ten major-element analyses from mid-Cretaceous plutons (Richter et al., 1975), and 30 major and trace, 13 REE, and 16 Sr-Nd isotope elemental analyses from a 0.78 km<sup>2</sup> intrusive body, the White Mountain pluton (Snyder and Hart, 2007). Short et al (2005) report 26 geochemistry, two <sup>40</sup>Ar/<sup>39</sup>Ar ages (116±1.3 to 113±1.3 Ma), as well as 10 Nd<sub>i</sub> and five (<sup>87</sup>Sr/<sup>86</sup>Sr)<sub>i</sub> isotope values from Bonanza Creek Chisana lavas, in an abstract. Six Lower Cretaceous aged granitoid and diorite plutons are present near our study areas. These six plutons have an age range from approximately 113 Ma to 105 Ma (Richter et al., 1975; Snyder and Hart, 2007), which are consistent with dates from the Chisana Formation (Short et al., 2005), and likely represent the plutonic equivalents of Chisana Formation volcanic rocks.

The Chisana Formation at the Bonanza Creek type section disconformably overlies the late Jurassic to early Cretaceous Nutzotin Mountains Sequence (Manuszak et al., 2007). The upper Nutzotin Mountain Sequence at Bonanza Creek (approximately the uppermost 50 m of the Nutzotin Mountains Sequence directly underneath the Chisana Formation) consists of fossil-rich mudstones, with minor amounts of volcanic-lithic sandstone, conglomerate, and fossiliferous limestone that grades into the lower Chisana Formation (Manuszak et al., 2007). The Chisana Formation is exposed along a slot canyon where Bonanza Creek has cut through the igneous and sedimentary strata. At the Jacksina Creek study location, the Chisana Formation also overlies the Nutzotin Mountains Sequence (Lowe et al., 1982; Figure 1-5 B). The uppermost lavas of the Chisana Formation are exposed approximately 4.5 km southeast of Bonanza Creek and are in direct erosional contact with sedimentary facies of the Beaver Lake Formation (Koepp et al., 2017). Overlying the Chisana Formation (located approximately 4.5km to the southeast) are nonmarine conglomerate, sandstone and mudrock of the Beaver Lake Formation (Koepp et al., 2017). Deposition is inferred to have taken place in channel-bar complexes and vegetated floodplains with poorly drained wetlands (Koepp et al., 2017). Volcaniclastic sediments from the Beaver Lake Formation were eroded from local igneous sources, including the underlying Chisana Formation (Koepp et al., 2017).

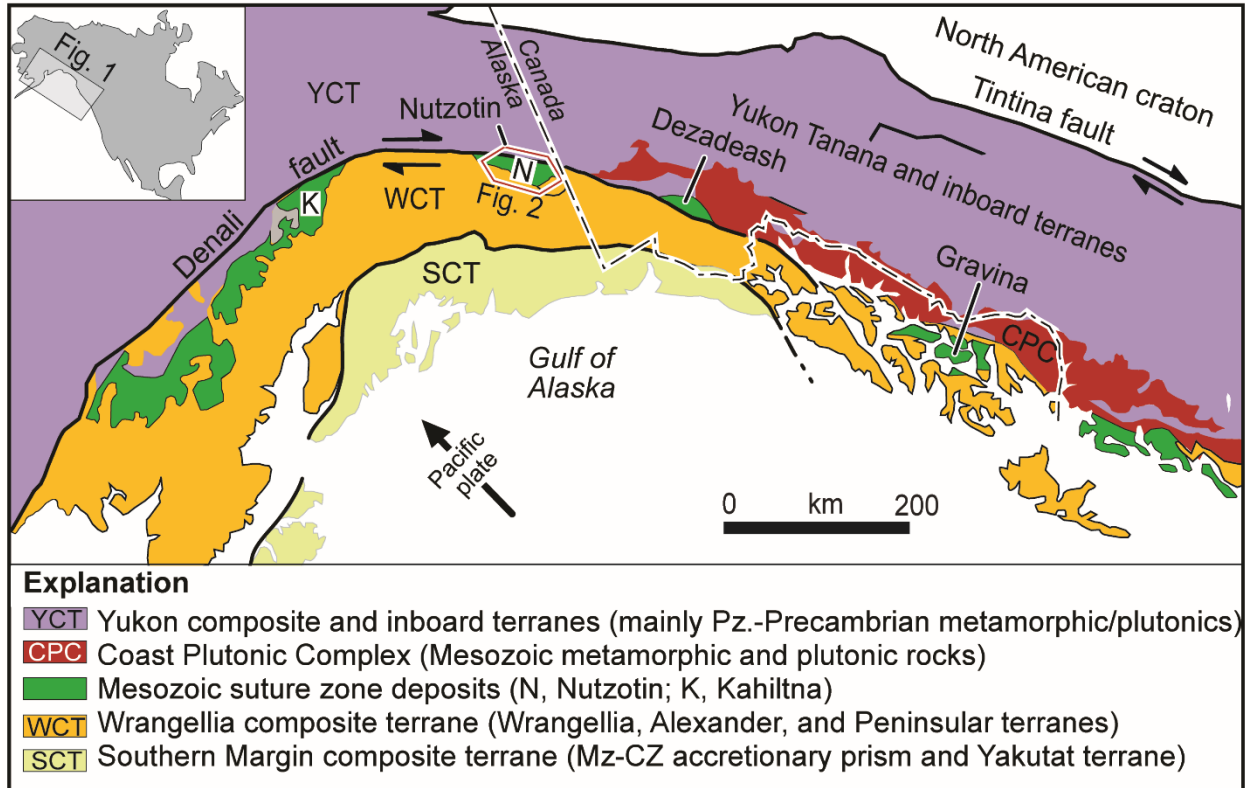


**Figure 1-1 Geologic map of south-central Alaska.**

Map showing major terranes, faults, and suture zones. Mesozoic (Mz) suture zone deposits (green) record accretion of the Wrangellia composite terrane (orange) against inboard terranes (purple). This study targets Chisana igneous rocks that are located in the Nutzotin area (N) of eastern Alaska (Fig. 1-2). (CZ-Cenozoic; Pz-Paleozoic) Adapted from Trop et al. (2002).

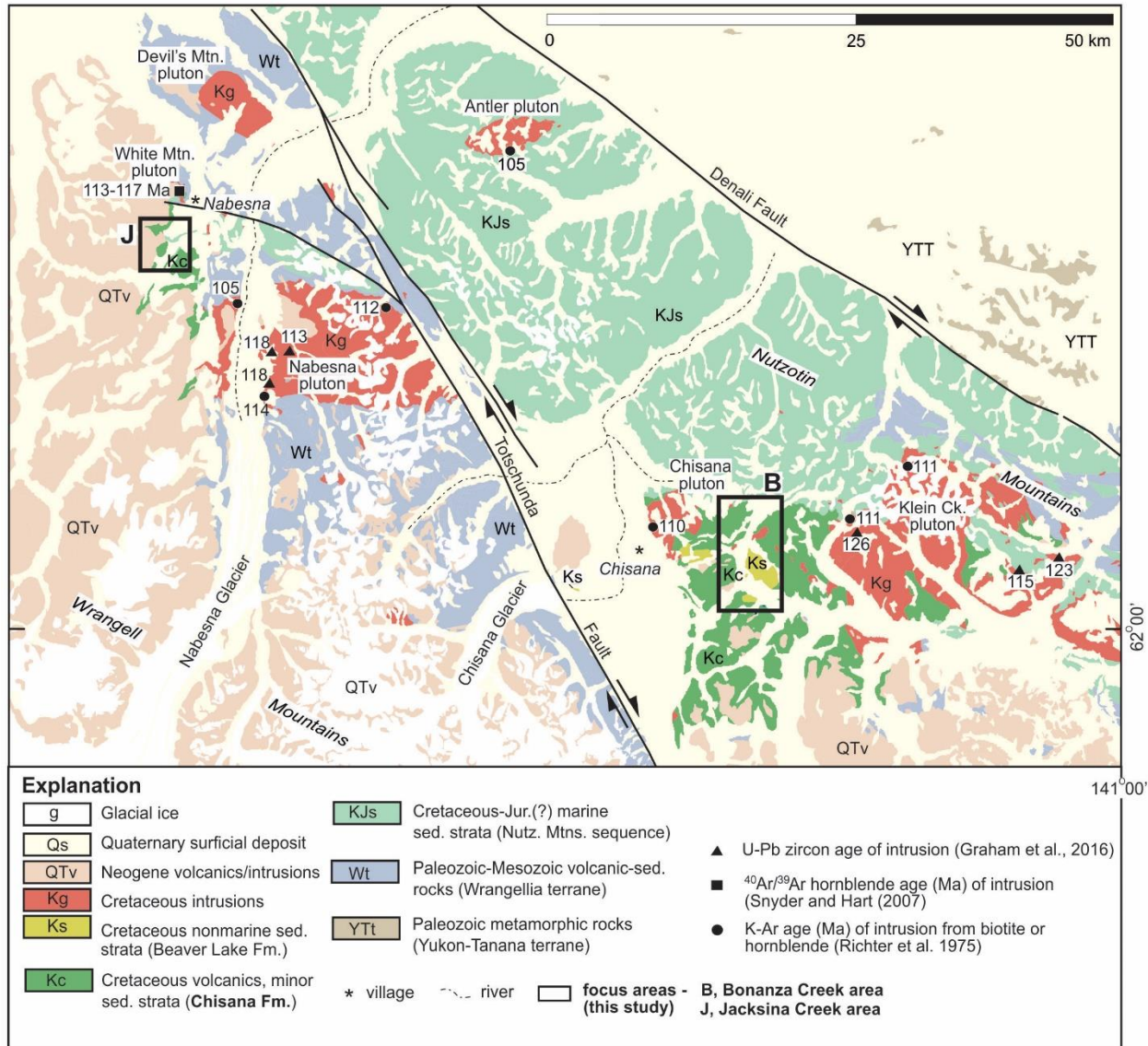


**Figure 1-2 Geologic Map of study areas.**

Geologic map showing the location of the Chisana Formation in dark green. Red rectangles mark focus areas for this study Chisana lavas in the Bonanza Creek study area were also studied by Short et al. (2005). Barker (1994) reports geochemical data from Chisana lavas from Bonanza creek and just southeast of the Jacksina Creek study area. Adapted from Richter and Jones, 1976. Geologic maps of outlined areas are present in Figure 1-3.

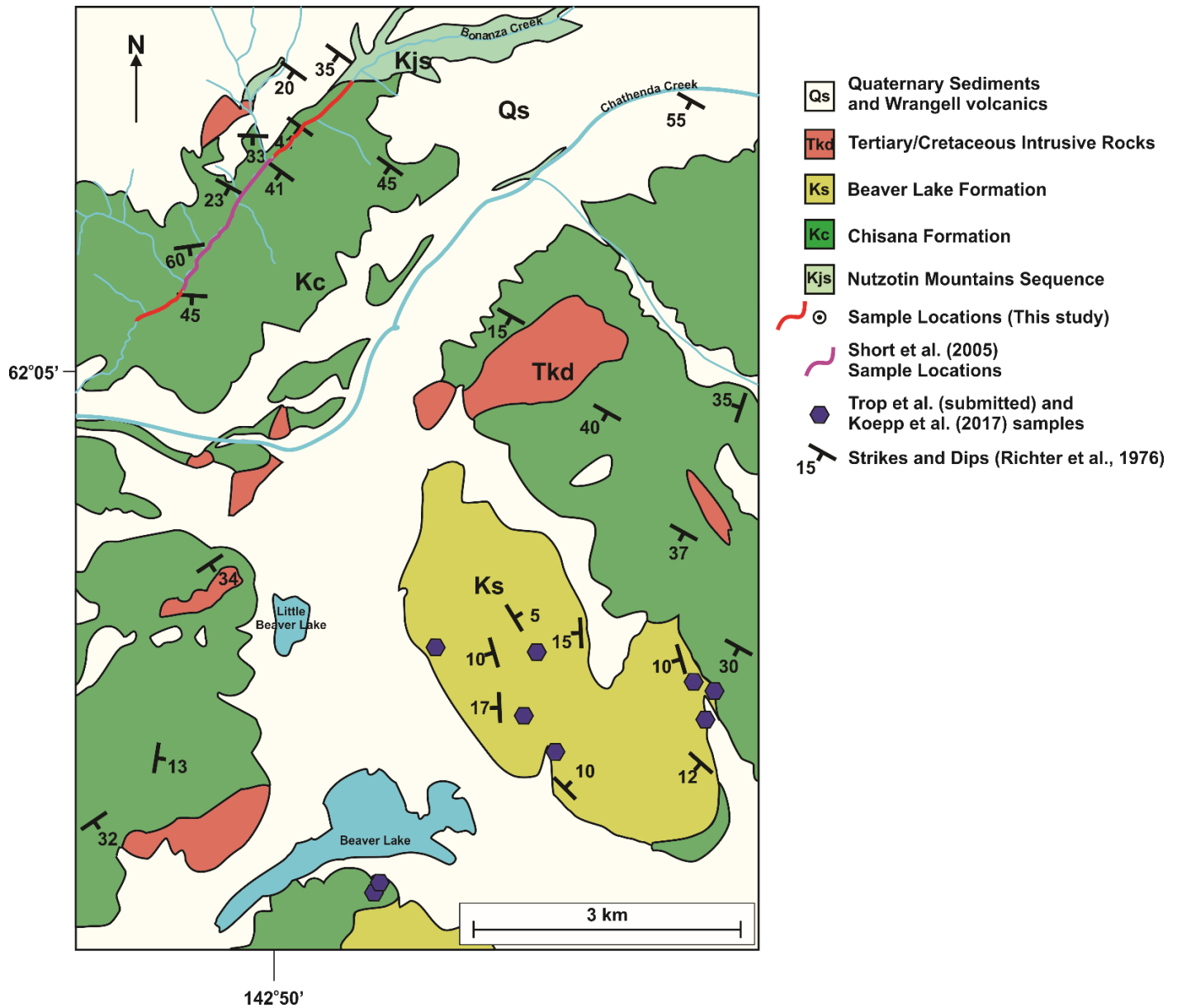
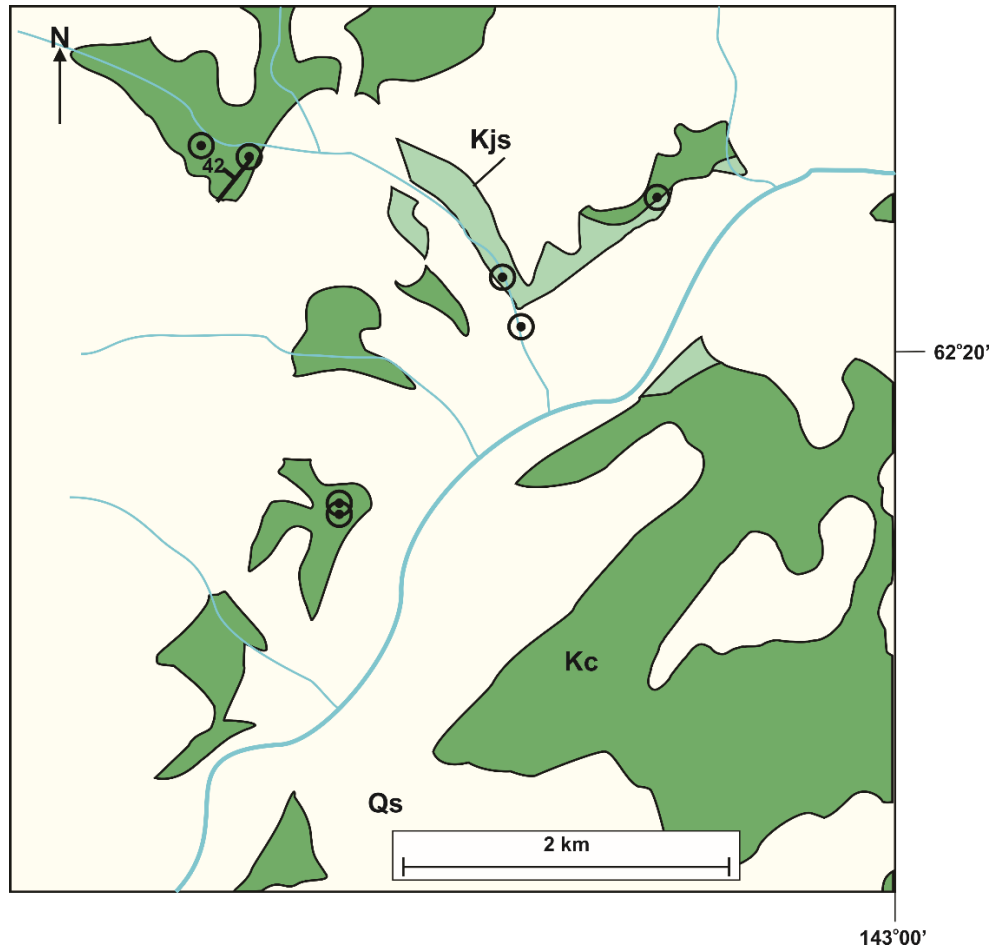


**Figure 1-3: Geologic map of the Bonanza Creek and Beaver Lake study areas**

Simplified geologic map of the Bonanza Creek study area (Richter and Jones, 1976), showing locations of samples taken. The sampled plutonic body is located approximately 5.3 km northwest of Bonanza Creek.





- Qs Quaternary Sediments and Wrangell volcanics
- Tkc Tertiary/Cretaceous Intrusive Rocks
- Ks Beaver Lake Formation
- Kc Chisana Formation
- Kjs Nutzotin Mountains Sequence
- ⊙ Sample Locations (This study)
- ⊙ Short et al. (2005) Sample Locations
- ⊙ Trop et al. (submitted) and Koepp et al. (2017) samples
- ↖ Strikes and Dips (Richter et al., 1976)

**Figure 1-4 Geologic Map of Bonanza Creek and Beaver Lake study areas.**

Simplified geologic map after Lowe et al. (1982) and this study showing the Jacksina Creek study area with sample locations.



**Figure 1-5 Overview Photographs of study areas.**

A.) Overview picture of the Chisana Formation at Bonanza Creek, near the contact between the lower and middle sections, person for scale. B.) Overview picture of the upper section of the Chisana Formation at Bonanza Creek, looking northeast. Note that as the formation became more lava dominated, the canyon became narrower and the creek typically becomes deeper. C.) Photograph of Chisana Formation lavas near Jacksina Creek, looking northwest along Canyon Creek.

## Chapter 2 - Methods

Stratigraphic observations of the volcanic and sedimentary lithologies of the Chisana Formation were made at both Bonanza Creek and Jacksina Creek study areas (Table 3-1). Lithologies were grouped into lithofacies and lithofacies associations on the basis of grain size, sedimentary structures, and igneous structures. Sampling locations were targeted based on published geologic maps and observations made in the field. At both Bonanza Creek and Jacksina Creek, sampling was guided by stratigraphic relationships between lithofacies. Only the freshest rocks were targeted for collection and further processing analysis for the igneous samples. After removing weathered surfaces from samples, a RockLabs hydraulic press was used to split fist-size samples into smaller pieces. These pieces were powdered using a Spex Industries shatterbox (alumina vessel).

Thirty-four samples (this study) were collected from sedimentary and igneous strata at both Bonanza Creek and Jacksina Creek in the Nutzotin Mountains, Alaska. Thin sections were made of twenty igneous rocks: 12 lavas, seven dikes, and one plutonic rock. Thin sections were used to help determine the extent of alteration before selecting samples for geochemical analyses and also for mineral and textural characterization. Modal percentages were made using visual estimations (thin section descriptions are present in Appendix A). Nineteen samples were selected for geochemical analyses based on the lack of obvious post-emplacement alteration in hand sample and thin section. A second suite of nine samples was collected from Chisana lavas and dikes in various locations surrounding Beaver Lake; their physical characteristics and relationships with overlying Cretaceous Beaver Lake formation strata are described in Koepf et al. (2017). A third suite of 15 samples was collected from the lower and middle sections of the Chisana Formation at Bonanza Creek (Short et al., 2005) and are incorporated into this study.

New Bonanza Creek, Jacksina Creek, and Beaver Lake samples from this study (samples starting with PM or JT in Appendix C) were sent to Franklin and Marshall College for XRF analysis of major and trace element compositions and loss on ignition (LOI) following the method outlined in (Mertzman, 2000, 2015) and online at <http://www.fandm.edu/earth-environment/laboratory-facilities/instrument-use-and-instructions>. One-gram of powder from each sample was placed in clean ceramic crucibles and heated at 900 °C in a muffle furnace for 60–75 min. After cooling to room temperature, samples were reweighed and the change in percent was reported as LOI. Following LOI determinations, 0.4 g of anhydrous powder was mixed with 3.6 g of lithium tetraborate ( $\text{Li}_2\text{B}_4\text{O}_7$ ) and melted in 95% Pt –5% Au crucibles. Samples were then quenched into glass disks, which were used for XRF analysis of major elements using a Panalytical, Inc. 2404 XRF vacuum spectrometer equipped with a 4 kW Rh X-ray tube. Major elements are reported as weight percent oxide ( $\text{SiO}_2$ ,  $\text{Al}_2\text{O}_3$ ,  $\text{CaO}$ ,  $\text{K}_2\text{O}$ ,  $\text{P}_2\text{O}_5$ ,  $\text{TiO}_2$ ,  $\text{Fe}_2\text{O}_3$ ,  $\text{MnO}$ ,  $\text{Na}_2\text{O}$ , and  $\text{MgO}$ ). Nineteen trace elements (Rb, Sr, Y, Zr, Ni, Nb, Ga, Zn, Cu, U, Th, Co, Pb, Sc, Cr, V, La, Ce, and Ba) were analyzed on pressed powder briquettes made from a mixture of 7.0 g of whole-rock sample powder and 1.4 g of high purity Copolywax powder. Working curves for each element are determined by analyzing geochemical rock standards from Abbey (1983) and Govindaraju (1994). The bulk rock data for all samples are presented in Appendix C, precision and accuracy of analyzed standards are presented in Appendix D. Major and trace element data for a subset (Denoted as samples beginning with CHI in Appendix C) of the Bonanza Creek samples were determined via Direct Current Argon Plasma Atomic Emission Spectroscopy (DCP-AES), at Miami University following methods outlined in Katoh et al. (1999) and Brueseke and Hart (2008). All trace element concentrations in this study are presented as parts per million (ppm) and major element data as weight percent

oxide (wt. %). Iron was split into  $\text{Fe}^{+2}$  and  $\text{Fe}^{+3}$  according to the procedure described by Le Maitre (1976), and all major element data used in diagrams and the discussion are reported as anhydrous using the split iron data.

Samples from all three locations (Beaver Lake, Bonanza Creek, Jacksina Creek) show signs of alteration, ranging from mildly altered (less than 10% alteration) to complete replacement of primary minerals. Samples that showed obvious signs of alteration in hand sample, such as phenocryst replacement, were eliminated from further analysis during the cutting phase. However, it is possible that alteration not immediately apparent in hand sample could still be present and affect the quality of geochemical analyses. In order to avoid biasing the geochemical analysis with samples that have been altered, a filter proposed by Beswick and Soucie (1978) was applied to the geochemical data (Appendix F). The “alteration filter” compares the molecular proportions of major element ratios ( $\text{Al}_2\text{O}_3/\text{K}_2\text{O}$ ,  $\text{SiO}_2/\text{K}_2\text{O}$ ,  $\text{CaO}/\text{K}_2\text{O}$  etc.) on logarithmic X Y-plots (Beswick and Soucie, 1978). Samples with compositions that are relatively unaffected by alteration plot as clustered, linear arrays on these diagrams whereas significant deviation from this array suggests post-eruptive alteration has affected the sample. Nine samples that did not fall along the linear array on multiple plots were removed from further consideration and are not reported or included in this study.

## **Chapter 3 - Results**

This study provides new major and trace element data in a combined dataset of 43 samples from Chisana volcanic rocks. Samples from Short et al. (2005) were collected from the Chisana Formation at Bonanza Creek, from 775 m above the base of the section to approximately 1695 m (Figure 3-7). The Chisana Formation at Bonanza Creek was split into three sections on the basis of field observations. Newly collected samples from this study are from the lower and upper part of the sections, from 69.4 m to 775 m and from 1695 m to 2115 m (Figure 3-7). Beaver Lake samples were collected from the uppermost lavas of the Chisana Formation approximately 4.5 km southeast of Bonanza Creek, near Beaver Lake (Figure 1-4). A complete list of samples and geochemical results is provided in Appendix C. Samples from Bonanza Creek include a mixture of lavas and dikes cutting through sedimentary facies in the lower section of the Chisana Formation. Samples from Jacksina Creek consist of lavas, from the Chisana Formation at Jacksina Creek, and of dikes cutting the Nutzotin Mountains Sequence that directly underlies the Chisana Formation.

### **Sedimentary and Volcanic Lithofacies**

Physical volcanic and sedimentologic observations from >2 km of combined Chisana Formation stratigraphic sections were made at the Bonanza Creek study location (Figure 3-7). There, the Chisana Formation is approximately 2.25 km-thick and can be divided into three sections: the lower, middle and upper sections, each of which is composed of seven different lithofacies associations that were identified through our field observations. Each section was demarcated based on the primary depositional environment of the associated lithofacies present in the section. Lithofacies were created based on rock type and environment of deposition and follow the example outlined in Trop et al. (2012). Table 3-1 summarizes the common facies in

the formation at the type section of Bonanza Creek and their key aspects. A stratigraphic column summarizing the Chisana Formation at Bonanza Creek is presented in Figure 3-7.

### **Marine Mudstones and minor fine-grained volcanoclastic sandstone (K<sub>CM</sub>)**

*Description.* This facies consists of very fine-grained mudstones with minor amounts of sandstones. It occurs in the lower Chisana Formation and upper Nutzotin Mountain Sequence, which directly underlies the Chisana Formation at Bonanza Creek. Marine brachiopods (Sandy and Blodgett, 1996) molluscs (Richter et al., 1975), and fragments of *Buchia* are present in the upper portions of the lower and middle section of the Chisana Formation at Bonanza Creek. Disarticulated brachiopods and molluscs are common. Sandstones occur in tabular beds but can be locally lenticular (Manuszak et al. 2007). This facies is depicted in Figure 3-1A.

*Interpretation.* This lithofacies reflects a subaqueous deposition in a marine environment, possibly representing suspensions settling. Evidence for marine deposition includes the presence of benthic marine fossils and very fine grain size. Deposits of disarticulated *Buchia* are interpreted by Manuszak et al. (2007) to represent fair-weather deposits on a marine shelf.

### **Volcanoclastic Conglomerate (K<sub>CGL</sub>)**

*Description.* This facies consists of a green, volcanoclastic granule to pebble conglomerate that represents the thickest facies in the lower section of the Chisana Formation at Bonanza Creek and is present throughout the entire formation. This lithofacies stops repeating at approximately 1982 m up section (Figure 3-7). Clasts are typically rounded to subrounded and poorly sorted, with a maximum clast size of 49.5 cm. Clasts are a mixture of volcanic and sedimentary rocks. Volcanic clasts appear to be consistent with the underlying mafic-intermediate Chisana lavas. Individual strata are typically matrix supported. In the lower section of the Chisana Formation, these rocks contain *Belemnite* and *Buchia* fragments. This facies is

seen in Figure 3-2C. *Inoceramus* fossils (Figure 3-2B.) and disarticulated and abraded fossil fragments are locally present in the conglomerates from the middle section of the Chisana Formation. Thickness of this facies can range from 8m to approximately 180 m. The parts of this facies that are in the lower section of the Chisana Formation at Bonanza Creek are frequently cut by mafic dikes. In a single location in the upper section at Bonanza Creek (Figure 3-7), this facies also contains thinly bedded (less than 6-cm-thick) tephra that are interbedded with the volcanoclastic conglomerate.

*Interpretation.* This lithofacies, which occurs throughout the middle and lower parts of the Chisana Formation at Bonanza Creek, implies subaqueous deposition via primary volcanic processes or by mass wasting onto the flanks of an active volcano. The presence of marine fossils, rare subaqueous structures, and interbedded pillow lavas in these facies are evidence of submarine deposition. Similar volcanoclastic strata can be seen in the Talkeetna arc (Clift et al., 2005), the Dezadeash basin (Lowey, 2011), and the Gravina belt (McClelland et al., 1992); they are interpreted by Draut et al. (2006) to represent similar depositional processes and environments.

### **Marine Lavas (K<sub>CLL</sub>)**

*Description.* Stratified basaltic andesite to basaltic lavas typify this lithofacies. Lavas are typically massive in nature, though pillow structures (1.1 m in length) are present from approximately 699 to 747 m in the lower section. Lavas are porphyritic, with fine-grained gray matrices and phenocrysts of plagioclase (typically 1-3 mm) and pyroxene (up to 3 mm). Plagioclase phenocrysts are more abundant than pyroxene phenocrysts, typically comprising 60-80% modally, while pyroxene typically makes up 5-10%. This facies is shown in Figure 3-1B. Autobrecciated lava tops and bottoms are present in K<sub>CLL</sub> lavas in the middle section of the



Chisana Formation. Lavas are interbedded with volcanoclastic conglomerates and mudstones containing marine fossils from the  $K_{CCGL}$  and  $K_{CM}$  facies, which imply marine deposition of the lavas.

*Interpretation.* This facies represents a subaqueous environment of emplacement for Chisana lavas. This is exhibited by the presence of pillow structures in lavas from the lower Bonanza Creek section and by interbedded sedimentary facies containing marine fossils.

### **Lahar Breccias ( $K_{CB}$ )**

*Description.* Inversely graded, poorly sorted and mud matrix-supported breccias define this facies, which is found at both the Bonanza Creek and Jacksina Creek locations. Clasts consist of underlying volcanic and sedimentary rocks from the Chisana Formation and are angular to subrounded and are poorly sorted. Clasts are more angular than clasts found in  $K_{CCGL}$ . The mud matrix, poor sorting, and angular nature of clasts are consistent with lahar breccias (Compton, 1985). This facies has an average clast size of approximately 8 cm. This facies is shown in Figure 3-3A, taken at Bonanza Creek, and Figure 3-5A, from the Jacksina Creek location.

*Interpretation.* This facies reflects volcanic aprons flanking an active volcano in a subaerial or shallow marine environment. The presence of a mud matrix, and the presence of more angular clasts distinguish this facies from previous sedimentary facies and establish it as a lahar. The poorly sorted, matrix-supported breccias are indicative of emplacement via debris flow, flood flow, and stream-bank collapse (Trop et al., 2012).

### **Block and Ash Flow deposit ( $K_{CBAF}$ )**

*Description.* This lithofacies consists of a matrix-supported volcanoclastic pebble conglomerate. Clasts are poorly sorted, composed primarily of subangular welded tuff, up to 15

cm in length. Matrix is fine-grained and grey-green. Rock is matrix supported but has more clasts than previous units. This facies is seen in Figure 3-2 F and I.

*Interpretation.* The presence of welded tuff clasts in this unit indicate the presence of elevated (relative to the area they were deposited in) lava domes that collapsed and produced pyroclastic density currents.

### **Oxidized Lavas (Kc<sub>UL</sub>)**

*Description.* This lithofacies is characterized by the presence of reddish-brown, oxidized lavas with autobrecciated tops and/or bottoms. These typically massive lavas occur in the upper section of the Chisana Formation at Bonanza Creek and directly overlie The Nutzotin Mountain Sequence in the Jacksina Creek area. In both locations, these occur as large packages of lavas that are distinguishable by autobreccias in interflow zones. These lavas range from basaltic andesites to andesites in composition, and typically contain 50-60% plagioclase, 0-24% pyroxene, and contain relict olivine phenocrysts. This is seen in Figure 3-4.

*Interpretation.* The presence of oxidation in the lava tops/bottoms indicates eruption in a subaerial environment.

### **Nutzotin Mountain Sequence at Bonanza Creek (Kjs)**

*Description.* This unit disconformably underlies the Chisana Formation at Bonanza Creek. At Bonanza Creek, this facies consists of mudstone with minor amounts of sandstone, conglomerate, and fossiliferous limestone.

*Interpretation.* At Bonanza Creek, this facies is interpreted to represent subaqueous deposition on a marine shelf (Manuszak et al., 2007; this study).

## **Nutzotin Mountains Sequence at Jacksina Creek (Kjs)**

At Jacksina Creek, the stratigraphy exposes nonmarine sedimentary strata (Figure 3-5B). Sedimentary strata at Jacksina Creek consist of mudrock, carbonaceous shale, fine-grained sandstone, and coal with abundant plant debris. Sandstones display symmetrical ripples and tidal bedding structures (flaser bedding, lenticular bedding, wavy bedding; Figure 3-6 A, B). Coal layers range from less than 5 cm to approximately 1.6 m in thickness.

*Interpretation.* At Jacksina Creek, this facies is interpreted to represent deposition that occurred in a coastal marine and terrestrial environment, influenced by fluvial, tidal, and wave processes (e.g., a fluvial-deltaic system).

## **Petrography**

Hand samples of both subaerial and subaqueous lavas are typically light to dark gray in color. Thin sections were made of 20 igneous and two sedimentary samples from this study; samples for petrographic analysis were limited to igneous rocks and combined with 26 thin sections from the study by Short et al. (2005). Thin sections were used to determine degrees of alteration of samples, and to provide visual estimates of mineralogy. In thin section, sampled lavas are porphyritic, and plutonic samples are phaneritic. Phenocrysts of plagioclase, 1-3 mm in size, are present in most of the lavas, with many samples also containing 1-4 mm pyroxene crystals. Alteration is clearly discernable in hand sample as pyrite blebs, veins of carbonates and sulfides, and as replacement of primary minerals by serpentine, epidote and other secondary alteration minerals. Alteration is pervasive and is distributed homogeneously throughout all samples collected. Alteration can make up anywhere from 10% to 100% of samples. In all but the most altered samples, phenocrysts typically exhibit less alteration than groundmass minerals (typically less than 30% alteration per phenocryst). Amphibole minerals are only present in

samples from the middle section of Bonanza Creek and from samples from Jacksina Creek. Amphiboles are typically completely replaced by chlorite, serpentine and/or opaque minerals, with the exception of a few samples from the middle section of the Chisana formation at Bonanza Creek (Figure 3-9 A, B) and samples from Jacksina Creek. Amphibole phenocrysts first appear at approximately 1185 m in the stratigraphic column in the middle section of the Chisana Formation at Bonanza Creek and continue until at least 1510 m. Amphibole phenocrysts range from greater than 2.5 mm to less than 0.125 mm. Alteration in amphibole phenocrysts and pseudomorphs can range from complete replacement by chlorite, sericite and opaque minerals to less than 5% replacement. In thin section, plagioclase is the dominant phenocryst phase for all samples. It is typically altered to sericite, epidote, carbonate, and opaque minerals. Plagioclase laths exhibit sieve textures, and are typically zoned (Figure 3-9 C, D). Plagioclase is present throughout the Chisana Formation at all localities sampled. Alteration ranges from total replacement of plagioclase minerals, to partial replacement present in certain zones, to homogenous alteration across the mineral to sericite and kaolinite. Chisana Lavas are locally amygduloidal, with vesicles filled by epidote, zeolites, serpentine, and calcite (Figure 3-9 E, F). Olivine pseudomorphs (Figure 3-9 G, H) are present only in samples from the upper section of Bonanza Creek and from Jacksina Creek. Olivine-bearing lavas first appear at about 1595m in the stratigraphic column and are found until approximately 1910 m. Olivine is typically replaced by serpentine, with minor chlorite and iddingsite also present. Clinopyroxene is the dominant mafic phenocryst found in samples from the upper and lower sections of the Chisana formation at Bonanza Creek. Orthopyroxene is typically less abundant than clinopyroxene. Alteration of pyroxenes is typically less than 5% of the phenocryst, and is concentrated around the rims of the minerals. Many pyroxenes are also normally zoned, and some are partially resorbed. Pyroxene

phenocrysts range in size from over 4 mm to microcrystalline. Many phenocrysts of pyroxene minerals exhibit twinning, and form as glomerocrysts (Figure 3-9 I, J). The groundmass of the volcanic samples contain plagioclase laths, pyroxene crystals, opaque minerals, serpentine, chlorite, zeolites, sericite, kaolinite, and epidote (Appendix B).

Multiple samples from the upper Chisana section at Bonanza Creek and Jacksina Creek exhibit trachytic textures in groundmass plagioclase. Samples from the lower section of the Chisana Formation at Bonanza Creek are typically porphyritic with glomerocrysts consisting of plagioclase and clinopyroxene. Glomerocrysts often are larger than 4 mm in diameter. Lower section samples typically contain amygdules that have been filled by calcite and/or zeolites. Lavas from the middle section also have plagioclase as the dominant mineral, but have more amphibole pseudomorphs and phenocrysts than pyroxene or olivine. Olivine pseudomorphs are present only in the uppermost portions of the middle section. In the upper section lavas, plagioclase is still the dominant mineral; however, pyroxene phenocrysts and olivine pseudomorphs are present mainly at the base of the upper section, and become less abundant and smaller upsection. Lavas from the Jacksina Creek region are plagioclase dominated; these include samples with trachytic texture with more than 90% plagioclase laths. Others contain large (greater than 1.65 mm in diameter) glomerocrysts of both clinopyroxene and hornblende, in addition to plagioclase. The stratigraphically lowest lavas sampled at Jacksina creek contain large (greater than 2.5 mm) amphibole pseudomorphs and medium (approximately 2 mm and smaller) clinopyroxene glomerocrysts. The uppermost samples from the Jacksina Creek region are trachytic and composed of approximately 85% plagioclase laths and 15% alteration minerals.

The plutonic sample collected from the Chisana Pluton near Bonanza Creek consists of plagioclase feldspar, amphibole pseudomorphs, trace apatite and secondary alteration minerals

such as serpentine, chlorite, kaolinite, and epidote. Alteration is extensive, making up approximately 45% of the sample. Plagioclase laths are typically euhedral to subhedral, and exhibit zoning, sieve textures, and extensive alteration to kaolinite (sometimes >50% of the mineral). Amphibole pseudomorphs are typically replaced by serpentine, epidote, and chlorite.

### **Geochemical classification and bulk rock geochemical characteristics**

On the total alkalis versus silica diagram (Le Maitre, 1989), the samples from Beaver Lake, Bonanza Creek and Jacksina Creek can be classified as transitional basalts to andesites, with SiO<sub>2</sub> values ranging from 44.7 wt.% to 63.4 wt.% (Figure 3-10). The samples show a broad array in which total alkali content increases with increasing silica content. Samples from Bonanza Creek and Jacksina Creek typically plot as basaltic andesites (Figure 3-9). Samples from Jacksina Creek and Beaver Lake range from basalts to andesites. On an alkali-FeO\*-MgO (AFM, where FeO\* is the total Fe expressed as FeO) diagram (Figure 3-10), samples from the upper Chisana Formation at Bonanza Creek follow a tholeiitic array whereas samples from middle and lower sections, Beaver Lake, and Jacksina Creek dike samples plot along a calc-alkaline array. Most of the Jacksina Creek lavas plot along a tholeiitic array, only the stratigraphically lowest lava collected from Jacksina creek plots along the calc-alkaline array. Samples also plot as subalkaline basaltic to andesitic compositions on a Zr/TiO<sub>2</sub> versus Nb/Y discrimination diagram (Figure 3-10). The similarity in classification using the two different schemes suggests that alteration has had a relatively small effect on the nomenclature and bulk chemical composition. CIPW normative estimations of basaltic samples plot as olivine tholeiites and tholeiites. (Appendix E)

Major element geochemical diagrams typically show increasing SiO<sub>2</sub> with Na<sub>2</sub>O and K<sub>2</sub>O and decreasing SiO<sub>2</sub> content with MgO, CaO, FeO and Fe<sub>2</sub>O (Figure 3-11). There are both high

FeO\* and low FeO\* groups present. Samples from the upper and Lower Chisana formation at Bonanza Creek tend to plot in a higher FeO\* group than samples from the middle section. Published data, as well as samples from Beaver Lake and Jacksina Creek typically plot within both groups. K<sub>2</sub>O and TiO<sub>2</sub> also have a small separation between the upper and middle sections of the Chisana Formation at Bonanza Creek. Samples from the middle section of Bonanza Creek commonly group together on most of the major and trace element diagrams. Data from the middle section show anomalously high values when plotting SiO<sub>2</sub> vs. K<sub>2</sub>O, Na<sub>2</sub>O, and Rb. Trace element diagrams (Figure 3-12) show that samples from the middle section are typically more elevated in Zr, Ba, and Rb; and more depleted in Sc than samples from the upper section. Samples from Beaver Lake show broadly similar elevations and depletions, except with higher concentrations of La, Y, Zr and Sc than the middle section of Bonanza Creek. These trace elements were chosen because they had the most overlap between the three datasets. Chemostratigraphic diagrams show that there are significant differences between lavas from the three sections of the Chisana Formation at Bonanza Creek (Figure 3-13).

A primitive mantle normalized multi-element diagram (Figure 3-14) shows enrichment of LILE (large ion lithophile elements) and depletion of HFSE (high field strength elements) relative to each other, characteristic of elemental enrichments and depletions associated with subduction.

Unit	Abbreviation	Description	Inferred Depositional processes	Facies Location
Subaerial Oxidized Lavas	KC <sub>UL</sub>	Andesite lava flows and flow top/bottom breccias that have been oxidized, typically occur as thick packages of massive andesites. Porphyritic, with fine-grained light to dark gray matrices. Phenocrysts include 1-3mm plag (sometimes replaced with epidote) as well as 1-2mm pyroxene and 1-4 mm amphibole phenocrysts	Effusive volcanism	Jacksina and Bonanza
Block and Ash Flow	KC <sub>BAF</sub>	Volcaniclastic pebble conglomerate, matrix supported with a fine-grained matrix, but more clasts than previous conglomerates. Poorly sorted clasts of what look like tuffs, up to 15 cm in length.	Explosive Volcanism	Bonanza
Lahar Breccias	KC <sub>B</sub>	Inversely graded, poorly sorted and matrix supported breccias, found in the lower parts of the section. Cut by andesite dikes.	Debris avalanche off volcano flank	Jacksina and Bonanza
Pillow and Marine Lavas	KC <sub>LL</sub>	Andesite and Basaltic lava flows, found interbedded with KC <sub>gI</sub> . Porphyritic, with fine grained light-to-dark colored matrixes. Frequently contain 1-3mm plagioclase laths. Frequently have lava flow top/bottom breccias.	Marine deposition indicated by pillows in andesite lavas, and by the interbedded sedimentary units containing marine fossils	Bonanza
Volcaniclastic Conglomerate	KC <sub>CgI</sub>	Volcaniclastic pebble conglomerate, found throughout the lower and middle sections of the formation. Coarsens upward, and contains <i>Inoceramus</i> fossils and fragments intermittently.	Shallow marine to deltaic deposition indicated by large clast size, and inverse grading of clasts.	Jacksina and Bonanza
Marine Mudstones and minor fine-grained volcaniclastic sandstone	KC <sub>M</sub>	Very fine-grained mudstones and volcaniclastic sandstones found in the lower third of the Chisana Formation. Marine brachiopods (Sandy and Blodgett 2000) and molluscs (Richter 1994) are present throughout the facies.	Deep marine environment, indicated by marine fossils and low energy deposition of mudstones	Bonanza
Upper Nutzotin Mountain Sequence	Kjs	Sandstone, mudrock, carbonaceous shale, and coal with abundant plant debris, symmetrical ripples, and tidal bedding.	Deposition in coastal marine and terrestrial environments influenced by fluvial, tidal, and wave processes such as a fluvial-deltaic system.	Jacksina
Upper Nutzotin Mountain Sequence	Kjs	Mudstone with minor amounts of sandstone, conglomerate, and fossiliferous limestone.	Deposition in submarine-fan systems (Manuszak et al., 2007)	Bonanza

**Table 3-1: Facies Table**

Table describing observed units from Bonanza Creek and Jacksina Creek and their inferred depositional processes. The Upper Nutzotin Mountains sequence is split into two facies here, as the description and inferred processes of deposition differs greatly between the two study areas.





**Figure 3-1: Pictures of Bonanza Creek Study area, lower section.**

A.) Dike in lower section of Bonanza Creek, cutting through marine mudstone facies. B.) Bonanza Creek pillow lavas in marine lavas facies. Person for scale.



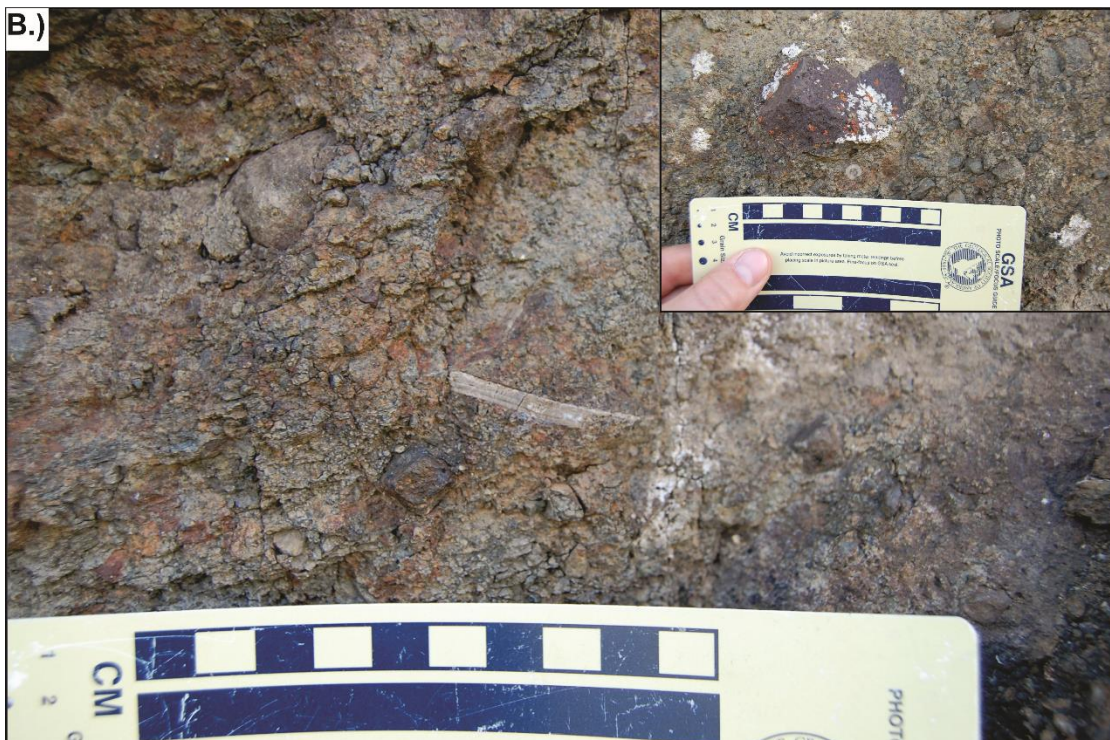


**Figure 3-2 Pictures of Bonanza Creek Study area, lower section.**

A.) Volcaniclastic conglomerate facies in lower section of Bonanza Creek, very poorly sorted, with pebble sized clasts and coarse sand-sized matrix. Clasts are volcanic in nature and are texturally consistent with derivation from underlying lavas (rock hammer for scale,

approximately 28cm). B.) Cross sections of *Inoceramus* and Belemnite fossils in volcanoclastic conglomerate facies at Bonanza Creek, indications of a marine environment.



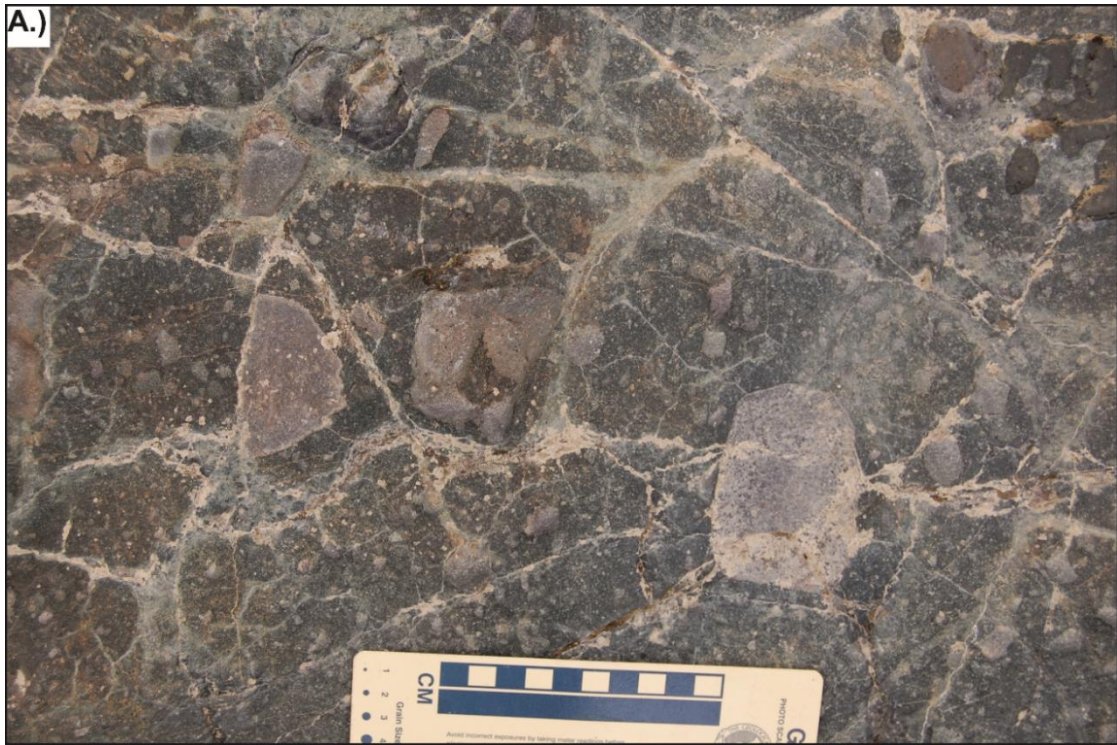


**Figure 3-3 Pictures of Bonanza Creek study area, middle section.**

A.) Lahar breccia facies in Bonanza Creek. Clasts are both sedimentary and volcanic. There are fewer clasts than previously seen in the formation, and clasts are more angular than previously

seen conglomerates. B.) Block and ash flow facies in Bonanza Creek. Clasts are made up of mostly pyroclastic rocks, but also include XXX rocks, and are also angular.



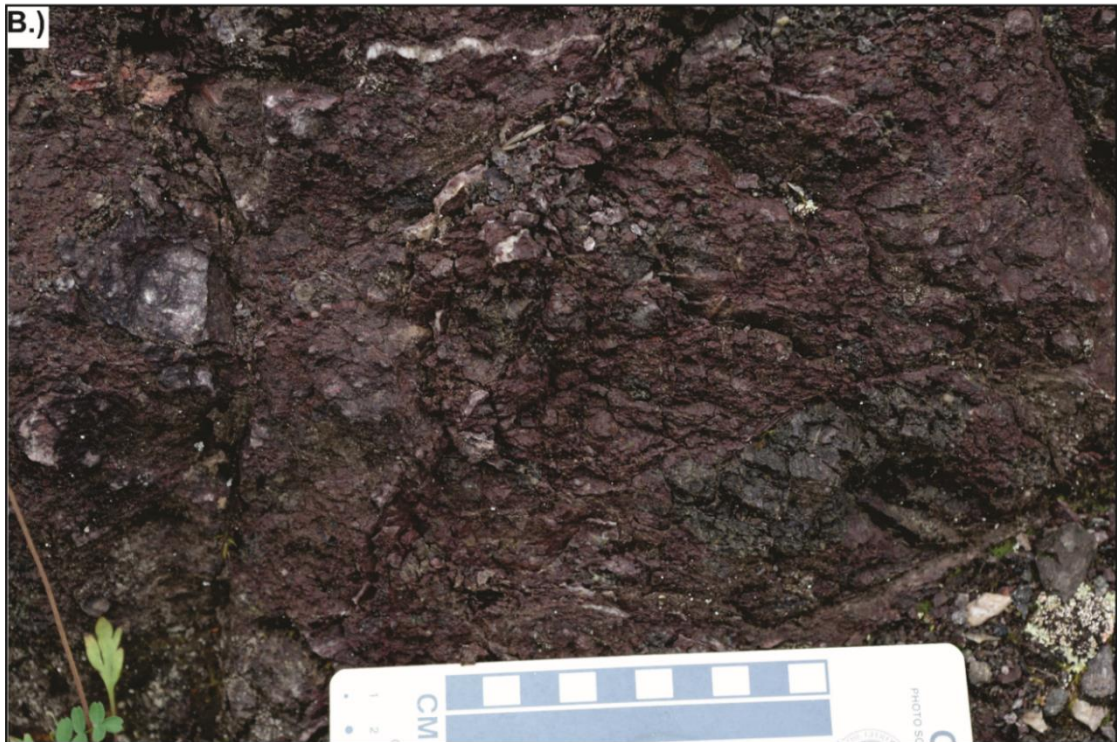


**Figure 3-4 Pictures of Bonanza Creek upper section and Jacksina Creek study areas.**

A.) Contact of first oxidized lava autobreccias (basalt autobreccia above red-colored zone of oxidation) facies signaling the beginning of subaerial lava facies. Previous lavas were not oxidized and were greenish-gray in color. B.) Subaerial lava facies at Jacksina Creek. Lowermost

stratigraphic part of the Chisana Formation at Jacksina Creek, very similar to upper Chisana section lavas at Bonanza Creek.





**Figure 3-5 Pictures of Jacksina Creek study area.**

A.) Lahar breccia facies at Jacksina Creek. Similar to the same facies from Bonanza Creek. B.) Chisana formation dike cutting through Nutzotin Mountains Sequence facies underlying Chisana



Formation at Jacksina Creek. Dike cuts through the sandstone and mudstone facies of the Nutzotin Mountains Sequence. Person for scale.



**Figure 3-6: Pictures of Nutzotin Mountains Sequence at Jacksina Creek**

A.) Symmetrical ripples in NMS sandstone as well as plant fossils in coal beds (inset). B.) Flaser bedding in sandstones.



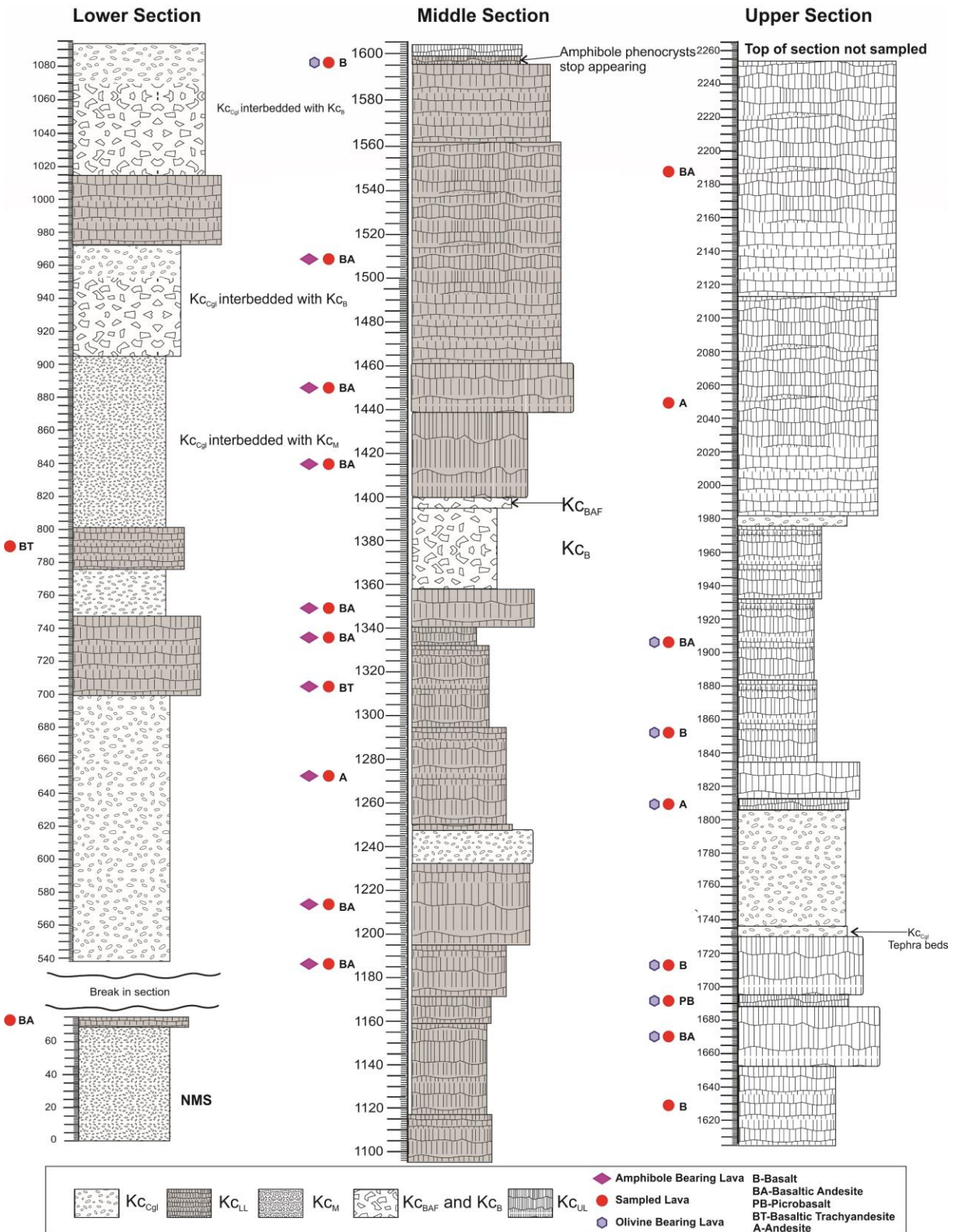


**Figure 3-7: Bonanza Creek stratigraphic column.**

Stratigraphic column for the Chisana Formation at Bonanza Creek. Unit consists of three sections, the upper, middle and lower, and is composed of six different facies. Facies

descriptions and abbreviations are taken from Table 3-1. The top of the section was eroded away and not documented.

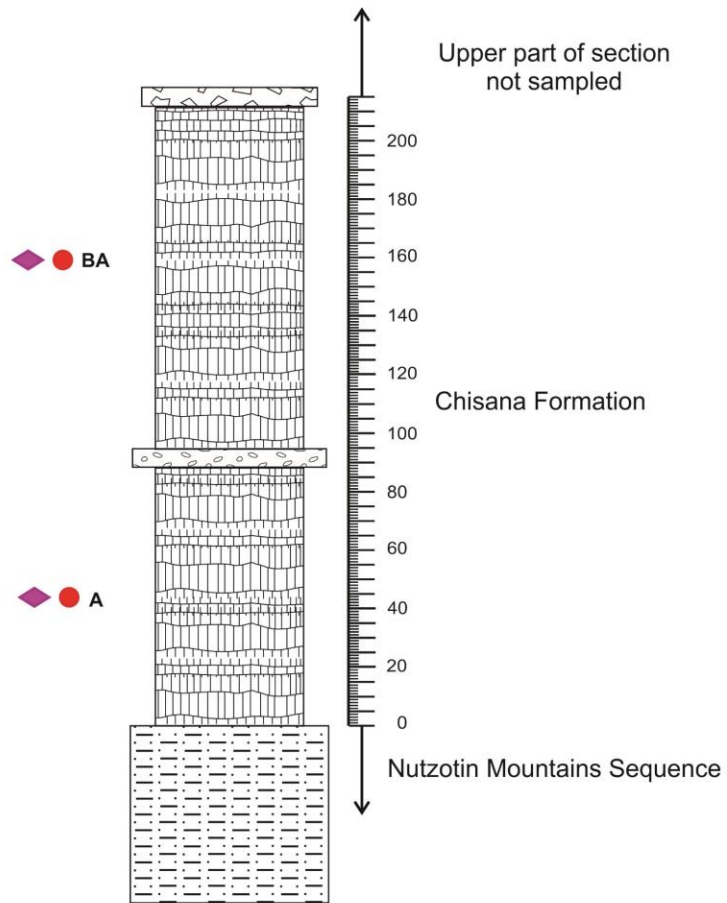


**Figure 3-8: Jacksina Creek stratigraphic column.**

Stratigraphic column showing the approximate stratigraphy of the Chisana Formation at Jacksina Creek.



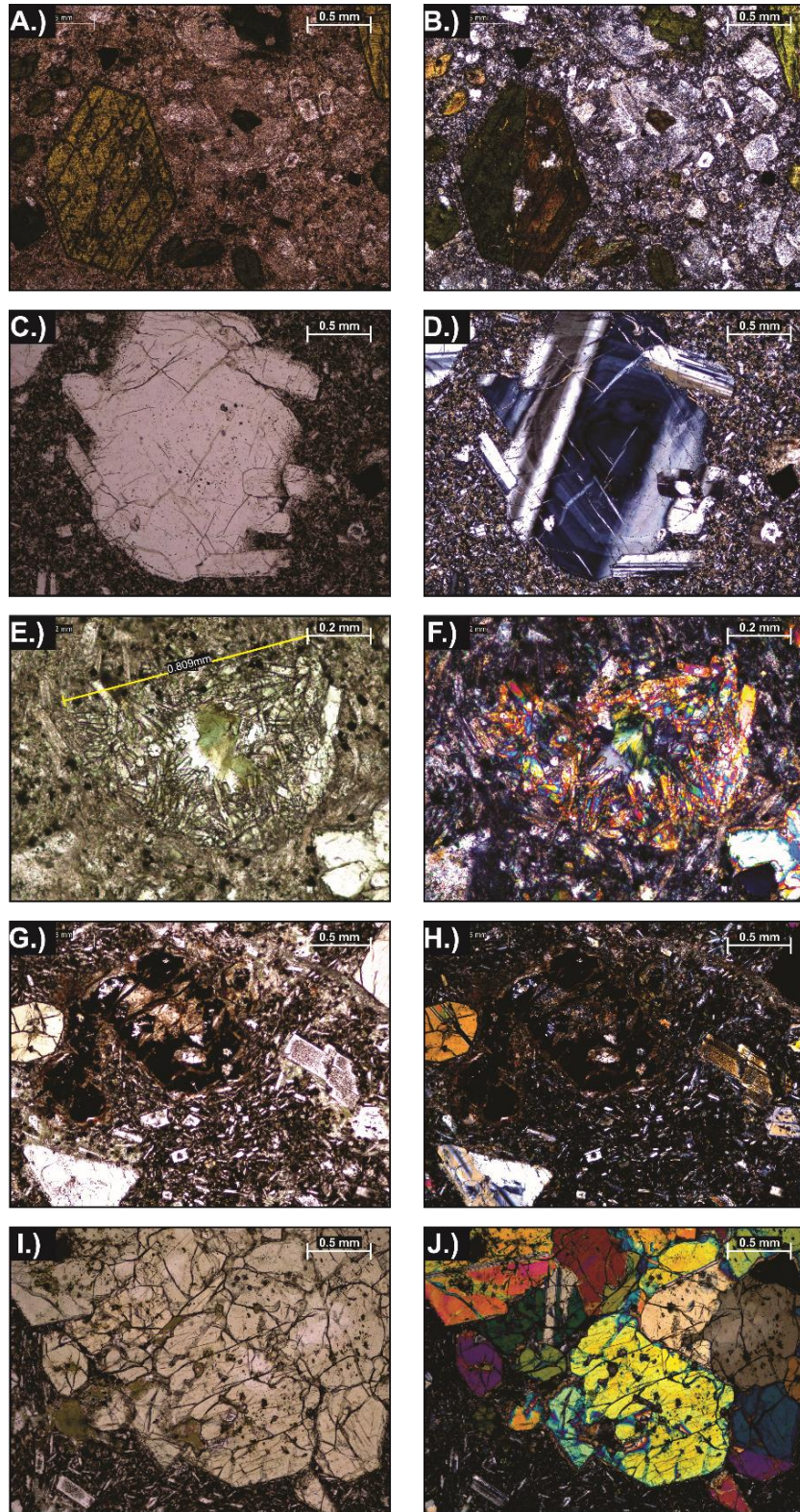


**Figure 3-9: Thin section photographs.**

Plane and cross-polarized light photomicrographs of: A, B) amphibole phenocrysts in an andesite from the middle section of the Chisana Formation. (4x) C, D) Phenocryst of zoned

plagioclase (4x). E, F) Vesicle filled with chlorite and epidote in a basaltic andesite from the Chisana Formation at Jacksina Creek (XPL, 10x). G, H) Olivine pseudomorph consisting of opaque minerals and iddingsite from lava from the upper section of the Chisana Formation at Bonanza Creek. (4x) I+J) Glomerocryst of clinopyroxene and orthopyroxene. Note twinning present in some pyroxenes. Sample from lower section of Bonanza Creek dike (4x).

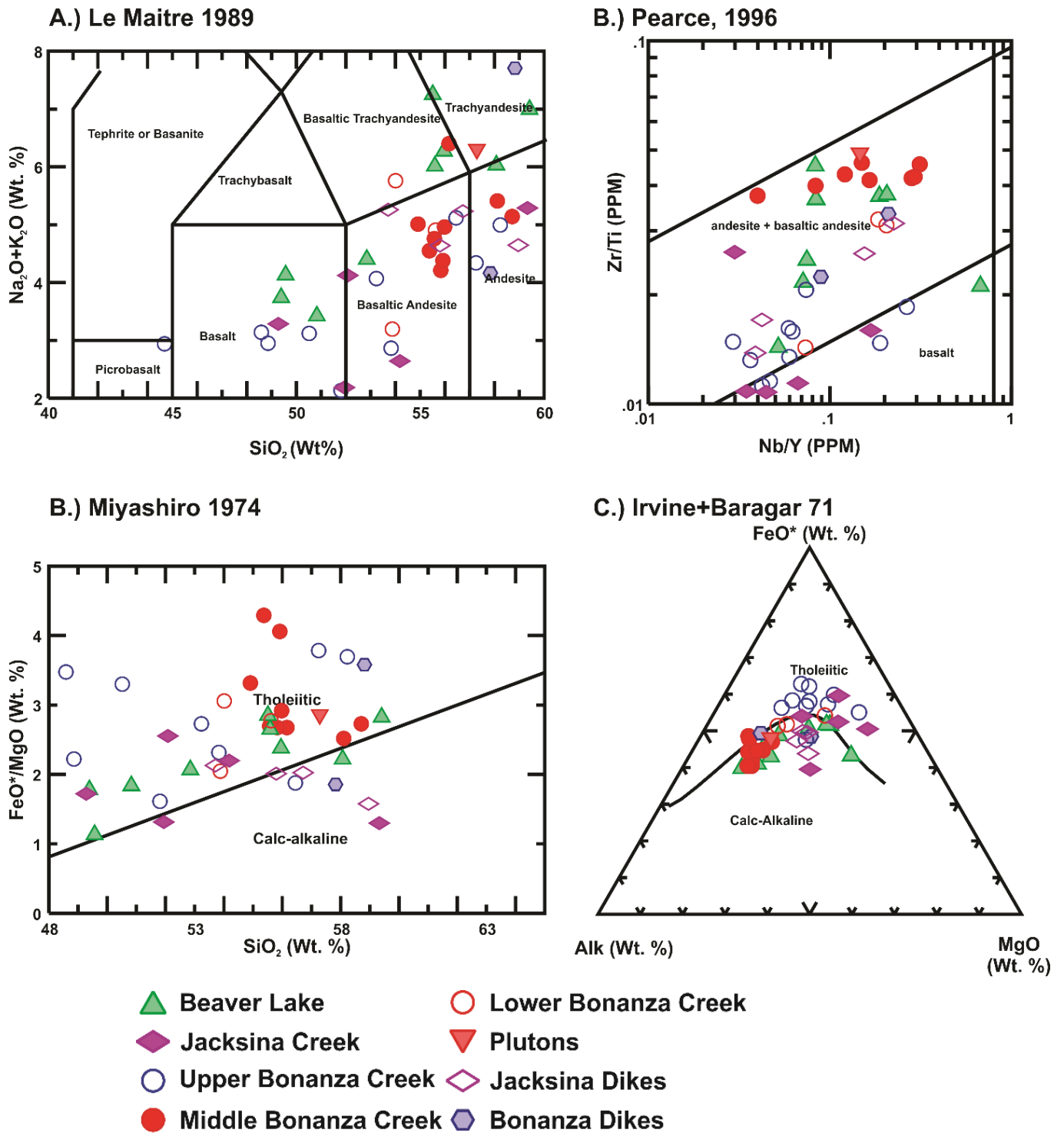


**Figure 3-10 Geochemical classification diagrams.**

A.) Volcanic rock classification diagram based on LeMaitre (1989). Chisana formation igneous rocks are composed primarily of basalts, basaltic andesites, and andesites. B.) Zr/Ti vs. Nb/Y classification scheme after Pearce (1996). The similar results yielded from both this diagram and the total alkalis vs. silica diagram indicates that any alteration has had minimal effect on the



behavior of incompatible trace elements and the overall bulk chemistry. C.) F/M vs. silica plot of Miyashiro (1974), showing the primarily tholeiitic rocks from the Chisana Formation. C.) AFM diagram after Irvine and Baragar, (1971), showing both tholeiitic and calc-alkaline arrays from the Chisana formation.

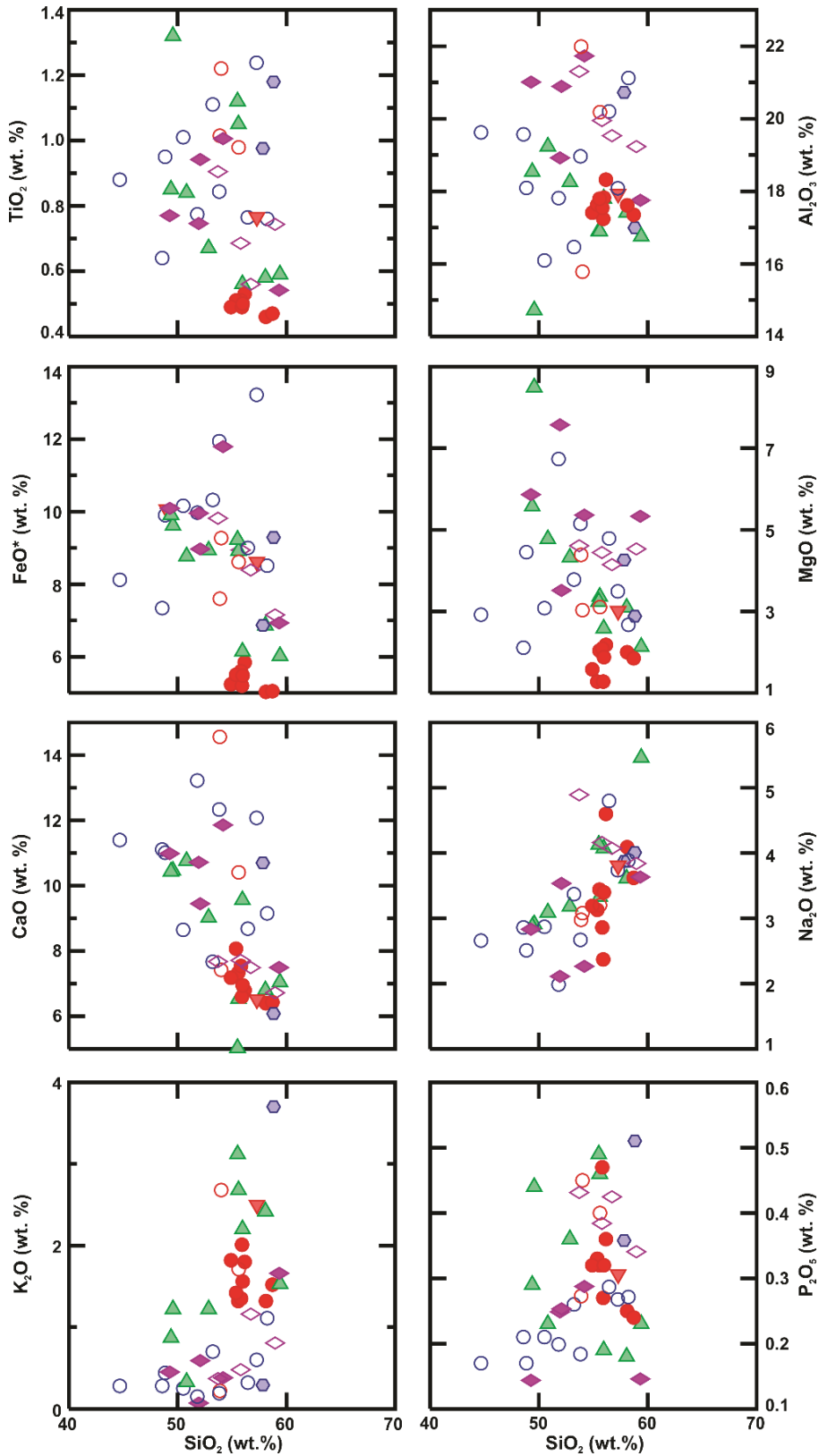


**Figure 3-11: Major element diagrams.**

Major elements vs. SiO<sub>2</sub>.

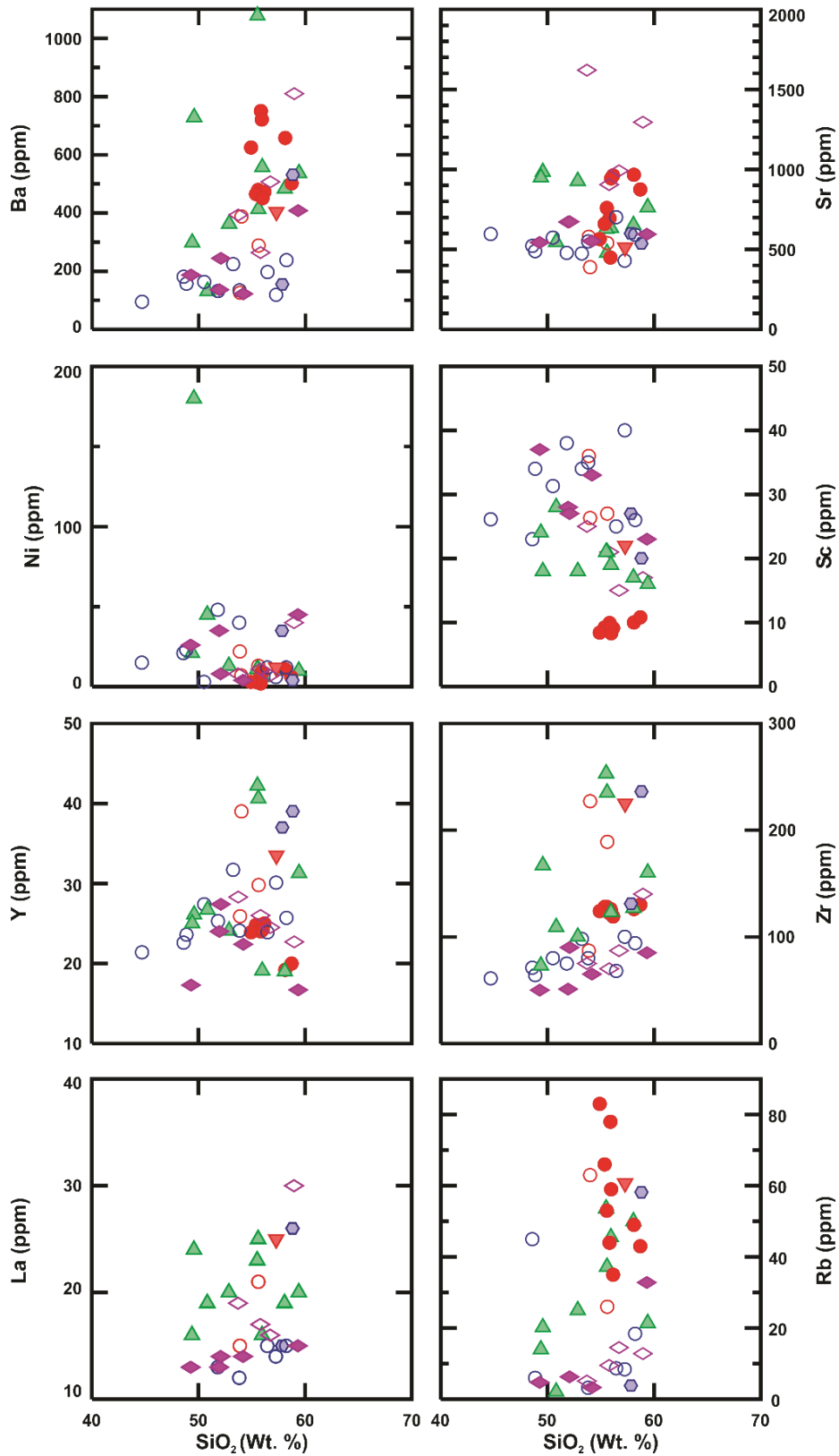


**Figure 3-12: Trace element diagrams.**

Select trace elements vs. SiO<sub>2</sub>.

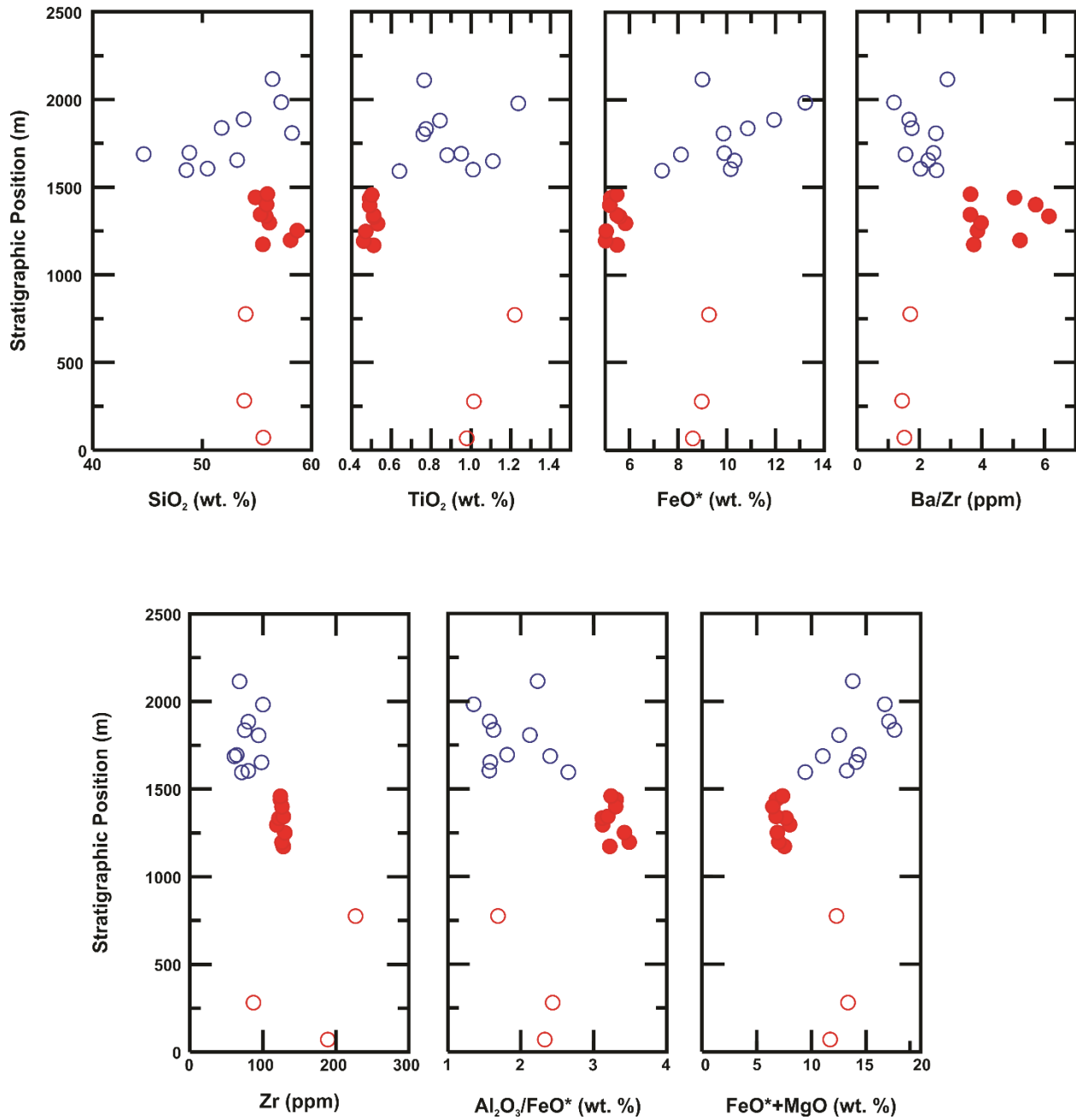


**Figure 3-13: Chemostratigraphic diagrams.**

Stratigraphically-controlled geochemical variations in the Chisana Formation at the Bonanza Creek type section. Differences between the middle sections and the upper and lower sections likely due to three different lava packages.

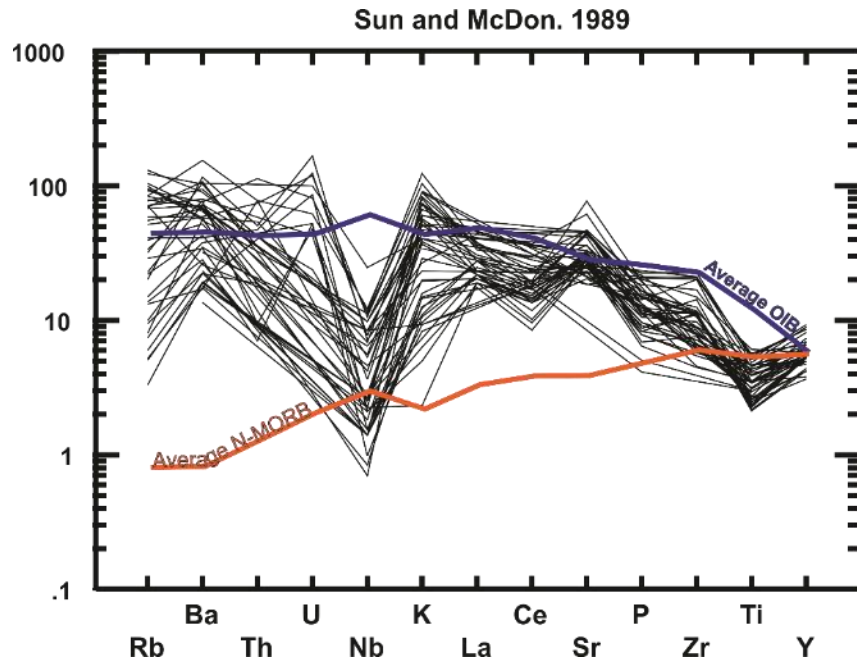


**Figure 3-14: Primitive mantle normalized multi-element diagram.**

Primitive mantle normalized multi-element diagram, normalizing values from Sun and McDonough, 1989. Overall, LILE enrichments and HFSE depletions relative to other elements are present, which is typical of arc magmatism. OIB-ocean island basalt, N-MORB-normal mid ocean ridge basalt (Sun and McDonough, 1989)

## **Chapter 4 - Discussion**

### **Stratigraphic Relationships of the Chisana Formation**

The Chisana Formation at Bonanza Creek is a record of a transition from subaqueous deposition and eruptions to subaerial deposition and eruptions. The presence of marine fossils and pillow lavas in the lower section, along with the inferred depositional setting of the locally exposed Nutzotin Mountains sequence (Berg et al., 1972; Richter and Jones, 1976; Manuszak et al., 2007) support a marine environment for deposition of the lower section of the Chisana Formation at Bonanza Creek. The middle section at Bonanza Creek contains a much higher proportion of lavas compared to the lower section and is interpreted to represent a transition between subaqueous and subaerial deposition. The interbedded sediments of the middle section are interpreted to have been deposited in a marine environment based on fossil evidence. Sedimentary layers thin, and eventually disappear upsection. The upper section of the Chisana Formation at Bonanza Creek, with its massive, oxidized lavas represents a primarily subaerial environment of deposition/emplacement. Manuszak et al. (2007) interpret structural imbrication and translation of the sedimentary strata of the Nutzotin basin during the Late-Early Cretaceous to represent accretion of the WCT onto the North American paleomargin. This is consistent with an interpretation where the transition from subaqueous to subaerial deposition/emplacement was caused by accretion of the WCT to the North American paleomargin.

The Chisana Formation at Jacksina Creek consists of oxidized lavas and autobrecciated lava tops/bottoms interbedded with the volcanoclastic conglomerate facies. The lavas and sedimentary rocks at Jacksina Creek are the same as the subaerial lava facies and upper section conglomerates at Bonanza Creek. Observations of the Nutzotin Mountains Sequence at the Jacksina Creek locality, however, indicate deposition of the Nutzotin Mountain Sequence at

Jacksina Creek to have occurred in a coastal marine and terrestrial environment influenced by fluvial, tidal, and wave processes. The Chisana Formation at Jacksina Creek is interpreted to represent a similar subaerial environment of deposition/emplacement as the subaerial lava facies from Bonanza Creek (Figure 4-1).

Chisana Formation chemostratigraphy at Bonanza Creek (Figure 3-13) show evidence of at least three distinct packages of lavas: chemically similar lower and upper section lavas, and a more evolved, middle section lava package. The upper section of the Chisana Formation at Bonanza Creek shows distinct enrichments in  $\text{FeO}^*$ , V, and  $\text{TiO}_2$ , and depletions in Ba and  $\text{K}_2\text{O}$  relative to lavas from the middle section (Figure 4-2). When plotted on a  $\text{SiO}_2$  vs  $\text{K}_2\text{O}$  discrimination diagram after Peccerillo and Taylor (1976), samples from the middle section of the Chisana Formation at Bonanza Creek typically plot as transitional from calc-alkaline to high-K calc-alkaline, and lavas from the upper formation plot as transitional from arc tholeiites to calc-alkaline affinities (Figure 4-2). Additional evidence of a change in magma composition are the petrographic differences present between the middle and upper sections of the Chisana Formation at Bonanza Creek (Figure 3-7; Figure 3-9). Phenocrysts of amphibole are abundant in middle section lavas but are absent in the upper and lower section lavas. Additionally, relict olivine phenocrysts are present in the upper section but absent in the lower and middle sections. These results indicate that lava packages in the middle and the upper Chisana Formation at Bonanza Creek came from different eruptions and potentially from different volcanic centers.

### **Geochemical constraints on Chisana Formation magmatism**

Geochemical analyses of new data gathered from the Chisana Formation, in addition to the minimal existing published data (Berg et al., 1972; Richter et al., 1975; Barker, 1994; Snyder and Hart, 2007) provide strong evidence that the Chisana Formation has an arc origin.

Subduction processes produce magmas that are enriched in LREEs and LILEs and depleted in HREEs and HFSEs (Smithies et al., 2007); these characteristic enrichments and depletions are present in the majority of samples from the Chisana Formation (Figure 3-14). Chisana Formation lavas show different trace element enrichments and depletions than OIB and N-MORB (Figure 3-14), that lack strong enrichments in Sr, K and Ba, which are present in most Chisana Formation samples. Basalts from the Chisana Formation primarily plot within the island arc array of a Zr-Ti-Sr diagram after Pearce and Cann, (1973) (Figure 4-5).

Plutonic rocks of similar ages (Richter et al., 1975; Snyder and Hart, 2007; Graham et al., 2016) to the volcanic rocks of the Chisana Formation crop out along the Nutzotin basin. Geochemical comparison of samples collected from the Chisana Formation (Berg et al., 1972; Barker, 1994, this study) to major element (Richter et al., 1975; Snyder and Hart, 2007) data from Cretaceous-aged plutons in the Nutzotin Mountains basin show similar arrays (Figure 4-3). Comparison with major, trace and REE geochemical data from the White Mountain pluton (Snyder and Hart, 2007) show that the White Mountain pluton in the Nutzotin basin plots within a similar range as samples from Chisana Formation volcanic rocks (Figure 4-3; Figure 4-4) and is compositionally similar. Radiogenic isotope data from Aleinikoff et al. (2000) show  $\epsilon\text{Nd}_i$  values range from 8.1-8.6 and  $^{87}\text{Sr}/^{86}\text{Sr}_i$  values range from 0.70289 to 0.70316 for four Chisana volcanic rocks. This is similar to radiogenic isotope ranges from the White Mountain pluton reported by Snyder and Hart (2007), who report  $\epsilon\text{Nd}_i = 7.2$  to  $9.1$  and  $^{87}\text{Sr}/^{86}\text{Sr}_i = 0.703189$  to  $0.704334$ . Short et al. (2005) report  $\epsilon\text{Nd}_i$  values of  $8.8$ - $9.1$  and  $^{87}\text{Sr}/^{86}\text{Sr}_i$  values ranging from  $0.70292$ - $0.70327$  for middle and lower lavas from the Chisana Formation at Bonanza Creek. Preliminary  $\epsilon\text{Nd}_i$  and  $^{87}\text{Sr}/^{86}\text{Sr}_i$  isotope data for samples from the Nabesna and Klein Creek plutons show a  $\epsilon\text{Nd}_i$  value of  $\sim 4.0$  and an  $^{87}\text{Sr}/^{86}\text{Sr}_i$  value of  $\sim 0.7040$  for the Nabesna pluton, and



an  $\epsilon\text{Nd}_i$  value of  $\sim 4.5$  with an  $^{87}\text{Sr}/^{86}\text{Sr}_i$  value of  $\sim 0.7045$  for a sample from the Klein Creek pluton (Graham et al., 2016). While these datasets are limited in scope, the similarity between radiogenic isotope values for the Chisana Formation lavas and Nutzotin basin plutons, as well as their geochemical overlap, is consistent with the interpretation that these igneous rocks all reflect magmatism in the same volcanic arc.

### **Origin of the Chisana Formation and tectonic implications**

Sedimentary facies similar to the volcanoclastic conglomerate facies we identified are found in modern arcs, such as the Mariana or Tonga arcs and are interpreted as primary volcanic and mass-wasting deposits proximal to an active arc volcano (Draut et al., 2006). The similarities of the sedimentary facies of the Chisana Formation and the sedimentary facies found in the Talkeetna, Mariana and Tonga arcs lend further credence to the hypothesis that the Chisana Formation was part of an island-arc system. Lithofacies of the lower and middle sections of the Chisana Formation at Bonanza Creek are very similar to lithofacies associations of the Talkeetna Formation at Sheep Mountain, or debris aprons formed around volcanic centers of the Tonga arc (Draut et al., 2006). Abundance of volcanoclastic turbidite facies, along with the presence of lahar breccias and block and ash flow deposits in the middle section of the Chisana Formation at Bonanza Creek, all suggest that deposition occurred less than 10 km from the volcanic vent (Draut et al., 2006). Lithofacies from the Chisana Formation are also consistent with lithofacies of island arcs, such as the Cretaceous Alisitos arc reported by Busby, (2004). Furthermore, thick successions of siliciclastic strata occur south of the Chisana Formation in the Wrangell Mountains basin and are interpreted to have been deposited in a forearc basin, relative to the Chisana arc (Plafker and Berg, 1994; Trop et al., 2002). Compositional data of volcanoclastic strata and volcanoclastic strata show that Late Cretaceous sediment in this basin was sourced

chiefly from the Chisana arc (Trop et al., 2002; Trop and Ridgway, 2007). The presence of these forearc deposits, support a model of island arc-formation for the Chisana Formation.

Chisana Formation igneous rocks originated in an island arc but differ slightly from “typical” island arcs, such as the Aleutians, because they would have been erupted/emplaced through/into an overthickened segment of oceanic crust in the Wrangellia terrane. This overthickened crust was created by the presence of the 3-6 km-thick package of Triassic Nikolai greenstone flood basalt lavas (and presumably, accompanying sub-volcanic magma plumbing systems) that represent an oceanic plateau that overlies older arc-related oceanic crust (Greene, 2010). Crustal thickness calculations using low magnesium intermediate (55-68 wt% SiO<sub>2</sub>) calc-alkaline Chisana Formation samples using Sr/Y concentrations and selection criteria after the method described by Profeta et al. (2015) (Appendix G) yield an average crustal thickness of the Wrangellia composite terrane crust of approximately 43 km, which is significantly thicker than the average island arc crust (Tetreault and Buitier, 2014). Supporting these calculations are La/Yb calculations (after Profeta et al., 2015) from four Chisana lavas that have Yb (Barker, 1994).

The arc-like signatures present in the geochemistry of the Chisana Formation, regional radiogenic isotope results, combined with marine depositional environments for lavas and interbedded sediments, local-regional geological setting and similarity between Chisana Formation sedimentary facies and sedimentary facies of other island arcs (Draut and Clift, 2006), all suggest that the Chisana Formation is the product of an island arc. Comparison of geochemical data from the Chisana Formation to geochemical data from volcanic rocks of the Gravina belt (Stowell et al., 2000) (Figure 4-6; Figure 4-7) exhibit very similar arrays and support the model of Plafker and Berg (1994) that Late Jurassic-Early Cretaceous volcanism in

the Gravina and Nutzotin belts were part of a single arc, dubbed the Gravina-Nutzotin arc (here called the Chisana arc).

The tectonic origin of the Gravina-Nutzotin belt is a highly debated subject (Yokelson et al., 2015; Lowey, 2017). Studies located in southeastern Alaska and British Columbia suggest that the WCT collision occurred during the Middle Jurassic, and that volcanism and sedimentation occurred in post-accretionary transtensional basins that were created by strike-slip fault systems (McClelland et al., 1992; Gehrels et al., 2009). Studies from southern Alaska and Yukon territory propose that volcanism is related to east-dipping subduction and that basin development evolved from an offshore Jurassic intra-oceanic arc to a Cretaceous collisional arc setting (Trop et al., 2002; Trop and Ridgway, 2007; Hampton et al., 2010). Recent tomography studies and studies of volcanoclastic rocks from the Dezadeash formation suggest that the Gravina-Nutzotin belt were the products of a west-dipping subduction related fore-arc basin (Sigloch and Mihalynuk, 2013, 2017; Lowey, 2017).

Chisana Formation-aged forearc deposits located south of our study area are interpreted by Trop et al. (2002) to represent deposition sediments derived from Chisana arc rocks into the Wrangell Mountains basin (Figure 4-8), located in a forearc position to the Chisana arc.

Radiogenic isotope analysis of Chisana volcanic rocks (Aleinikoff et al., 2000; Short et al., 2005) give a composite range of  $\epsilon\text{Nd}_i$  values from 7.2-9.1 and a range of  $^{87}\text{Sr}/^{86}\text{Sr}_i$  values from 0.70289 to 0.704334. Radiogenic isotope analysis of Yukon Tanana terrane (craton) granitoids give a range of  $\epsilon\text{Nd}_i$  values from -6.93 to -11.14, and a range of  $^{87}\text{Sr}/^{86}\text{Sr}_i$  values from 0.70706 to 0.711535 (Aleinikoff et al., 2000). The differences between  $\epsilon\text{Nd}_i$  values from the Chisana Formation volcanic rocks and Yukon Tanana granitoids suggest that Chisana magmas were not influenced by interaction with the North American craton. This indicates that Chisana

Formation volcanism occurred prior to accretion of the WCT onto the North American continent and the arc was not in close spatial proximity to the continental margin.

Data from this study alone cannot distinguish between an east-dipping subduction model and a west-dipping subduction model; however, when taken in context with other studies from southern Alaska, the results of this study provide more evidence for east-dipping subduction under the WCT than the alternatively proposed, west-dipping subduction model. Studies from the Chugach terrane to the west of the study area (Plafker and Berg, 1994; Amato et al., 2013) yield evidence that the Chugach terrane represents the remains of Late Jurassic-Early Cretaceous accretionary prism. Middle Jurassic to Early Cretaceous siliciclastic strata located inboard of the Chugach Terrane and outboard of the Chisana Formation are interpreted to represent intra-arc and forearc depocenters relating to the Chisana-Chitina-Talkeetna formations (Plafker and Berg, 1994; Trop and Ridgway, 2007). Our data, when combined with these other studies from across southern Alaska, support a model where formation of the Gravina-Nutzotin belt was dominated by subduction-related arc volcanism through overthickened island arc crust and underlain by an east-dipping subduction zone beneath the WCT.

### **Comparison to other volcanic arcs and other tectonomagmatic environments**

New data presented in this study, when combined with published data (Berg et al., 1972; Barker, 1994) allow for a detailed characterization of the Chisana Formation. This combined dataset allows us to compare the Chisana Formation with rocks from other volcanic arcs, such as the modern Honshu or Jurassic Talkeetna arcs. The Talkeetna Formation is an oceanic volcanic arc complex within the Peninsular terrane of south-central Alaska and was formed during the Early Jurassic (Clift et al., 2005). This formation is comprised of lavas, tuffs and volcanoclastic debris-flow and turbidite deposits. Geochemical comparison of rocks from the Chisana

Formation (Barker, 1994; this study) to geochemical analyses of igneous rocks from the Talkeetna Formation (Clift et al., 2005) show similarities between the two arcs. This is to be expected, as the two both represent arc magmatism within the WCT, albeit at different times. Chisana Formation samples plot in a similar range as samples from the older (182-177 Ma) Talkeetna arc (Clift et al., 2005) (Figure 4-9). Sedimentary facies in the Chisana Formation are very similar to volcanoclastic turbidites from other arcs, such as the Talkeetna arc (Clift et al., 2005).

Comparison of the Chisana Formation to the younger continental arc, the Wrangell arc (Preece and Hart, 2004; Brueseke et al., 2019) show that, while the two arcs have similarities in some elements, there are significant differences in others (Figure 4-10). Samples from the Wrangell arc are significantly more depleted in Ti, Sr, and P, and more enriched in Zr. An AFM diagram (Irvine and Baragar, 1971) show that Chisana Formation samples plot as more transitional tholeiitic to calc-alkaline, whereas samples from the Wrangell arc plot almost exclusively in the calc-alkaline field.

We compared samples of the Chisana Formation to samples from the modern Honshu arc, as we infer it to be a possible modern-day proxy for the Chisana arc due to the accretionary nature of both arcs. Compared to representative samples from the central and northeastern Honshu arc (Nobuyuki, 1988; Allan and Gorton, 1992; Jones et al., 1993; Morris and Itaya, 1997; Kawabata and Shuto, 2005; Safonova et al., 2015), the Chisana Formation typically shows greater trace element enrichments than Honshu and has greater Nb depletions (Figure 4-11), however, major element chemistries show overlap and the two arcs plot along similar transitional calc-alkaline to tholeiitic arrays on an AFM diagram. Trace element diagram comparisons between the two arcs show that, while they are similar, the Chisana Formation has higher

concentrations of La, Zr, Ce, Rb, Ba, and Nb/Y and Sr/Y. Similarities between the two arcs are consistent with the interpretation that the Honshu arc represents a modern-day proxy for Chisana Formation igneous rocks.

Trace element data from Chisana Formation igneous rocks with SiO<sub>2</sub> less than 64 wt.% were compared to Quaternary samples of basaltic to andesitic composition from the East African Rift (Giordano et al., 2014). Chisana Formation volcanic rocks are typically more depleted in Sr, and Ti, and more depleted in Ba and Nb than East African Rift (EAR) rocks. Chisana Formation volcanic rocks are significantly more depleted in Zr, Nb and Th than samples from the EAR. Differences between the two sets of geochemical data do not support the hypothesis that Chisana Formation volcanism occurred due to continental rifting.

Comparison of trace element geochemistry from igneous rocks from the Chisana Formation to samples from the Mariana back arc (Hart et al., 1972; Bougault et al., 1982; Stern et al., 1990; Gribble et al., 1998; Newman et al., 2000; Pearce et al., 2005; Straub et al., 2015) show broad similarities. Trace element ratios from samples from the Marianas back arc are similar to trace element ratios from samples of the Chisana Formation (Figure 4-13). Geochemical similarities are consistent with the model where the Gravina Nutzotin belt was formed in a back arc environment (Berg et al., 1972). However, back arc basin mantle source geochemistry can be influenced by subduction related processes which can cause back arc derived magmas to exhibit arc-like geochemical signatures (Saunders and Tarney, 1984; Pearce and Stern, 2006). Additionally, strata of the Wrangell Mountains basin that are inferred to represent fore arc deposits of the Chisana arc (Trop et al., 2002) are inconsistent with this model.

Another suggested model for the formation of the Chisana Formation and associated igneous rocks is formation via transtensional rifting during northward translation along strike-

slip faults (McClelland et al., 1992). Volcanic activity along strike-slip fault zones is primarily related to local extensional processes occurring at pull-apart basins or at releasing bend basins (Tibaldi et al., 2010) and in small volumes (relative to belts of arc volcanoes). Chisana Formation igneous rocks help define a ~2,000 km-long zone of magmatism (Plafker and Berg, 1994), which is inconsistent with a transtensional-related model of formation. Additionally, magmas produced in a transtensional tectonic regime are usually less hydrous than what is seen in Chisana Formation lavas and plutons (e.g., hydrous mineral-bearing). Overall, the hydrous nature and long linear array of coeval igneous rocks from south-central through southeastern Alaska are inconsistent with a model where Chisana Formation igneous rocks were formed in a transtensional tectonic setting.

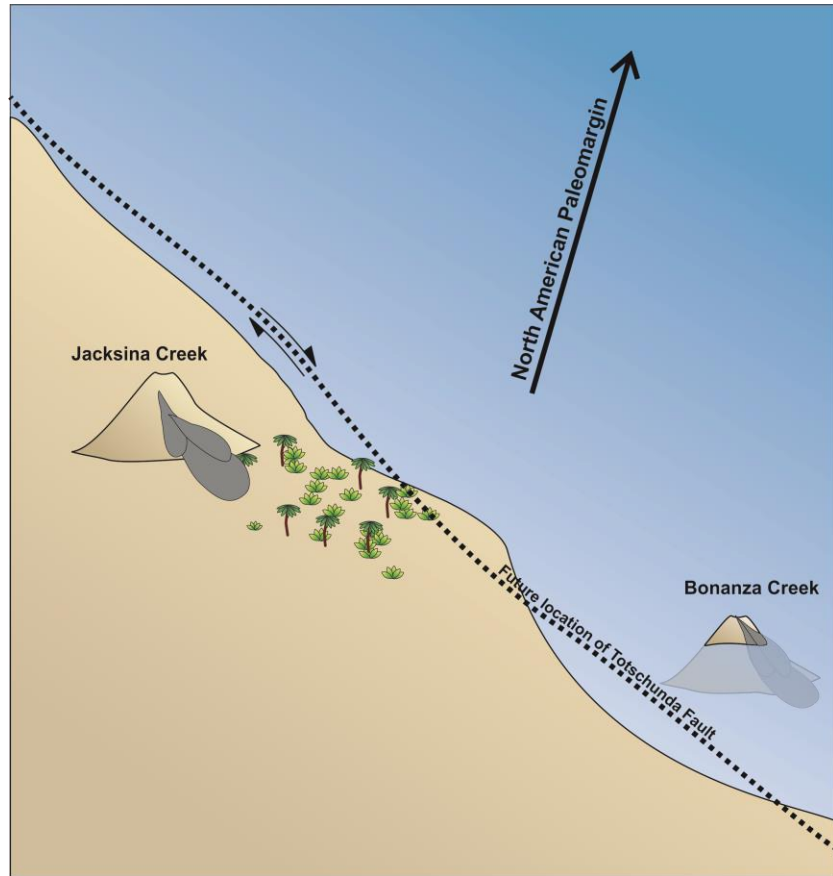


**Figure 4-1 Depiction of differences in depositional environments between study areas.**

Cartoon showing inferred depositional differences between Bonanza Creek and Jacksina Creek locales, based on field relationships from this study. This diagram illustrates that the Chisana Formation at Jacksina Creek was deposited in a subaerial (Tan) environment alongside deltaic facies, while at the same time, the lower Chisana Formation at Bonanza Creek was being deposited in a subaqueous (Blue) environment alongside marine sediments



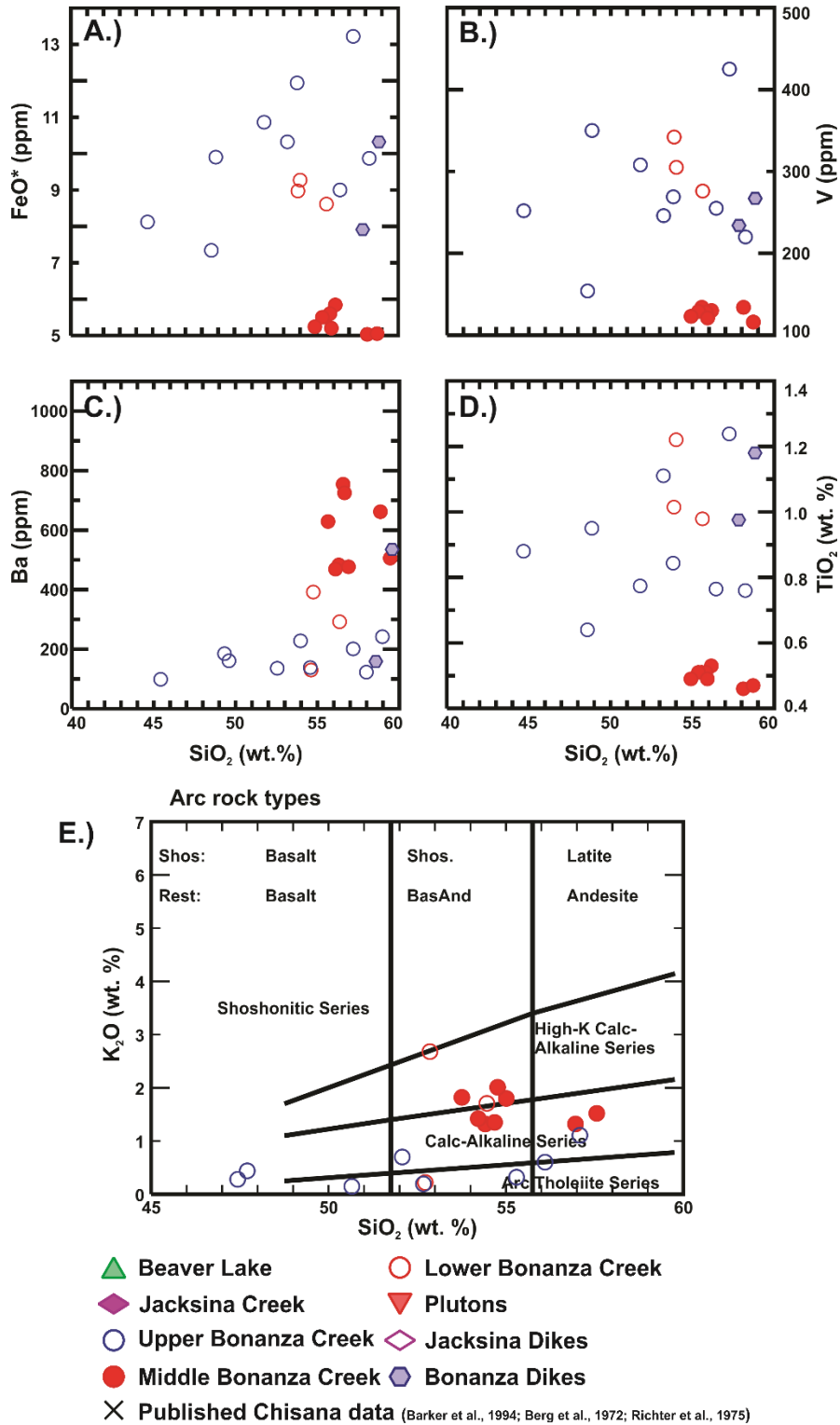


**Figure 4-2: Selected geochemical diagrams showing differences between upper and middle packages of Chisana Formation lavas at Bonanza Creek.**

A.) SiO<sub>2</sub> vs FeO\* diagram showing two different arrays from lavas from Bonanza Creek, one array for the middle section and one array for the lower and upper sections. B.) SiO<sub>2</sub> vs. V

diagram showing elevated levels of V in upper and lower section Chisana lavas at Bonanza Creek relative to the middle section. C.) SiO<sub>2</sub> vs. Ba diagram showing different arrays between the middle section and upper and lower section lavas at Bonanza Creek. D.) SiO<sub>2</sub> vs. TiO<sub>2</sub> diagram illustrating similar to the SiO<sub>2</sub> vs. V diagram where the upper and lower Chisana formation show elevated TiO<sub>2</sub> relative to the middle section of the Chisana Formation at Bonanza Creek. E.) SiO<sub>2</sub> vs. K<sub>2</sub>O diagram (Peccerillo and Taylor, 1976) showing calc-alkaline and high-K calc-alkaline affinity of middle and lower Chisana Formation lavas at Bonanza Creek, and the arc-tholeiitic and calc-alkaline affinities of the lower section of the Chisana Formation lavas at Bonanza Creek.

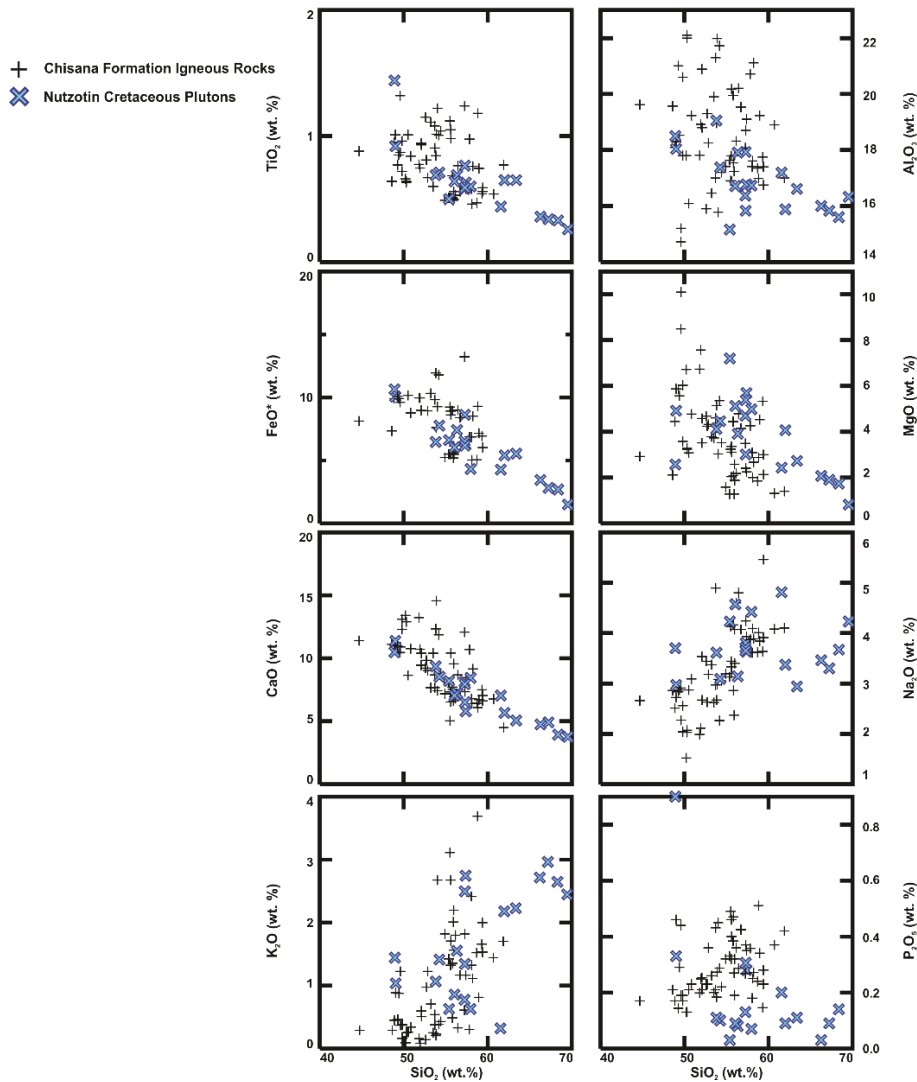
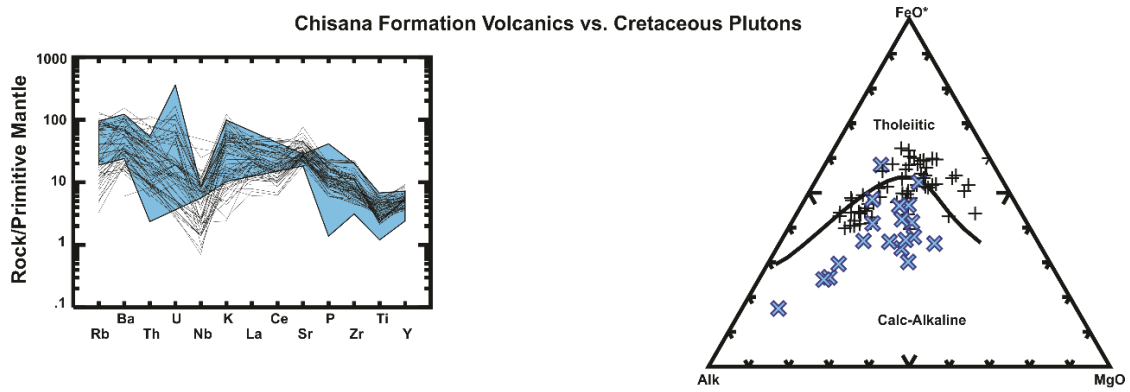


**Figure 4-3: Comparison of the Chisana Formation igneous rocks to Cretaceous plutons in the Nutzotin belt.**

Multi-element diagram comparing geochemistry from the Cretaceous-aged plutons in blue (Richter et al., 1975; Snyder and Hart, 2007) to geochemical data from the Chisana Formation (black)(Barker, 1994; this study), showing REE overlap between the plutons and volcanic rocks

from the Chisana Formation. AFM diagrams after Irvine and Baragar (1971) and major elements vs. silica plots show additional similarities between the two groups.

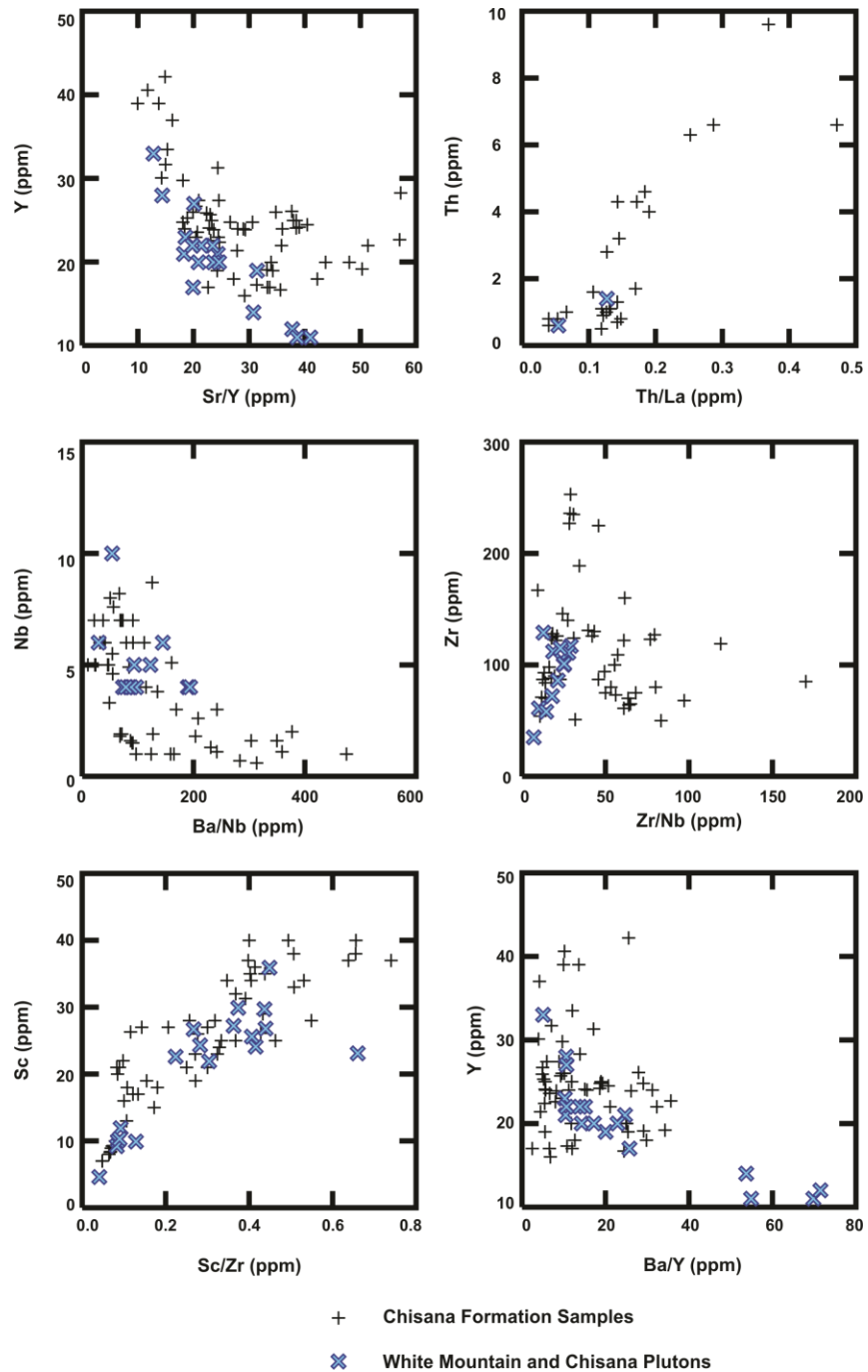


**Figure 4-4: Trace element comparison of Chisana Formation igneous rocks to White Mountain plutons**

Geochemical diagram showing trace element overlap between samples of the Chisana Formation and samples of the White Mountain pluton (Snyder and Hart, 2007).

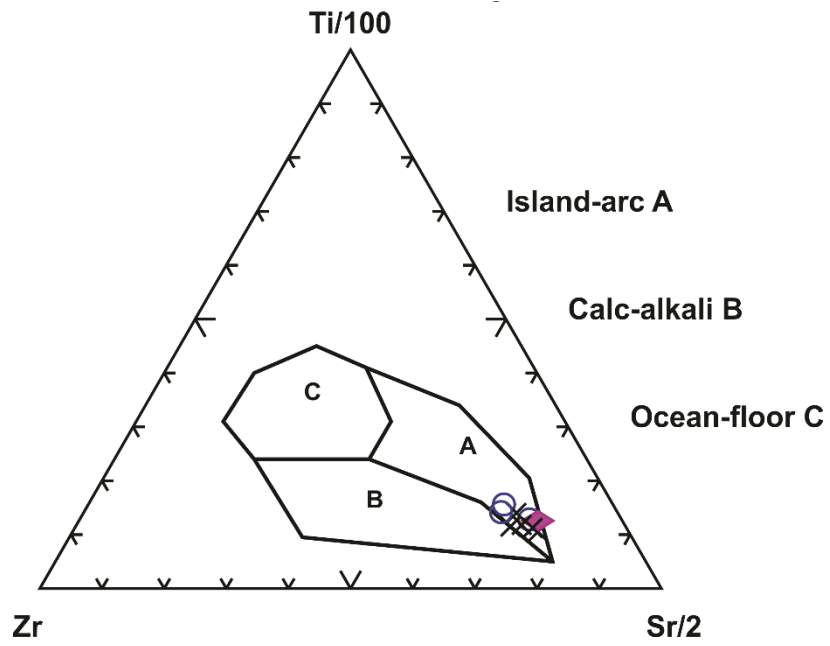


**Figure 4-5 Ternary diagram of tholeiitic basalts from the Chisana Formation.**

Ternary diagram after Pearce and Cann. (1973), showing island-arc affinity for Chisana Formation tholeiitic basalts.

Chisana Formation Volcanics vs. Gravina Volcanic Rocks

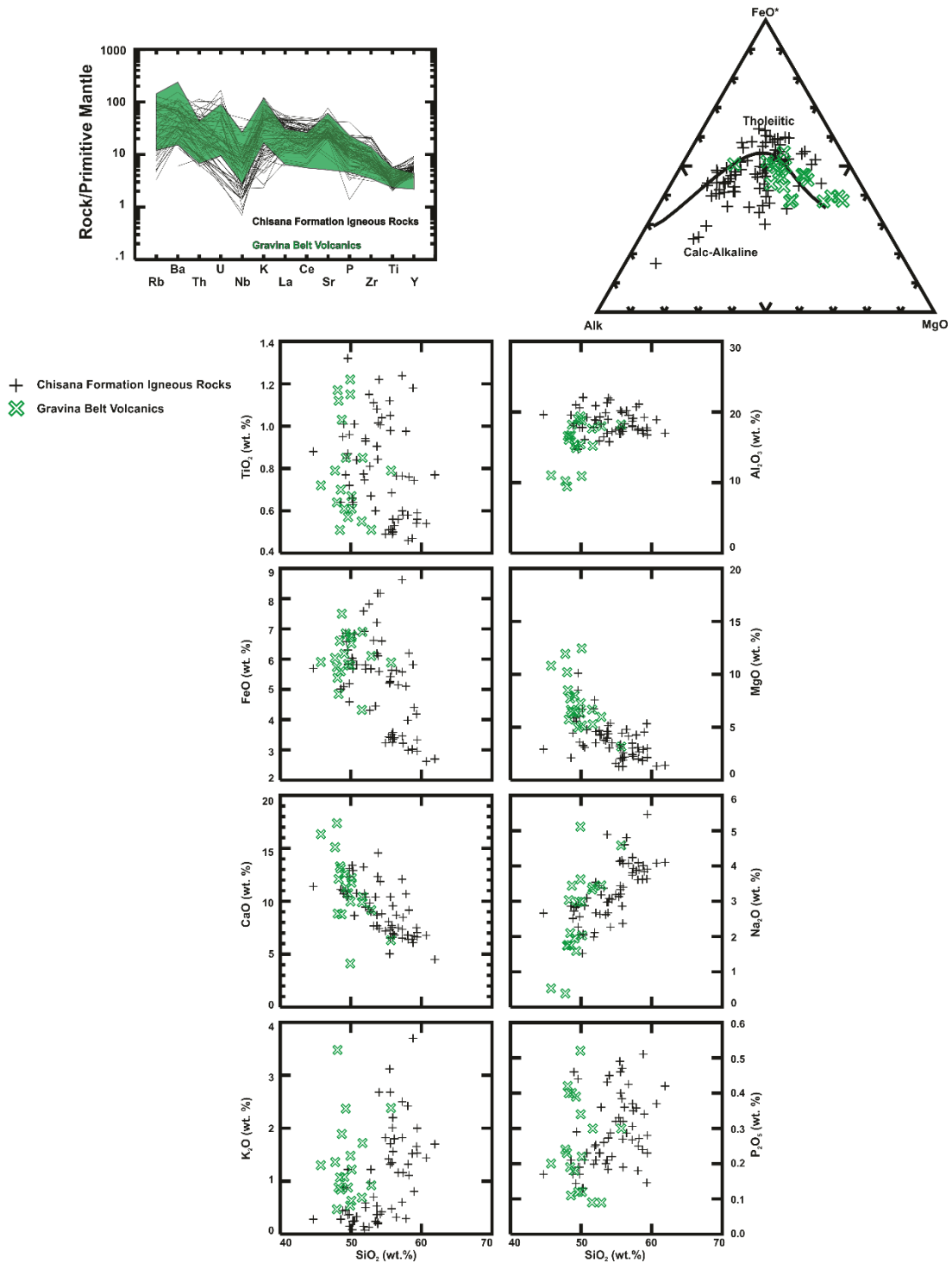


**Figure 4-6: Geochemical comparison of the Chisana Formation to Gravina belt volcanic rocks.**

Multi-element (normalizing values Sun and McDonough, 1989) and Trace element diagrams comparing the Chisana Formation to basalts from the Gravina belt (Rubin and Saleeby, 1991;

McClelland et al., 1992; Stowell et al., 2000). Similarities between the two suggest that both were part of the same arc.



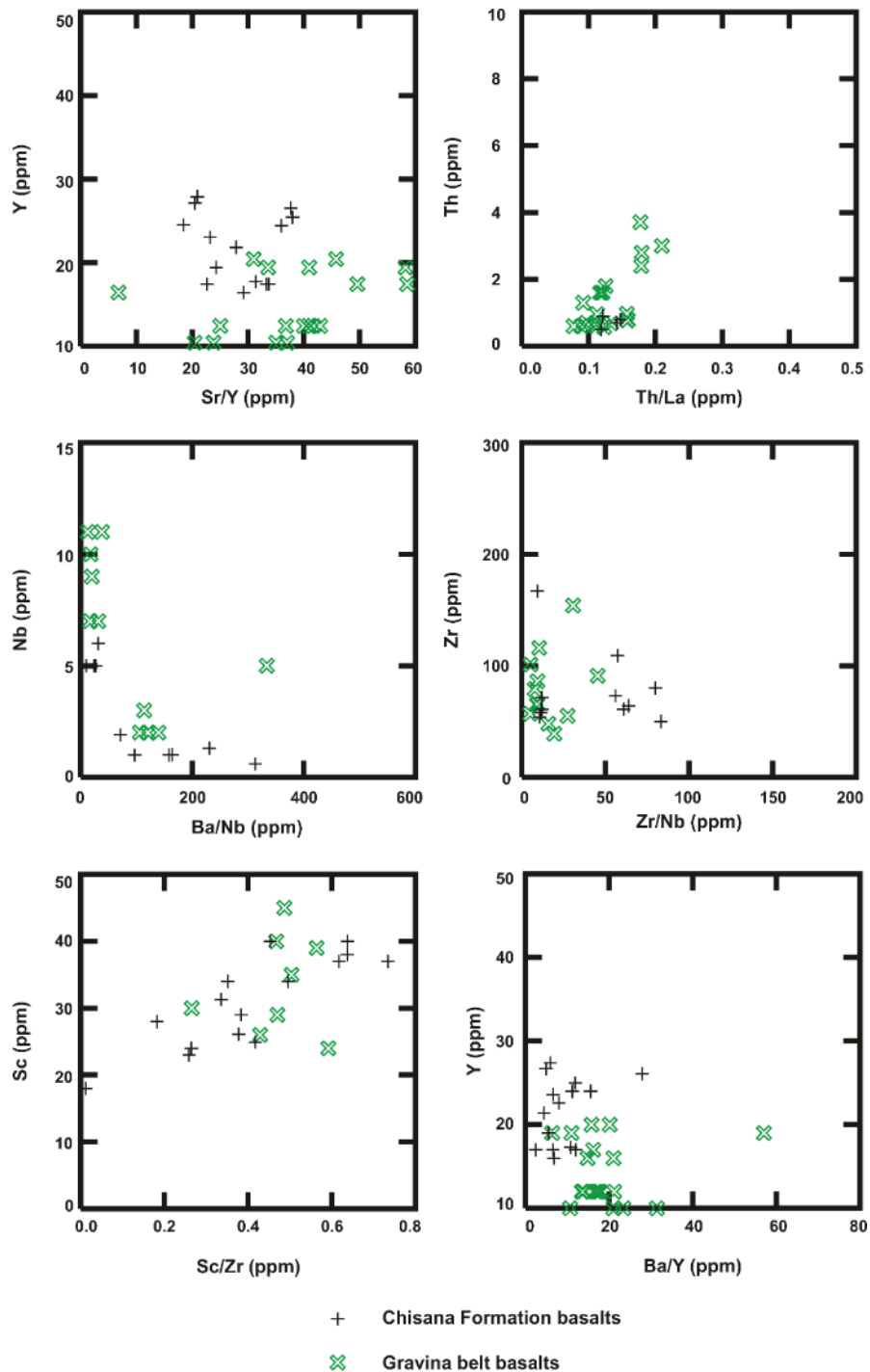


**Figure 4-7: Trace element comparison of Chisana Formation igneous rocks to Gravina metabasalts**

Geochemical diagram showing trace element overlap between igneous rocks from the Chisana Formation and samples of the Gravina belt (Rubin and Saleeby, 1991; McClelland et al., 1992; Stowell et al., 2000).

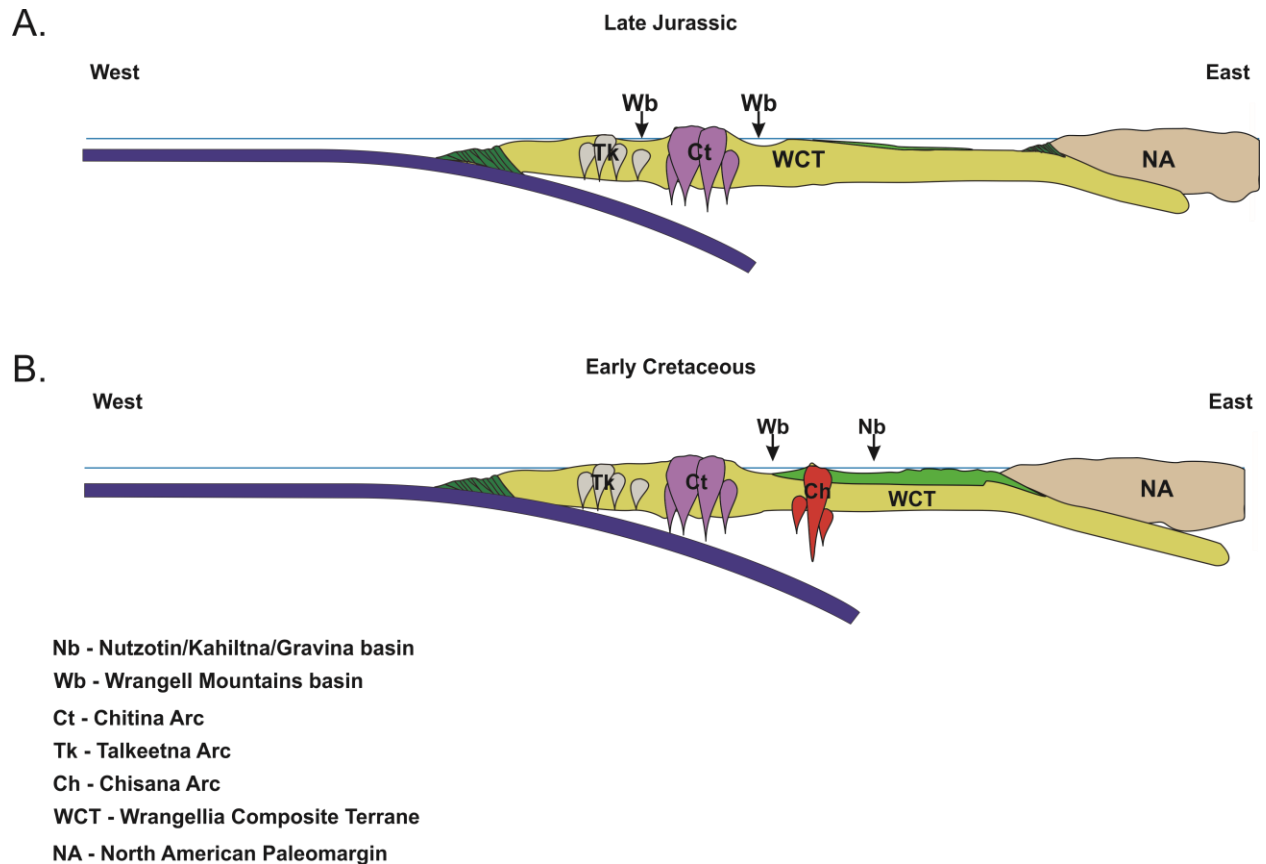


**Figure 4-8: Cartoon depicting favored model of formation for Chisana Formation and Gravina-Nutzotin belt.**

Cartoon showing the formation of the Chisana Formation magmatic arc relative to other Jurassic-Cretaceous arcs as well as the position of forearc and backarc basin deposits. Adapted from Trop and Ridgway (2007).

Chisana Formation Vs. Talkeetna Arc

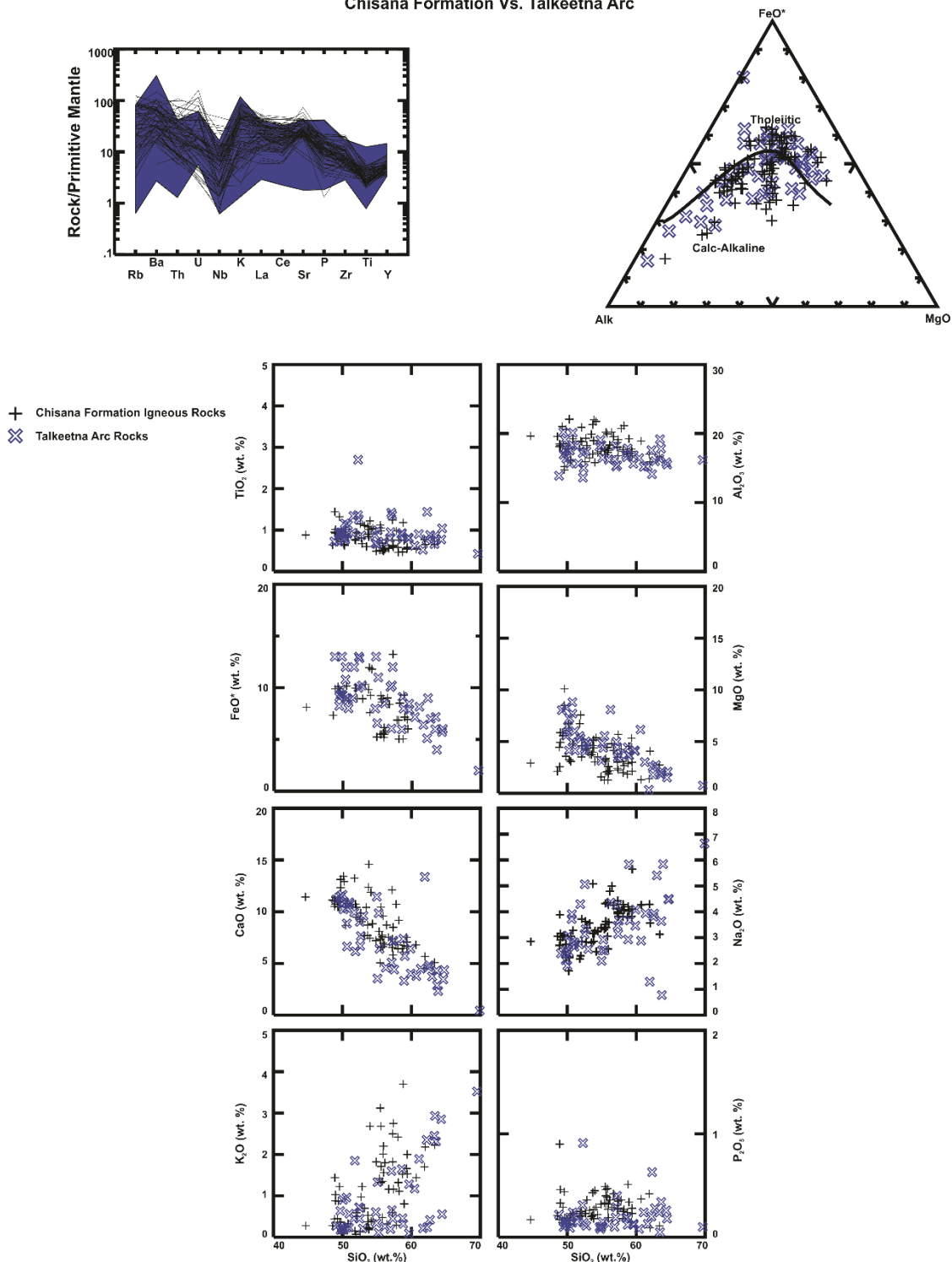


**Figure 4-9: Geochemical comparison of the Chisana Formation to the Talkeetna arc.**

Multi-element (normalizing values Sun and McDonough, 1989) and Trace element diagrams comparing the Chisana Formation to the Talkeetna arc (Clift et al., 2005). Samples from the Chisana Formation overlap with geochemical fields representing the Talkeetna Formation.

Chisana Formation Volcanics vs. Wrangell Igneous Rocks

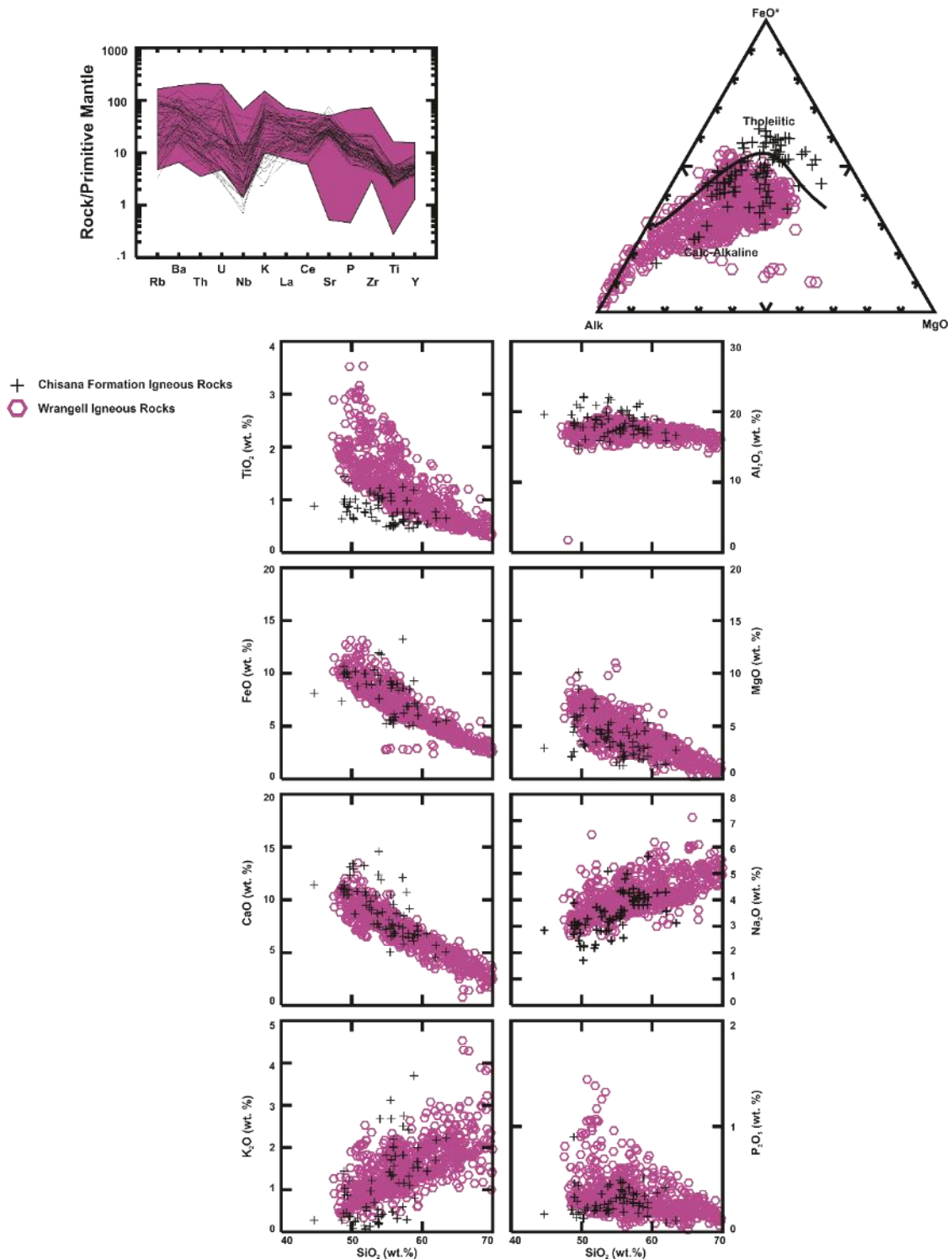


**Figure 4-10: Geochemical Comparison of the Chisana Formation igneous rocks to the Wrangell Arc.**

Multi-element (normalizing values from Sun and McDonough, 1989) and Trace element diagrams comparing the Chisana Formation to representative samples from Wrangell arc (Preece

and Hart, 2004; Trop et al., 2012; Brueseke et al., 2019). Samples from the Wrangell arc are significantly more depleted in Sr, P, and Ti than samples from the Chisana Formation.

Chisana Formation vs. Honshu Arc

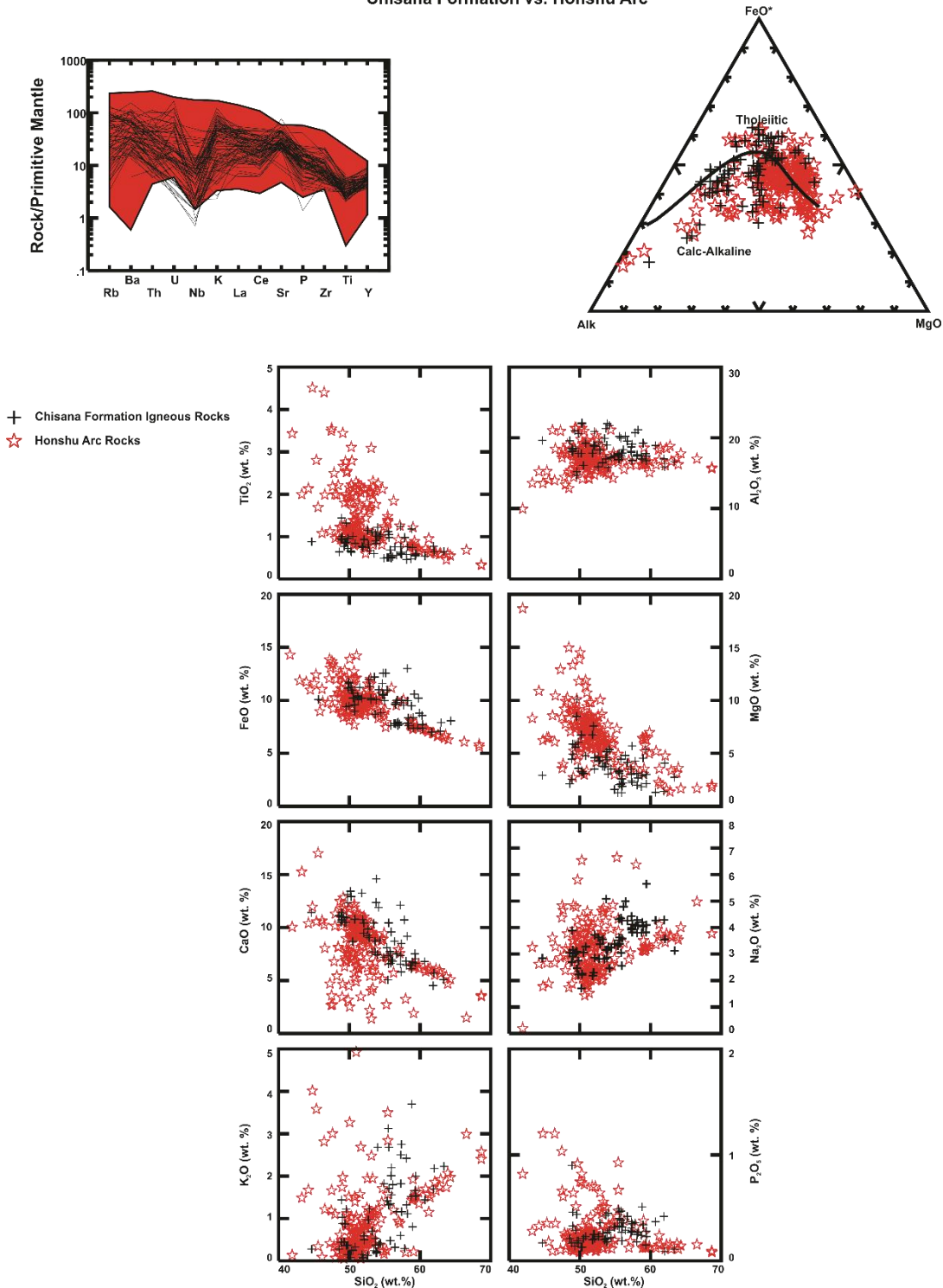


**Figure 4-11: Geochemical comparison of igneous rocks from the Chisana Formation to the modern Honshu arc.**

Multi-element (Sun and McDonough, 1989) and Trace element diagrams comparing the Chisana Formation to representative samples from Honshu arc (Nobuyuki, 1988; Allan et al., 1992; Jones et al., 1993; Morris et al., 2006; Kawabata and Shuto, 2005; Safonova et al., 2015). The Chisana

Formation shows greater enrichments of trace elements, and greater depletion of Nb than the Honshu arc.

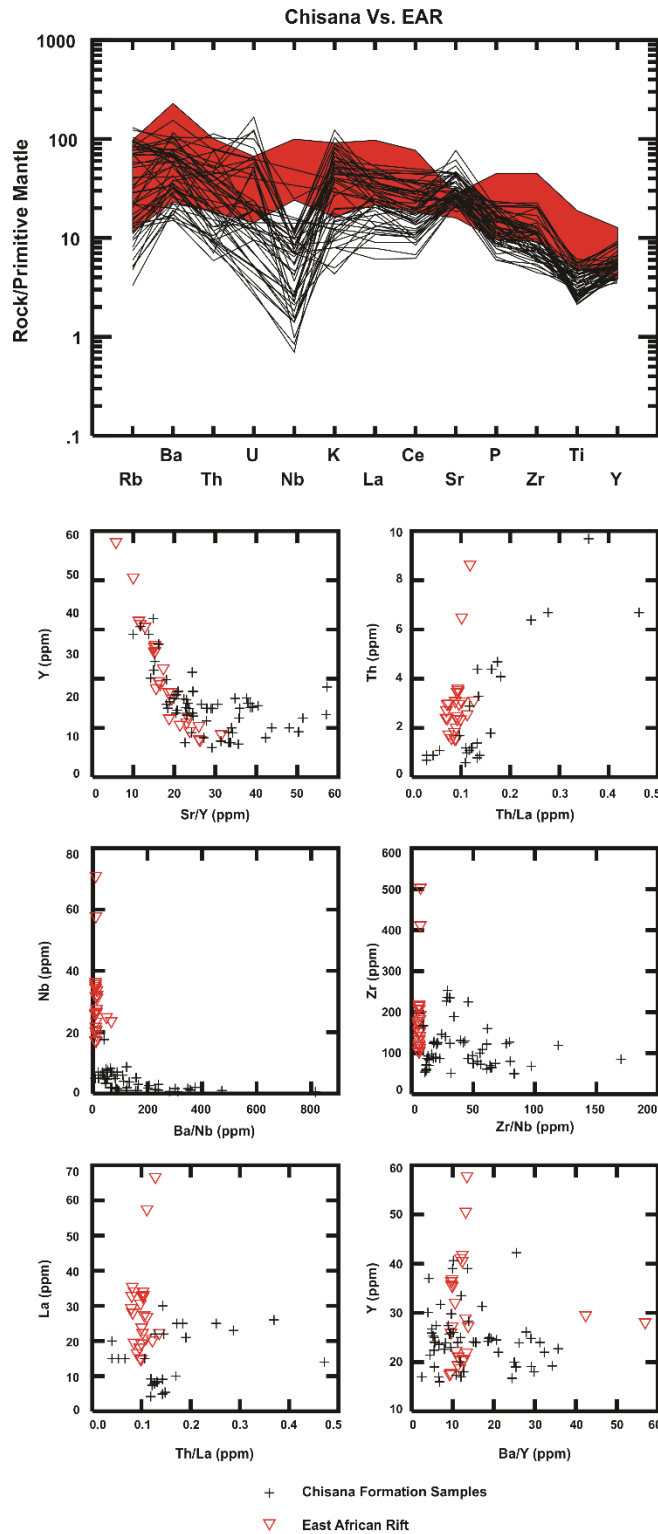


**Figure 4-12: Geochemical comparison of igneous rocks from the Chisana Formation igneous rocks to the East African Rift.**

Trace element diagrams comparing samples from the Chisana Formation to samples from the East African Rift (Giordano et al., 2014).



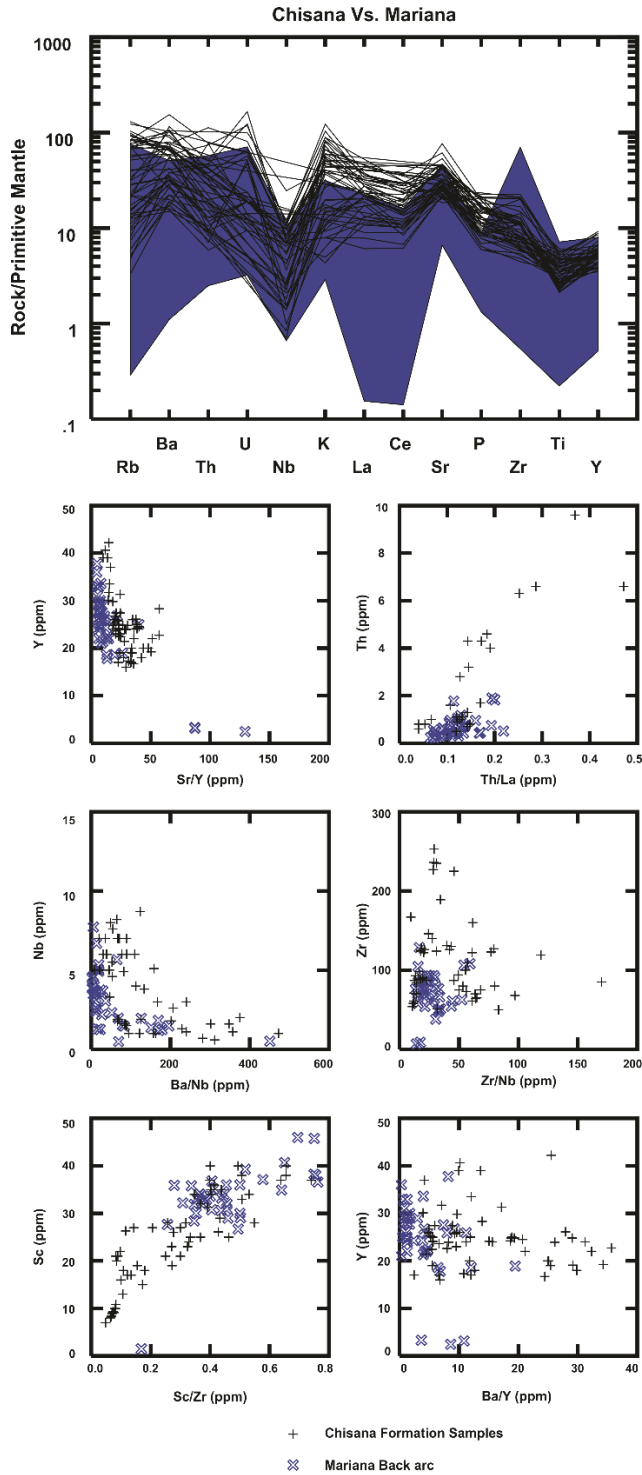


**Figure 4-13: Geochemical Comparison of igneous rocks from the Chisana Formation to samples from the Mariana trough back arc.**

Trace element diagrams comparing samples from the Chisana Formation to samples from the Mariana trough (Hart et al., 1972; Bougault et al., 1982; Stern et al., 1990; Gribble et al., 1998; Newman et al., 2000; Pearce et al., 2005; Straub et al., 2015).

## Chapter 5 - Conclusions

The Chisana Formation is an approximately 2-3 km-thick sequence of Early Cretaceous volcanic and volcanoclastic rocks that are exposed at their type section at Bonanza Creek, in the vicinity of Jacksina Creek, in small outcrops near Beaver Lake, and in other locations near our study areas (Figure 1-2; Figure 1-4). Geochemical data and sedimentary lithofacies comparisons strongly support a subduction-related origin for the Chisana Formation. Furthermore, paleogeographic reconstructions of underlying formations (Manuszak et al., 2007), geochemistry, and reconstructions of the crust through which Chisana Formation volcanic rocks erupted (Greene et al., 2004; Greene, 2010) suggest that the Chisana Formation was an island arc that erupted through significantly overthickened oceanic crust.

Geochemical data presented here can be used to directly correlate to metabasalts exposed in Gravina belt to the south (Rubin and Saleeby, 1991; McClelland et al., 1992; Stowell et al., 2000) and used to verify earlier conclusions that the Chisana Formation in the Nutzotin basin is part of a long-lived Chisana Arc (Plafker and Berg, 1994).

Geochemical similarities between Cretaceous-aged plutons in the Nutzotin Mountains and Chisana Formation igneous rocks are consistent with the hypothesis that these Cretaceous plutons also represent magmatism in the Chisana arc. Data from this study, combined with: [1] accretionary wedge deposits coeval with the Chisana Formation in the Chugach Mountains (Plafker and Berg, 1994); [2] Chisana Formation-aged basinal sediments located in a forearc position relative to the Chisana Magmatic arc (Trop et al., 2002), and [3] Chisana-derived sediments located in a backarc position to the Chisana Formation in the Nutzotin and Kahiltna basins (Trop and Ridgway, 2007; Manuszak et al., 2007) can only reflect an arc origin, with an east-dipping subduction zone under the WCT.

## References

- Abbey, S., 1974, Studies in "Standard Samples" of Silicate Rocks and Minerals: Geological Survey of Canada Papers, p. 1–114, doi: 10.4095/104657.
- Abbott, D., and Mooney, W., 1995, The structural and geochemical evolution of the continental crust: Support for the oceanic plateau model of continental growth: *Reviews of Geophysics*, v. 33, p. 231–242, doi: 10.1029/95rg00551.
- Aleinikoff, J.N., Farmer, G.L., Rye, R.O., and Nokleberg, W.J., 2000, Isotopic evidence for the sources of Cretaceous and Tertiary granitic rocks, east-central Alaska: implications for the tectonic evolution of the Yukon-Tanana Terrane: *Canadian Journal of Earth Sciences*, v. 37, p. 945–956, doi: 10.1139/e00-006.
- Allan, J., and Gorton, M., 1992, Geochemistry of Igneous Rocks from Legs 127 and 128, Sea of Japan: Proceedings of the Ocean Drilling Program, 127/128 Scientific Results Proceedings of the Ocean Drilling Program, doi: 10.2973/odp.proc.sr.127128.208.1992.
- Amato, J.M., Pavlis, T.L., Clift, P.D., Kochelek, E.J., Hecker, J.P., Worthman, C.M., and Day, E.M., 2013, Architecture of the Chugach accretionary complex as revealed by detrital zircon ages and lithologic variations: Evidence for Mesozoic subduction erosion in south-central Alaska: *Geological Society of America Bulletin*, v. 125, p. 1891–1911, doi: 10.1130/b30818.1.
- Barker, F., 1994, Some accreted volcanic rocks of Alaska and their elemental abundances, *in* Plafker, G., and Berg, H. C., eds., *The Geology of Alaska: Boulder, Colorado, Geological Society of America, The Geology of North America*, v. G-1
- Berg, H. C., Jones, D. L., and Richter, D. H., 1972, Gravina-Nutzotin belt; Tectonic significance of an upper Mesozoic sedimentary and volcanic sequence in southern and southeastern Alaska: *U.S. Geological Survey Professional Paper 800-D*, p. D1-D24.
- Beswick, A., and Soucie, G., 1978, A correction procedure for metasomatism in an Archean greenstone belt: *Precambrian Research*, v. 6, p. 235–248, doi: 10.1016/0301-9268(78)90015-3.
- Bougault, H., Maury, R., Azzouzi, M.E., Joron, J.-L., Cotton, J., and Treuil, M., 1982, Tholeiites, Basaltic Andesites, and Andesites from Leg 60 Sites: Geochemistry, Mineralogy, and Low Partition Coefficient Elements: Initial Reports of the Deep Sea Drilling Project, 60 Initial Reports of the Deep Sea Drilling Project, p. 657–677, doi: 10.2973/dsdp.proc.60.135.1982.
- Brueseke, M.E. and Hart, W.K., 2008, Geology and petrology of the mid-Miocene Santa Rosa-Calico volcanic field, northern Nevada. *Nevada Bureau of Mines and Geology Bulletin #113*

- Brueseke, M.E., Benowitz, J.A., Trop, J.M., Davis, K.N., Berkelhammer, S.E., Layer, P.W., and Morter, B.K., 2019, The Alaska Wrangell Arc: ~30 million years of subduction-related magmatism along a still active arc-transform junction: *Terra Nova*, p. 59–66, doi: 10.1111/ter.12369.
- Busby, C., 2004, Continental growth at convergent margins facing large ocean basins: a case study from Mesozoic convergent-margin basins of Baja California, Mexico: *Tectonophysics*, v. 392, p. 241–277, doi: 10.1016/j.tecto.2004.04.017.
- Compton, R.R., 1985, *Geology in the field*: Cape Town, Earthspun Books.
- Draut, A.E., and Clift, P.D., 2006, Sedimentary Processes in Modern and Ancient Oceanic Arc Settings: Evidence from the Jurassic Talkeetna Formation of Alaska and the Mariana and Tonga Arcs, Western Pacific: *Journal of Sedimentary Research*, v. 76, p. 493–514, doi: 10.2110/jsr.2006.044.
- Ferrari, L., Esquivel, T.O., Bryan, S., and Martínez, M.L., 2018, Cenozoic Extension And Magmatism In Western Mexico: Linking The Sierra Madre Occidental Silicic Large Igneous Province And The Comondú Group With The Gulf Of California Rift: *Earth Science Reviews*, v. 183, p. 115–152, doi: 10.1130/abs/2017cd-292843.
- Gehrels, G., Rusmore, M., Woodsworth, G., Crawford, M., Andronicos, C., Hollister, L., Patchett, J., Ducea, M., Butler, R., Klepeis, K., Davidson, C., Friedman, R., Haggart, J., Mahoney, B., et al., 2009, U-Th-Pb geochronology of the Coast Mountains batholith in north-coastal British Columbia: Constraints on age and tectonic evolution: *Geological Society of America Bulletin*, v. 121, p. 1341–1361, doi: 10.1130/b26404.1.
- Giordano, F., Dantonio, M., Civetta, L., Tonarini, S., Orsi, G., Ayalew, D., Yirgu, G., Dellerba, F., Vito, M.D., and Isaia, R., 2014, Genesis and evolution of mafic and felsic magmas at Quaternary volcanoes within the Main Ethiopian Rift: Insights from Gedemsa and Fanta Ale complexes: *Lithos*, v. 188, p. 130–144, doi: 10.1016/j.lithos.2013.08.008.
- Govindaraju, K., 1994, 1994 Compilation Of Working Values And Sample Description For 383 Geostandards: *Geostandards and Geoanalytical Research*, v. 18, p. 1–58, doi: 10.1111/j.1751-908x.1994.tb00526.x.
- Graham, G., Kelley, K., Holm-Denoma, C., Ayuso, R., Kokaly, R., Hoefen, T., & Selby, D., 2016, Geochronology and Nd-Sr-Pb isotopic compositions of Early intrusions and associated porphyry Cu deposits in eastern Alaska. 4858. Abstract 35th International Geological Congress. Capetown, South Africa.
- Greene, A. R., Scoates J. S., Weis D., 2004, Flood basalts of the Wrangellia Terrane, southwest Yukon: Implications for the formation of oceanic plateaus, continental crust and Ni-Cu-PGE mineralization. *Yukon Exploration and Geology 2004*, Yukon Geological Survey, Whitehorse, p. 109-120

- Greene, A., 2010, The architecture of oceanic plateaus revealed by the volcanic stratigraphy of the accreted Wrangellia oceanic plateau: *Geosphere*, v. 6, p. 47–73, doi: 10.1130/ges00212.s1.
- Gribble, R., Stern, R.J., Bloomer, S.H., and O'Hearn, T., 1998, Chemical and Isotopic Composition of Lavas from the Northern Mariana Trough: Implications for Magmagenesis in Back-arc Basins: *Journal of Petrology*, v. 39, p. 125–154, doi: 10.1093/petrology/39.1.125.
- Hampton, B.A., Ridgway, K.D., and Gehrels, G.E., 2010, A detrital record of Mesozoic island arc accretion and exhumation in the North American Cordillera: U-Pb geochronology of the Kahiltna basin, southern Alaska: *Tectonics*, v. 29, doi: 10.1029/2009tc002544.
- Hart, S., Glassley, W., and Karig, D., 1972, Basalts and sea floor spreading behind the Mariana Island arc: *Earth and Planetary Science Letters*, v. 15, p. 12–18, doi: 10.1016/0012-821x(72)90023-4.
- Jahn, B.-M., Wu, F., and Chen, B., 2000, Granitoids of the Central Asian Orogenic Belt and continental growth in the Phanerozoic: Special Paper 350: The Fourth Hutton Symposium on the Origin of Granites and Related Rocks, p. 181–193, doi: 10.1130/0-8137-2350-7.181.
- Jones, G., Sano, H., and Valsami-Jones, E., 1993, Nature and tectonic setting of accreted basalts from the Mino terrane, central Japan: *Journal of the Geological Society*, v. 150, p. 1167–1181, doi: 10.1144/gsjgs.150.6.1167.
- Kalbas, J.L., Ridgway, K.D., and Gehrels, G.E., 2007, Stratigraphy, depositional systems, and provenance of the Lower Cretaceous Kahiltna assemblage, western Alaska Range: Basin development in response to oblique collision: Special Paper 431: Tectonic Growth of a Collisional Continental Margin: *Crustal Evolution of Southern Alaska*, p. 307–343, doi: 10.1130/2007.2431(13).
- Kapp, P.A., and Gehrels, G.E., 1998, Detrital zircon constraints on the tectonic evolution of the Gravina belt, southeastern Alaska: *Canadian Journal of Earth Sciences*, v. 35, p. 253–268, doi: 10.1139/e97-110.
- Katoh, K. S., Danhara, T., Hart, W. K., and WoldeGabriel, G., 1999, Use of Sodium polytungstate solution in the purification of volcanic glass shards for bulk chemical analysis: *Nature and Human Activities* v. 4, p.45-54
- Kawabata, H., and Shuto, K., 2005, Magma mixing recorded in intermediate rocks associated with high-Mg andesites from the Setouchi volcanic belt, Japan: implications for Archean TTG formation: *Journal of Volcanology and Geothermal Research*, v. 140, p. 241–271, doi: 10.1016/j.jvolgeores.2004.08.013.
- Koepp, D.Q., Trop, J.M., Benowitz, J.A., Layer, P.W., Zippi, P.A., and Brueseke, M.E., 2017, Mid-Cretaceous Volcanism And Fluvial Sedimentation In The Alaska Range Suture Zone: Implications For The Accretionary History Of The Wrangellia composite terrane:

- Geological Society of America Abstracts with Programs, doi: 10.1130/abs/2017am-298406.
- Le Maitre, R.W., 1976, The Chemical Variability of some Common Igneous Rocks: *Journal of Petrology*, v. 17, p. 589–598, doi: 10.1093/petrology/17.4.589.
- Lowey, G.W., 2011, Volcaniclastic gravity flow deposits in the Dezadeash Formation (Jura-Cretaceous), Yukon, Canada: Implications regarding the tectonomagmatic evolution of the Chitina arc in the northern Cordillera of North America: *Lithos*, v. 125, p. 86–100, doi: 10.1016/j.lithos.2011.01.014.
- Lowey, G. W., 2017, Comment on “U-Pb and Hf isotope analysis of detrital zircons from Mesozoic strata of the Gravina belt, southeast Alaska” by Yokelson et al. (2015): *Tectonics*, 36. <https://doi.org/10.1002/2017TC004507>
- Lowey, G.W., 2019, Provenance analysis of the Dezadeash Formation (Jurassic–Cretaceous), Yukon, Canada: implications regarding a linkage between the Wrangellia composite terrane and the western margin of Laurasia: *Canadian Journal of Earth Sciences*, v. 56, p. 77–100, doi: 10.1139/cjes-2017-0244.
- Löwe P. C., Richter, D.H., and Schmoll, H.R., 1982, Geologic map of the Nabesna B-5 quadrangle, Alaska: U.S. Geological Survey map.
- Manuszak, J.D., Ridgway, K.D., Trop, J.M., and Gehrels, G.E., 2007, Sedimentary record of the tectonic growth of a collisional continental margin: Upper Jurassic–Lower Cretaceous Nutzotin Mountains sequence, eastern Alaska Range, Alaska: Special Paper 431: *Tectonic Growth of a Collisional Continental Margin: Crustal Evolution of Southern Alaska*, p. 345–377, doi: 10.1130/2007.2431(14).
- McClelland, W.C., Gehrels, G.E., and Saleeby, J.B., 1992, Upper Jurassic-Lower Cretaceous basinal strata along the Cordilleran Margin: Implications for the accretionary history of the Alexander-Wrangellia-Peninsular Terrane: *Tectonics*, v. 11, p. 823–835, doi: 10.1029/92tc00241.
- McClelland, W.C., and Mattinson, J.M., 2000, Cretaceous-Tertiary evolution of the western Coast Mountains, central Southeastern Alaska: Special Paper 343: *Tectonics of the Coast Mountains, Southeastern Alaska and British Columbia*, p. 159–182, doi: 10.1130/0-8137-2343-4.159.
- McDonough, W., and Sun, S.-S., 1995, The composition of the Earth: *Chemical Geology*, v. 120, p. 223–253, doi: 10.1016/0009-2541(94)00140-4.
- Mertzman, S.A., 2000, K-Ar results from the southern Oregon-northern California Cascade Range: *Oregon Geology*, v. 62, p. 99-122
- Mertzman, S.A., 2015, XRF Laboratory: Overview and analytical procedures: <http://www.fandm.edu/earth-environment/laboratory-facilities/instrument-use-and-instructions>. (accessed 4 April 2019)

- Mezger, J.E., Creaser, R.A., Erdmer, P., and Johnston, S.T., 2001, A Cretaceous back-arc basin in the Coast Belt of the northern Canadian Cordillera: evidence from geochemical and neodymium isotope characteristics of the Kluane metamorphic assemblage, southwest Yukon: *Canadian Journal of Earth Sciences*, v. 38, p. 91–103, doi: 10.1139/e00-076.
- Miyashiro, A., 1974, Volcanic rock series in island arcs and active continental margins: *American Journal of Science*, v. 274, p. 321–355, doi: 10.2475/ajs.274.4.321.
- Morris, P.A., and Itaya, T., 1997, The Matsue Formation: Evidence for gross mantle heterogeneity beneath Southwest Japan at 11 Ma: *The Island Arc*, v. 6, p. 337–352, doi: 10.1111/j.1440-1738.1997.tb00044.x.
- Newman, S., Stolper, E., and Stern, R., 2000, H<sub>2</sub>O and CO<sub>2</sub> in magmas from the Mariana arc and back arc systems: *Geochemistry, Geophysics, Geosystems*, v. 1, doi: 10.1029/1999gc000027.
- Nokleberg, W.J., Plafker, G., and Wilson, F.H., 1994, Geology of south-central Alaska, *in* Plafker, G., and Berg, H.C., eds., *The geology of Alaska: Boulder, Colorado, Geological Society of America, Geology of North America*, v. G-1, p. 311-365
- Nokleberg, W.J., 2000, Phanerozoic tectonic evolution of the Circum-North Pacific: Reston, VA, U.S. Geological Survey.
- Pearce, J., and Cann, J., 1973, Tectonic setting of basic volcanic rocks determined using trace element analyses: *Earth and Planetary Science Letters*, v. 19, p. 290–300, doi: 10.1016/0012-821x(73)90129-5.
- Pearce, J.A., 1996, A user's guide to basalt discrimination diagrams: *in* Wyman, D.A., eds., *Trace Element Geochemistry of Volcanic Rocks: Applications for Massive Sulphide Exploration*: vol. 12. Geological Association of Canada Short Course Notes, p. 79-113
- Pearce, J.A., Stern, R.J., Bloomer, S.H., and Fryer, P., 2005, Geochemical mapping of the Mariana arc-basin system: Implications for the nature and distribution of subduction components: *Geochemistry, Geophysics, Geosystems*, v. 6, doi: 10.1029/2004gc000895.
- Pearce, J.A., and Stern, R.J., 2006, Origin of back-arc basin magmas: Trace element and isotope perspectives: *Back-Arc Spreading Systems: Geological, Biological, Chemical, and Physical Interactions Geophysical Monograph Series*, p. 63–86, doi: 10.1029/166gm06
- Plafker, G., and Berg, H.C., 1994, Overview of the geology and tectonic evolution of Alaska, *in* Plafker, G., and Berg, H.C., eds., *The geology of Alaska: Geological Society of America, Geology of North America*, v. G-1, p. 989-1021
- Preece, S.J., and Hart, W.K., 2004, Geochemical variations in the <5 Ma Wrangell Volcanic Field, Alaska: implications for the magmatic and tectonic development of a complex continental arc system: *Tectonophysics*, v. 392, p. 165–191, doi: 10.1016/j.tecto.2004.04.011.

- Profeta, L., Ducea, M.N., Chapman, J.B., Paterson, S.R., Gonzales, S.M.H., Kirsch, M., Petrescu, L., and Decelles, P.G., 2015, Quantifying crustal thickness over time in magmatic arcs: *Scientific Reports*, v. 5, doi: 10.1038/srep17786.
- Richter, D.H., and Jones, D.L., 1976, Geologic map of the Nabesna quadrangle, Alaska: U.S. Geological Survey map.
- Richter, D.H., Lanphere, M.A., and Matson, N.A., 1975, Granitic Plutonism and Metamorphism, Eastern Alaska Range, Alaska: *Geological Society of America Bulletin*, v. 86, p. 819–829, doi: 10.1130/0016-7606(1975)86<819:gpagea>2.0.co;2.
- Rioux, M., Hacker, B., Mattinson, J., Kelemen, P., Blusztajn, J., and Gehrels, G., 2007, Magmatic development of an intra-oceanic arc: High-precision U-Pb zircon and whole-rock isotopic analyses from the accreted Talkeetna arc, south-central Alaska: *Geological Society of America Bulletin*, v. 119, p. 1168–1184, doi: 10.1130/b25964.1.
- Rubin, C.M., and Saleeby, J.B., 1991, The Gravina Sequence: Remnants of a Mid-Mesozoic oceanic arc in southern southeast Alaska: *Journal of Geophysical Research: Solid Earth*, v. 96, p. 14551–14568, doi: 10.1029/91jb00591.
- Sandy, M.R., and Blodgett, R.B., 1996, *Peregrinella* (Brachiopoda; Rynchonellida) from the Early Cretaceous, Wrangellia terrane, Alaska in Copper, P., and Jin, J., eds., *Brachiopods, Proceedings of the Third International Brachiopod Congress: A.A. Balkema/Rotterdam/Brookfield*.239-242.
- Safonova, I., Kojima, S., Nakae, S., Romer, R., Seltmann, R., Sano, H., and Onoue, T., 2015, Oceanic island basalts in accretionary complexes of SW Japan: Tectonic and petrogenetic implications: *Journal of Asian Earth Sciences*, v. 113, p. 508–523, doi: 10.1016/j.jseas.2014.09.015.
- Saunders, A.D., and Tarney, J., 1984, Geochemical characteristics of basaltic volcanism within back-arc basins: *Geological Society, London, Special Publications*, v. 16, p. 59–76, doi: 10.1144/gsl.sp.1984.016.01.05.
- Short, E., Snyder, D.C., Trop, J.M., Hart, W.K., and Layer, P.W., 2005, New Findings on Early Cretaceous volcanism within the allochthonous Wrangellia terrane, south-central Alaska: stratigraphic, geochronologic, and geochemical data from the Chisana Formation, Nutzotin Mountains: *Geological Society of America Abstracts with Programs*, v.37, no.7, p. 81.
- Sigloch, K., and Mihalynuk, M.G., 2013, Intra-oceanic subduction shaped the assembly of Cordilleran North America: *Nature*, v. 496, p. 50–56, doi: 10.1038/nature12019.
- Sigloch, K., and Mihalynuk, M.G., 2017, Mantle and geological evidence for a Late Jurassic–Cretaceous suture spanning North America: *GSA Bulletin*, v. 129, p. 1489–1520, doi: 10.1130/b31529.1.



- Smithies, R.H., Champion, D.C., and Sun, S., 2004, Evidence for Early LREE-enriched Mantle Source Regions: Diverse Magmas from the c. 3{middle dot}0 Ga Mallina Basin, Pilbara Craton, NW Australia: *Journal of Petrology*, v. 45, p. 1515–1537, doi: 10.1093/petrology/egh014.
- Smithies, R.H., Van Kranendonk, M.J., and Champion, D.C., 2007, The Mesoarchean emergence of modern-style subduction: *Gondwana Research*, v. 11, p. 50–68, doi: 10.1016/j.gr.2006.02.001.
- Snyder, D.C., and Hart, W.K., 2007, The White Mountain Granitoid Suite: Isotopic constraints on source reservoirs for Cretaceous magmatism within the Wrangellia Terrane: Special Paper 431: Tectonic Growth of a Collisional Continental Margin: *Crustal Evolution of Southern Alaska*, p. 379–399, doi: 10.1130/2007.2431(15).
- Stern, R.J., Lin, P.-N., Morris, J.D., Jackson, M.C., Fryer, P., Bloomer, S.H., and Ito, E., 1990, Enriched back-arc basin basalts from the northern Mariana Trough: implications for the magmatic evolution of back-arc basins: *Earth and Planetary Science Letters*, v. 100, p. 210–225, doi: 10.1016/0012-821x(90)90186-2.
- Stowell, H., Green, N. L., and Hooper, R. J., 2000, Geochemistry and Tectonic Setting of Basaltic Volcanism, Northern Coast Mountains, Southeastern Alaska, *in* Stowell, H.H., and McClelland, W.C., eds., *Tectonics of the Coast Mountains, Southeastern Alaska and British Columbia*: Boulder, Colorado: Geological Society of America Special Paper 343, p. 235-256.
- Straub, S.M., Woodhead, J.D., and Arculus, R.J., 2015, Temporal Evolution of the Mariana Arc: Mantle Wedge and Subducted Slab Controls Revealed with a Tephra Perspective: *Journal of Petrology*, v. 56, p. 409–439, doi: 10.1093/petrology/egv005.
- Sun, S., and McDonough, W. F., 1989, Chemical and isotopic systematics of oceanic basalts: implications for mantle composition and processes, *in* Saunders, A. D., and Norry, M. J., eds., *Magmatism in the ocean basins: geological Society of London Special Publication 42*, p. 313-345.
- Tetreault, J.L., and Buitter, S.J.H., 2014, Future accreted terranes: a compilation of island arcs, oceanic plateaus, submarine ridges, seamounts, and continental fragments: *Solid Earth Discussions*, v. 6, p. 1451–1521, doi: 10.5194/sed-6-1451-2014.
- Tibaldi A., Pasquarè F., Tormey D., 2009, Volcanism in Reverse and Strike-Slip Fault Settings, *in*, Cloetingh S., Negendank J., eds., *New Frontiers in Integrated Solid Earth Sciences: International Year of Planet Earth*, Springer, Dordrecht, p. 315-348
- Trop, J.M., Ridgway, K.D., Manuszak, J.D., and Layer, P., 2002, Mesozoic sedimentary-basin development on the allochthonous Wrangellia composite terrane, Wrangell Mountains basin, Alaska: A long-term record of terrane migration and arc construction: *Geological Society of America Bulletin*, v. 114, p. 693–717, doi: 10.1130/0016-7606(2002)114<0693:msbdot>2.0.co;2.

- Trop, J.M., Szuch, D.A., Rioux, M., and Blodgett, R.B., 2005, Sedimentology and provenance of the Upper Jurassic Naknek Formation, Talkeetna Mountains, Alaska: Bearings on the accretionary tectonic history of the Wrangellia composite terrane: *Geological Society of America Bulletin*, v. 117, p. 570–588, doi: 10.1130/b25575.1.
- Trop, J.M., and Ridgway, K.D., 2007, Mesozoic and Cenozoic tectonic growth of southern Alaska: A sedimentary basin perspective: *Special Paper 431: Tectonic Growth of a Collisional Continental Margin: Crustal Evolution of Southern Alaska*, p. 55–94, doi: 10.1130/2007.2431(04).
- Trop, J.M., Snyder, D., Hart, W.K., and Idleman, B.D., 2012, Miocene basin development and volcanism along a strike-slip to flat-slab subduction transition: stratigraphy, geochemistry, and geochronology of the central Wrangell volcanic belt, Yakutat-North America collision zone: *Geosphere*, v. 8, p. 805–834.
- Tsuchiya, N., 1988, Distribution and chemical composition of the Middle Miocene Basaltic Rocks in Akita-Yamagata oil fields of northeastern Japan.: *The Journal of the Geological Society of Japan*, v. 94, p. 591–608, doi: 10.5575/geosoc.94.591.
- van der Heyden, P., 1992, A Middle Jurassic to Early Tertiary Andean-Sierran Arc Model for the Coast Belt of British Columbia: *Tectonics*, v. 11, p. 82–97, doi: 10.1029/91tc02183.
- Yokelson, I., Gehrels, G.E., Pecha, M., Giesler, D., White, C., and McClelland, W.C., 2015, U-Pb and Hf isotope analysis of detrital zircons from Mesozoic strata of the Gravina belt, southeast Alaska: *Tectonics*, v. 34, p. 2052–2066, doi: 10.1002/2015tc003955.
- Zhu, D.-C., Wang, Q., Cawood, P.A., Zhao, Z.-D., and Mo, X.-X., 2017, Raising the Gangdese Mountains in southern Tibet: *Journal of Geophysical Research: Solid Earth*, v. 122, p. 214–223, doi: 10.1002/2016jb013508.

## Appendix A - Petrography

All modal percentages are visual estimates.

**Sample ID:** PM18-1                      **Latitude:** 62.11155  
**Rock Type:** Basalt                      **Longitude:** -141.81622

**Thin Section:** This rock consists of approximately 99% groundmass, 1% phenocrysts. Phenocrysts consist of only subhedral plagioclase laths. The groundmass consists of 50% subhedral plagioclase, 40% dark green alteration mineral, 5% anhedral calcite, 3% opaque minerals, and 2% anhedral to subhedral biotite. Phenocryst plagioclase, up to 0.772 mm in length, exhibit varying degrees of alteration, and are partially replaced by calcite. Groundmass plagioclase, cryptocrystalline to 0.2 mm in length, exhibit extensive alteration to calcite, chlorite, and a dark green alteration mineral. Calcite occurs as a replacement mineral, and in veins along with minor quartz and clusters of opaque minerals, probably pyrite.

**Sample ID:** PM18-2                      **Latitude:** 62.11068  
**Rock Type:** Basaltic Andesite **Longitude:** -141.81697

**Thin Section:** This is a seriate glomeroporphyritic basaltic andesite, with glomerocrysts greater than 4mm in size. Glomerocrysts are composed entirely of subhedral to euhedral plagioclase. The rock is approximately 45% glomerocrysts and 55% groundmass. Glomerocryst plagioclase is typically zoned, and exhibit both regular and irregular alteration patterns as well as alteration rims around some crystals. Plagioclase exhibits both normal and oscillatory zoning patterns. Relict glomerocrysts, accounting for approximately 10% of glomerocrysts, are typically composed varying combinations of calcite, chlorite, smectite and minor quartz. Plagioclase in glomerocrysts contain multiple inclusions, including opaque minerals and zircon. The groundmass is composed of approximately 45% euhedral to subhedral opaque minerals, 25% smectite and clay minerals, 25% euhedral to subhedral plagioclase laths, and 5% chlorite and other alteration products. Opaque minerals in the groundmass are evenly distributed throughout the sample, with concentrations around certain glomerocrysts as alteration rims. They occur as individual crystals <0.3 mm in size, and as aggregates of 0.708 mm in length. Groundmass

plagioclase contain numerous opaque mineral inclusions, and exhibit alteration to smectite or other clays and, rarely, calcite. Calcite and zeolites are present as amygdaloidal vesicle fill minerals. Amygdules range in diameter from 0.75mm to less than 0.25mm.

**Sample ID:** PM18-3

**Latitude:** 62.10862

**Rock Type:** Basaltic Andesite

**Longitude:** -141.82146

**Thin Section:** This rock is a seriate, glomeroporphyritic basaltic andesite, with glomerocrysts greater than 4mm in size. Glomerocrysts are composed of plagioclase, orthopyroxene, and clinopyroxene. The rock is approximately 50% glomerocrysts and phenocrysts, and 50% groundmass, not including xenoliths present in this rock. Glomerocrysts and phenocrysts are approximately 95% euhedral to subhedral plagioclase, 3% euhedral to subhedral clinopyroxene, and 2% euhedral orthopyroxene. Groundmass consists of approximately 60% subhedral plagioclase, 38% alteration minerals and clays, 1% subhedral clinopyroxene, and 1% subhedral orthopyroxene. Glomerocryst clinopyroxene is typically large (up to 2.7mm) and euhedral to subhedral. They exhibit less alteration than plagioclase laths, and contain inclusions of opaque minerals, zircon, and plagioclase. Phenocryst clinopyroxene consist of subhedral to euhedral crystals, ranging in size from 0.7mm to 0.06mm. It is also relatively unaltered, and contains inclusions of oxides, plagioclase, and rare zircon. Glomerocryst plagioclase is typically subhedral, and ranges in size from 1.45mm to 0.4mm. Many plagioclase crystals exhibit either normal or oscillatory zoning. Glomerocryst plagioclase contain alteration zones with opaque and clay alteration present. Bow-tie structures are also exhibited. Plagioclase phenocrysts are also subhedral and range in size from 1.2mm to 0.4mm. They are similar to glomerocryst plagioclase, with the same inclusions and alteration patterns. Sieve textures are common. Groundmass plagioclase are subhedral, with sizes ranging from 0.4mm to cryptocrystalline. They also exhibit extensive alteration and are interbedded with clays and other alteration minerals. Calcite is present as a post-eruption vein mineral. Xenoliths in this sample are composed typically of calcite and plagioclase laths and are more extensively altered than the host rock. They have subhedral plagioclase, typically less than 0.5mm in length. They seem to be clasts of previously erupted igneous rocks and clasts of the volcanoclastic pebble conglomerate that is commonly interbedded with Chisana volcanic rocks.

**Sample ID:** PM18-4

**Latitude:** 62.10767

**Rock Type:** Andesite

**Longitude:** -141.82329

**Thin Section:** This rock is an amygdaloidal glomeroporphyritic andesite. This rock consists of 30% glomerocrysts and phenocrysts, 15% amygdaloids, and 55% groundmass. The glomerocrysts and phenocrysts in this rock consist of 90% subhedral plagioclase and 10% subhedral to euhedral chlorite. The groundmass is composed of roughly 5% opaque minerals, 50% plagioclase, and 45% alteration minerals. Glomerocryst and phenocryst plagioclase is extensively altered, showing alteration to calcite and clay minerals, and can be larger than 4mm in length. Chlorite has completely replaced what I assume to be clinopyroxene in this rock, and is typically euhedral to subhedral, with a maximum size of 2mm. Chlorite phenocrysts also contain more opaque mineral inclusions than plagioclase phenocrysts. Groundmass plagioclase is typically subhedral, with a maximum size of 0.3mm. They too are extensively altered, many having been replaced by calcite and clay minerals. Chlorite is also found extensively in the groundmass, possibly replacing clinopyroxene. Amygdules range in diameter from larger than 4mm to less than 0.40mm, and are filled mainly by carbonates, and some zeolite minerals.

**Sample ID:** PM18-5

**Latitude:** 62.10657

**Rock Type:** Trachyandesite

**Longitude:** -141.82689

**Thin Section:** This rock is a trachyandesite porphyry. It consists of approximately 1% subhedral to euhedral phenocrysts and 99% groundmass. Phenocrysts consist of 99% euhedral to subhedral clinopyroxene, and 1% subhedral plagioclase. Clinopyroxene phenocrysts are largely unaltered and have a maximum size of mm. Plagioclase phenocrysts have a maximum size of >4mm. They have been extensively replaced by clay minerals, and exhibit sieve textures. The groundmass of this rock is approximately 35% subhedral plagioclase laths, and 45% alteration minerals, 10% opaque minerals, and 10% subhedral pyroxene phenocrysts. Plagioclase laths in the groundmass are less than 0.25 mm in length, however, the extensive alteration present makes determining their original sizes difficult. Three different alteration minerals are present throughout the sample. There is an olive-green mineral with low interference colors that may be chlorite or

serpentine. Calcite is present in very low (<1%) abundance as subhedral crystals in parts of the slide. Kaolinite is present throughout, especially in plagioclase laths, as the primary plagioclase alteration mineral. Opaque minerals are typically euhedral, equant in shape, and are less than 0.1mm in diameter. Groups of opaque minerals can grow up to 0.875mm. Pyroxene crystals are typically less than 0.125mm in diameter and are euhedral to subhedral. Pyroxene crystals in both the groundmass and phenocrysts show very little, if any, alteration.

**Sample ID:** PM18-8

**Latitude:** 62.08989

**Rock Type:** Andesite

**Longitude:** -141.85278

**Thin Section:** This sample is an andesite that has been completely replaced by secondary alteration. There are relict crystals of what appear to have been plagioclase that have been entirely replaced by calcite, quartz, and kaolinite. Relict pyroxenes have been replaced by chlorite, kaolinite and quartz.

**Sample ID:** PM18-9

**Latitude:** 62.08965

**Rock Type:** Basalt

**Longitude:** -141.85352

**Thin Section:** This sample is a seriate porphyritic basalt. It is approximately 60% phenocrysts and 40% groundmass. Phenocrysts are comprised of approximately 55% subhedral to euhedral plagioclase, 40% subhedral to euhedral pyroxene, and 5% relict olivine. Phenocryst plagioclase exhibit zoning, with sieve alteration textures present in certain zones of the mineral. Some plagioclase display alteration rims of opaque minerals. Plagioclase laths frequently show kaolinite alteration, and some have chlorite alteration present as well. Pyroxene phenocrysts are subhedral to euhedral, with a max size of >4mm. Pyroxene is present as both individual phenocrysts and as glomerocrysts. Many pyroxenes exhibit simple twins. Pyroxene phenocrysts contain numerous inclusions, including clay minerals, opaque minerals, and chlorite. Relict olivine are typically euhedral to subhedral, with a maximum size of 1.525 mm. Olivine phenocrysts have been entirely replaced by opaque minerals, iddingsite, chlorite, and other clay minerals. The groundmass of this rock is composed of 60% plagioclase laths, 20% alteration minerals, 10% opaque minerals, and pyroxene crystals. Groundmass plagioclase is typically

subhedral and range in size from cryptocrystalline to less than 0.5 mm in length. Groundmass plagioclase also shows some zoning. Groundmass opaque minerals are typically subhedral to euhedral and are concentrated around the rims of groundmass pyroxene and phenocryst olivine. Groundmass clinopyroxene are typically subhedral, showing pseudo-hexagonal sections, and typically are extensively replaced by opaque minerals.

**Sample ID:** PM18-10

**Latitude:** 62.08912

**Rock Type:** Basaltic Andesite

**Longitude:** -141.85454

**Thin Section:** This sample is an extensively altered basaltic andesite porphyry. This sample contains approximately 60% phenocrysts and 40% groundmass. Phenocrysts consist of approximately 70% plagioclase, and 30% alteration and relict minerals. Phenocryst plagioclase is typically subhedral, with a maximum size of more than 4mm in one glomerocryst. Phenocryst plagioclase typically shows extensive alteration to clay minerals, and rarely to chlorite. Phenocryst relict minerals include pyroxenes that have been replaced by chlorite, and olivines that have been replaced by quartz, calcite, and iddingsite. These relict minerals are typically subhedral, with pyroxene relicts up to 1.375 mm in length, and olivine relicts up to 1.5 mm. Phenocryst alteration minerals include anhedral serpentine, calcite and quartz up to 4 mm in length. The groundmass of this sample is approximately 10% plagioclase, 30% alteration minerals, and 60% opaque minerals. Groundmass plagioclase is subhedral and is typically extensively altered. Alteration minerals in the groundmass are typically clay minerals, or chlorite intergrown with quartz. Groundmass opaque minerals are subhedral, with square to rounded cross sections, and individual crystals less than 0.125mm in diameter. In part of this rock, the groundmass has been completely filled with hematite.

**Sample ID:** PM18-12

**Latitude:** 62.08833

**Rock Type:** Andesite

**Longitude:** -141.85738

**Thin Section:** This sample is an extensively altered andesite. This sample consists entirely of clay minerals, chlorite, calcite, and quartz. There are relict plagioclase laths present, that have been completely replaced by clay minerals.

**Sample ID:** PM18-13

**Latitude:** 62.08754

**Rock Type:** Basaltic Andesite

**Longitude:** -141.86189

**Thin Section:** This sample is a porphyritic basaltic andesite. It is approximately 20% phenocrysts, and 80% groundmass. The phenocrysts are composed of approximately 96% plagioclase relics, 2% calcite, 1% epidote, and 1% clasts. Plagioclase relict phenocrysts up to 1.750 mm in length are present. These plagioclase relics are replaced by calcite, sericite, and kaolinite. Calcite phenocrysts are anhedral and can be up longer than 4 mm. Epidote phenocrysts are typically subhedral and up to 1mm in length. They have many inclusions of clay minerals, and some exhibit simple twinning. The groundmass of this rock has been completely replaced by kaolinite, chlorite, quartz, calcite, and opaque minerals. Calcite, quartz, chlorite and kaolinite are typically massive. Opaque minerals are typically euhedral to subhedral and equant, with larger crystals growing up to 0.375mm in diameter.

**Sample ID:** PM18-15

**Latitude:** 62.11954

**Rock Type:** Diorite

**Longitude:** -141.93036

**Thin Section:** This sample is a diorite, composed of roughly 55% plagioclase laths, and 45% alteration minerals. Plagioclase laths are euhedral to subhedral, lath shaped, and grow up to >4mm in length. Some plagioclase laths exhibit zoning, and some show preferential alteration confined to certain zones. All plagioclase minerals show some alteration to kaolinite and sericite, some show additional alteration to epidote, calcite, or zeolites. Small (<1mm) apatite crystals are also present as euhedral prisms. Alteration minerals are typically serpentine, chlorite, epidote, and opaque minerals.

**Sample ID:** PM18-17

**Latitude:** 62.3453

**Rock Type:** Basaltic Andesite

**Longitude:** -143.08243

**Thin Section:** This rock is a porphyritic basaltic andesite. It is composed of roughly 80% phenocrysts and 20% groundmass. Phenocrysts are composed of approximately 10% euhedral to



subhedral clinopyroxene, and 90% subhedral to anhedral plagioclase relicts. Clinopyroxene phenocrysts are typically zoned, and some exhibit twins. Clinopyroxene phenocrysts can be found up to 2.45mm in length. Plagioclase relicts have a maximum clast size of larger than 3mm. Plagioclase relicts have been replaced by clay minerals, zeolites, serpentine and opaque minerals. The groundmass of this rock consists of approximately 5% plagioclase relicts, 94% alteration minerals, and 1% clinopyroxene. Groundmass plagioclase and clinopyroxene are very similar to phenocryst plagioclase and clinopyroxene. Alteration minerals in the groundmass include oxides, serpentine, kaolinite, sericite, calcite and zeolites. This sample was gathered from an autobrecciated lava flow and contains multiple clasts of similar lavas.

**Sample ID:** PM18-18

**Latitude:** 62.346115

**Rock Type:** Andesite

**Longitude:** -143.07751

**Thin Section:** This sample is a porphyritic andesite, containing approximately 20% phenocrysts and 80% groundmass. Phenocrysts range in size from more than 2.5mm to 0.625mm. They consist of approximately 60% subhedral plagioclase laths, 20% relict amphiboles, 5% quartz, and 5% pyroxene phenocrysts. Plagioclase is subhedral, ranging in size from less than 0.625mm to greater than 2.5mm, and exhibits zoning in places. Plagioclase laths show extensive alteration to sericite and kaolinite. Amphibole relicts range from 0.625mm to greater than 2.5mm. They have been replaced by chlorite, and opaque minerals. Quartz is present as a vesicle-fill mineral and is typically rimmed by a fibrous mineral, possibly epidote, or vesuvianite. Pyroxene glomerocrysts range from 2mm to less than 0.625mm. Pyroxene phenocrysts are euhedral to subhedral and range in size from larger than 3mm to less than 0.625mm. Pyroxene phenocrysts are typically zoned and exhibit alteration to serpentine and clay minerals, possibly kaolinite or sericite. A large xenocryst, approximately 24mm in length, is present in the sample. The xenocryst is comprised of approximately 75% plagioclase laths, 5% relict amphibole and 20% alteration minerals. Plagioclase laths grow to over 4mm in length. Plagioclase show extensive alteration to sericite and kaolinite. Amphibole relicts are composed of serpentine and opaque minerals, and exhibit amphibole-like shapes.

**Sample ID:** PM18-19

**Latitude:** 62.33818

**Rock Type:** Basalt

**Longitude:** -143.04895

**Thin Section:** This sample is a seriate porphyritic basalt containing roughly 75% phenocrysts and 25% groundmass. Phenocrysts are composed of 80% plagioclase, 15% clinopyroxene, and 5% amphibole. Plagioclase phenocrysts are euhedral to subhedral, and lath like in shape. They range in size from 2.75mm to cryptocrystalline. Multiple phenocrysts show zoning and alteration to sericite. Clinopyroxene phenocrysts range in size from larger than 3mm to cryptocrystalline, and from euhedral to anhedral. Clinopyroxene phenocrysts contain numerous inclusions of opaque minerals and plagioclase. Many phenocrysts exhibit zoning textures and simple twinning. Amphibole occurs as two phenocrysts larger than 3mm in size. They are anhedral, and exhibit both twinning and a reaction rim of opaque minerals. Alteration is present as abundant replacement of the groundmass by chlorite. Calcite and quartz are also present as alteration products.

**Sample ID:** PM18-20

**Latitude:** 62.343437

**Rock Type:** Basaltic Andesite

**Longitude:** -143.023676

**Thin Section:** This is a phaneritic, porphyritic basalt. This sample consists of approximately 85% groundmass and 15% phenocrysts. The phenocryst assemblage consists of approximately 15% clinopyroxene, 85% alteration minerals. Clinopyroxene phenocrysts have a maximum clast size of greater than 3mm. They are typically are euhedral and occur in glomerocrysts. Pyroxenes are commonly zoned, and contain inclusions of opaque minerals, clays, apatite, serpentine, and epidote. Alteration mineral phenocrysts are composed of zeolites, clay minerals, epidote, serpentine, chlorite, epidote, calcite and apatite. Groundmass is completely altered to clay minerals and zeolites.

**Sample ID:** PM18-21

**Latitude:** 62.33508

**Rock Type:** Basaltic Andesite

**Longitude:** -143.07706

**Thin Section:** This rock is a porphyritic basaltic andesite, composed of approximately 70% groundmass and 30% phenocrysts. Phenocrysts consist of approximately 90% relict plagioclase

minerals, 9% pyroxene phenocrysts, and 1% calcite phenocryst. Plagioclase relicts are subhedral to euhedral and are replaced by sericite. Phenocrysts of plagioclase have a maximum size of 2.75mm. Clinopyroxene phenocrysts have a max size of approximately 2.5mm and are zoned. Phenocrysts contain numerous inclusions of apatite, sericite, serpentine and opaque minerals. The calcite phenocryst is anhedral and appears to be an amygdule. The groundmass of this sample has been completely altered to fine clays, serpentine, and epidote.

**Sample ID:** PM18-22

**Latitude:** 62.3255

**Rock Type:** Basalt

**Longitude:** -143.067

**Thin Section:** This sample is a seriate porphyritic basalt containing roughly 85% phenocrysts and 15% groundmass. Phenocrysts consist of about 75% plagioclase, 20% relict olivine and 5% clinopyroxene. Plagioclase laths range in size from 2.25mm to less than 0.625mm in length. Plagioclase laths are euhedral to subhedral, showing alteration to sericite, kaolinite, and zeolite minerals. Plagioclase phenocrysts exhibit zoned textures. Serpentine, iddingsite and opaque minerals have completely replaced olivine crystals. These relict crystals grow up to 1.625mm in length. They are euhedral to subhedral and exhibit reaction rims of opaque minerals. Clinopyroxene glomerocrysts range from 2 to 1.25mm in size. They are euhedral to subhedral and exhibit zoning textures. The groundmass is composed of 40% plagioclase, 30% opaque minerals, and 30% alteration minerals, including zeolites, quartz, sericite, and kaolinite. Groundmass plagioclase ranges in size from cryptocrystalline to greater than 0.625mm. Plagioclase laths are euhedral to subhedral, and typically contain numerous inclusions of zeolites, quartz and opaque minerals. Opaque minerals are round, and typically subhedral to euhedral.

**Sample ID:** PM18-23

**Latitude:** 62.32255

**Rock Type:** Basalt

**Longitude:** -143.0672

**Thin Section:** This sample is a glomeroporphyritic, pilotaxitic basalt, composed of approximately 90% phenocrysts and 10% groundmass. Phenocrysts consist entirely of plagioclase laths, and the groundmass consists of 90% plagioclase, and 9% alteration minerals,

and less than 1% pyroxene minerals. Plagioclase phenocrysts range in size from larger than 4mm to 0.5mm. Phenocrysts are typically euhedral to subhedral and consist of both individual phenocrysts and glomerocrysts. Plagioclase phenocrysts exhibit zoning textures with alteration to opaque minerals, zeolites, and clays. Some phenocrysts exhibit reaction rims consisting of opaque minerals located in certain zones of zoned plagioclase. Groundmass plagioclase ranges in size from cryptocrystalline to 0.375mm in length. They are typically euhedral to subhedral, and exhibit sericite alteration. Groundmass alteration consists of serpentine, opaque minerals, iddingsite, and possibly zeolite minerals. Clinopyroxene minerals range from 0.45mm to 0.0375mm.

**Sample ID:** Jacksina-01

**Latitude:**

**Rock Type:** Andesite

**Longitude:**

**Thin Section:** This porphyritic andesite is composed of approximately 50% phenocrysts and 50% groundmass. Phenocrysts are approximately 80% subhedral plagioclase, 15% euhedral to subhedral amphibole, and 5% subhedral clinopyroxene. Plagioclase is extensively altered by sericite and has a max size of approximately 0.77mm. Plagioclase is typically lath shaped. Amphibole has a maximum size of approximately 1mm and is typically lath or rhomb shaped. Amphibole phenocrysts are locally zoned, with many displaying alteration rims and inclusions of opaque minerals. Clinopyroxene phenocrysts have a maximum size of approximately 0.875mm. They exhibit simple twinning and are zoned. The groundmass is almost completely composed of secondary minerals. These include Sericite, opaque minerals, serpentine, epidote, chlorite, and zeolites.

**Sample ID:** Jacksina-02

**Latitude:**

**Rock Type:** Basaltic Andesite

**Longitude:**

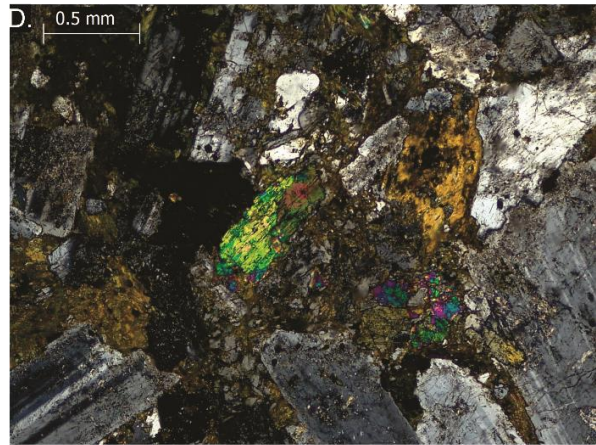
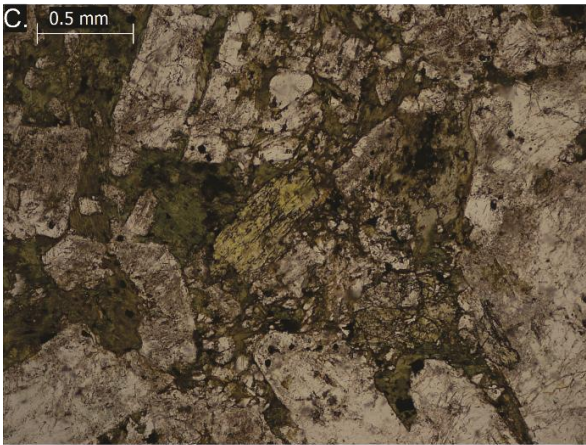
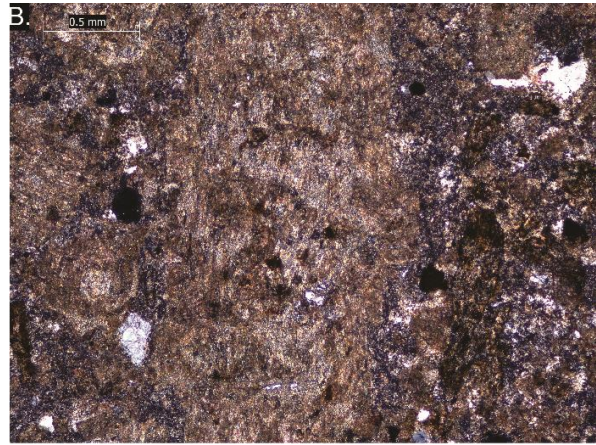
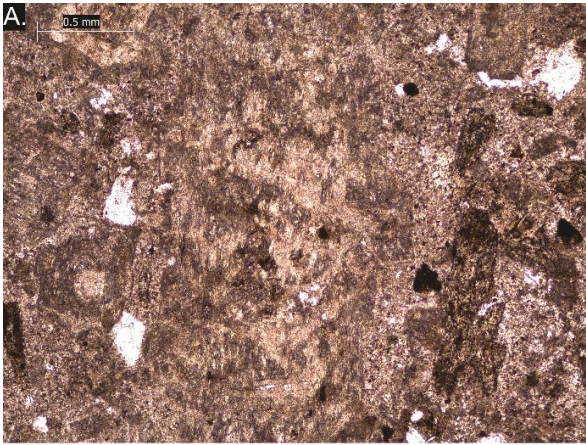
**Thin Section:** This sample is a porphyritic basaltic andesite and consists of approximately 80% phenocrysts and 20% groundmass. Phenocrysts are composed of 85% plagioclase, 10% clinopyroxene, and 5% amphibole. Plagioclase phenocrysts are typically euhedral to subhedral and have a maximum clast size of approximately 1.87mm in length. Plagioclase laths are

extensively altered, with 80-100% of the phenocryst being composed of sericite or kaolinite. Clinopyroxene phenocrysts are typically euhedral, with few subhedral phenocrysts, and have a maximum size of 1.75mm. Clinopyroxene phenocrysts exhibit simple twinning and oscillatory zonation. Amphibole phenocrysts are typically subhedral and have a maximum size of greater than 4.55mm. Amphibole phenocrysts typically display an alteration rim of opaque minerals, and some form around phenocrysts of clinopyroxene. The groundmass of this sample is composed entirely of secondary minerals such as kaolinite, sericite, opaque minerals, chlorite, and small amounts of epidote.



## Appendix B - Alteration Photomicrographs

Representative photomicrographs of kaolinite and sericite alteration (A-PPL, B-XPL; CHI-1066; 4x), epidote, sericite alteration (C-PPL, D-XPL; PM18-15; 4x), and chlorite alteration (E-PPL, F-XPL; PM18-4; 4x)



## Appendix C - Geochemical Analyses

New geochemical data presented from this study that passed the alteration filter (labeled PM18-# and Jacksina-#, and JT#) analyzed by XRF, and unpublished data from Short et al. (2005) (labeled CHI-#) analyzed by DCP-AES.

Sample ID	PM18-2	PM18-3	PM18-4	PM18-5	PM18-8	PM18-9	PM18-10	PM18-12	PM18-13
Rock Unit/Location	Low Bonanza	Low Bonanza	Bonanza Dike	Bonanza Dike	Upper Bonanza	Upper Bonanza	Upper Bonanza	Upper Bonanza	Upper Bonanza
<b>SiO<sub>2</sub></b>	52.84	49.40	53.35	55.34	53.64	49.56	49.79	51.34	53.17
<b>TiO<sub>2</sub></b>	0.93	0.93	0.90	1.11	0.70	0.74	0.78	1.11	0.72
<b>Al<sub>2</sub>O<sub>3</sub></b>	19.17	20.16	19.11	15.98	19.45	17.04	17.54	16.21	19.03
<b>Fe<sub>2</sub>O<sub>3</sub>*</b>	9.08	9.13	8.10	10.78	10.09	11.53	12.26	13.16	9.41
<b>MnO</b>	0.11	0.12	0.08	0.21	0.18	0.16	0.18	0.28	0.20
<b>MgO</b>	2.95	4.02	3.93	2.71	2.46	6.44	4.76	3.13	4.51
<b>CaO</b>	9.89	13.35	9.87	5.72	8.43	12.65	11.41	10.83	8.18
<b>Na<sub>2</sub>O</b>	3.04	2.73	3.57	3.77	3.58	1.90	2.47	3.35	4.52
<b>K<sub>2</sub>O</b>	1.62	0.20	0.27	3.48	1.02	0.14	0.18	0.54	0.30
<b>P<sub>2</sub>O<sub>5</sub></b>	0.38	0.25	0.33	0.48	0.25	0.19	0.17	0.24	0.27
<b>Total</b>	100.01	100.29	99.51	99.58	99.80	100.35	99.54	100.19	100.31
<b>LOI</b>	5	8.6	7.26	5.5	7.69	4.69	7.04	10.52	6.12
<b>Rb</b>	26.0	<0.5	3.8	58.2	18.4	<0.5	3.2	8.4	8.7
<b>Sr</b>	540	579	600	537	591	478	550	430	701
<b>Y</b>	29.8	25.9	37.0	39.0	25.7	25.3	24.1	30.1	23.9
<b>Zr</b>	189	87	131	236	94	75	80	100	68
<b>V</b>	276	342	234	267	220	308	269	425	255
<b>Ni</b>	13	22	35	4	12	48	40	6	12
<b>Cr</b>	43	36	81	12	27	59	79	10	19
<b>Nb</b>	5.5	1.9	3.3	8.2	1.9	1.5	1.5	1.8	0.7
<b>Ga</b>	19.9	18.2	17.3	18.8	17.1	15.5	15.4	15.3	17.6
<b>Cu</b>	216	111	125	244	62	51	69	63	18
<b>Zn</b>	95	82	92	108	94	76	84	116	100
<b>Co</b>	39	18	27	38	23	23	12	34	26
<b>Ba</b>	288	126	155	531	238	132	134	119	197
<b>La</b>	21	15	15	26	15	13	12	14	15
<b>Ce</b>	42	21	30	41	26	26	15	24	25
<b>U</b>	2.6	<0.5	<0.5	1.7	<0.5	1.8	<0.5	<0.5	1.1
<b>Th</b>	4.0	<0.5	1.6	9.6	0.8	<0.5	<0.5	6.6	0.6
<b>Sc</b>	27	36	27	20	26	38	35	40	25
<b>Pb</b>	<1	<1	<1	6	<1	<1	<1	<1	<1

Sample ID	PM18-15	PM18-17	PM18-18	PM18-19	PM18-20	PM18-21	PM18-22	PM18-23	Jacksina-01
Rock Unit/Location	Pluton	Jacksina	Jacksina	Jacksina Dike	Jacksina Dike	Jacksina Dike	Jacksina	Jacksina	Jacksina Dike
<b>SiO<sub>2</sub></b>	56.17	49.03	56.99	50.16	54.75	51.06	48.01	51.43	57.12
<b>TiO<sub>2</sub></b>	0.75	0.91	0.52	0.72	0.54	0.86	0.75	0.93	0.72
<b>Al<sub>2</sub>O<sub>3</sub></b>	17.58	19.66	17.05	18.27	18.85	20.25	20.47	20.63	18.63
<b>Fe<sub>2</sub>O<sub>3</sub>*</b>	9.38	11.84	7.39	10.67	8.99	10.36	10.91	9.83	7.69
<b>MnO</b>	0.19	0.18	0.17	0.19	0.18	0.18	0.16	0.20	0.12
<b>MgO</b>	2.95	4.85	5.12	7.31	4.00	4.38	5.71	3.47	4.39
<b>CaO</b>	6.39	10.73	7.20	10.35	7.23	7.30	10.70	9.33	6.51
<b>Na<sub>2</sub>O</b>	3.73	2.05	3.49	2.04	3.93	4.65	2.76	3.49	3.72
<b>K<sub>2</sub>O</b>	2.45	0.34	1.59	0.07	1.12	0.35	0.44	0.58	0.78
<b>P<sub>2</sub>O<sub>5</sub></b>	0.30	0.26	0.14	0.24	0.41	0.41	0.14	0.25	0.33
<b>Total</b>	99.89	99.85	99.66	100.02	100.00	99.80	100.05	100.14	100.01
<b>LOI</b>	1.84	9.36	3.6	3.45	3.48	4.73	2.62	1.39	3.13
<b>Rb</b>	60.7	3.3	32.8	<0.5	14.5	5.1	4.7	6.3	12.8
<b>Sr</b>	513	552	595	671	991	1620	543	673	1295
<b>Y</b>	33.5	22.4	16.7	24.0	24.5	28.3	17.3	27.4	22.7
<b>Zr</b>	225	65	85	51	87	75	50	90	140
<b>V</b>	220	352	192	276	155	271	348	263	197
<b>Ni</b>	12	4	45	35	7	8	26	8	40
<b>Cr</b>	35	17	110	55	14	15	34	11	78
<b>Nb</b>	4.9	1.0	0.5	1.6	3.8	1.1	0.6	4.6	5.1
<b>Ga</b>	19.6	17.3	15.9	15.6	18.0	19.2	18.3	18.5	20.0
<b>Cu</b>	153	49	85	53	34	74	63	62	45
<b>Zn</b>	116	81	100	75	94	102	73	75	91
<b>Co</b>	24	33	21	41	24	30	36	28	33
<b>Ba</b>	404	122	408	136	507	393	187	244	810
<b>La</b>	25	14	15	13	16	19	13	14	30
<b>Ce</b>	45	26	18	24	40	35	17	27	66
<b>U</b>	<0.5	<0.5	<0.5	<0.5	0.5	<0.5	<0.5	<0.5	3.5
<b>Th</b>	4.6	<0.5	1.0	<0.5	<0.5	<0.5	<0.5	<0.5	4.3
<b>Sc</b>	22	33	23	28	15	25	37	27	17
<b>Pb</b>	5	<1	7	<1	1	<1	10	<1	<1



Sample ID	Jacksina-02	JT08LA	JT09LA	JT15LA	JT22LA	JT23LA	JT24LA	JT01LA	JT02LA
Rock Unit/Location	Jacksina Dike	Beaver Lake	Beaver Lake	Beaver Lake	Beaver Lake	Beaver Lake	Beaver Lake	Beaver Lake	Beaver Lake
SiO <sub>2</sub>	53.76	57.83	55.82	59.25	49.37	49.21	52.76	50.88	55.37
TiO <sub>2</sub>	0.66	0.58	0.56	0.59	1.31	0.85	0.67	0.84	1.05
Al <sub>2</sub> O <sub>3</sub>	19.22	17.34	17.76	16.7	14.66	18.46	18.22	19.25	16.82
Fe <sub>2</sub> O <sub>3</sub> *	9.56	7.58	6.8	6.67	10.62	10.96	9.9	9.74	9.85
MnO	0.16	0.22	0.26	0.17	0.2	0.2	0.22	0.19	0.22
MgO	4.28	3.08	2.57	2.12	8.46	5.55	4.31	4.77	3.35
CaO	7.43	6.77	9.54	7.02	10.42	10.39	9	10.77	6.5
Na <sub>2</sub> O	4.01	3.59	4.06	5.45	2.9	2.86	3.17	3.09	3.32
K <sub>2</sub> O	0.46	2.41	2.19	1.53	1.22	0.87	1.22	0.33	2.67
P <sub>2</sub> O <sub>5</sub>	0.37	0.18	0.19	0.23	0.44	0.29	0.36	0.23	0.46
Total	99.91	99.58	99.75	99.73	99.6	99.64	99.83	100.09	99.61
LOI	3.56	2.61	4.56	5.2	2.11	2.96	2.99	2.88	2.65
Rb	9.5	50	45.5	21.4	20.2	14	25	2.1	37.2
Sr	905	651	634	763	983	949	927	546	478
Y	26.0	19	19.1	31.3	26.1	25	24.1	26.7	40.6
Zr	70	127	123	160	167	73	100	109	235
V	206	185	160	145	199	304	196	285	241
Ni	11	10	6	10	180	21	13	45	11
Cr	20	25	20	21	331	29	48	78	33
Nb	1.1	1.6	1.6	2.6	17.6	1.3	1.8	1.9	7.6
Ga	17.5	18.4	16.2	16.2	17	19.4	19.8	18.4	20
Cu	39	47	36	60	82	145	98	60	242
Zn	108	54	56	83	159	53	72	80	102
Co	26	18	11	13	36	35	27	32	23
Ba	264	483	557	537	729	298	363	132	413
La	17	19	16	20	24	16	20	19	25
Ce	33	30	28	43	53	31	34	24	50
U	1.1	<0.5	0.9	1	2.1	<0.5	<0.5	<0.5	2.5
Th	<0.5	<0.5	<0.5	0.8	<0.5	<0.5	<0.5	<0.5	6.3
Sc	21	17	19	16	18	24	18	28	21
Pb	<1	10	<1	<1	<1	3	<1	4	10

Sample ID	JT07LA	CH1-704	CH1-1109	CH1-1130	CH1-1191	CH1-1232	CH1-1291	CH1-1299	CH1-1311
Rock Unit/Location	Beaver Lake	Lower Bonanza	Middle Bonanza	Middle Bonanza	Middle Bonanza	Middle Bonanza	Middle Bonanza	Middle Bonanza	Middle Bonanza
SiO <sub>2</sub>	55.32	53.82	55.15	57.80	58.32	55.61	55.77	55.06	54.51
TiO <sub>2</sub>	1.12	1.21	0.50	0.46	0.47	0.52	0.51	0.51	0.48
Al <sub>2</sub> O <sub>3</sub>	16.84	15.73	17.65	17.51	17.24	18.14	17.52	17.53	17.28
Fe <sub>2</sub> O <sub>3</sub> *	10.21	10.25	6.06	5.56	5.56	6.42	6.21	6.07	5.78
MnO	0.21	0.18	0.17	0.14	0.14	0.18	0.14	0.15	0.16
MgO	3.23	3.02	2.02	1.99	1.84	2.16	2.09	1.28	1.56
CaO	5.01	7.39	7.27	6.37	6.38	6.74	7.53	8.02	7.12
Na <sub>2</sub> O	4.12	3.07	3.41	4.07	3.60	4.55	2.85	3.11	3.17
K <sub>2</sub> O	3.11	2.67	1.31	1.31	1.51	1.78	1.35	1.41	1.81
P <sub>2</sub> O <sub>5</sub>	0.49	0.45	0.32	0.25	0.23	0.36	0.47	0.33	0.32
Total	99.66	99.65	93.88	95.46	99.34	99.02	99.89	93.47	92.20
LOI	3.09	1.856843	5.356786	4.006795	4.04826	2.556166	5.444755	5.96	7.078853
Rb	53.6	63	53	49	43	35	44	66	83
Sr	629	389	759	966	875	962	695	660	565
Y	42.2	39	24.8	19.2	20	25	24	24.8	23.9
Zr	253	227	128	126	130	119	122	128	124
V	247	305	134	134	116	130	128	129	123
Ni	11	7	4	11	6		2	3	3
Cr	32	7		4	9	2	3		
Nb	8.7	8	7	6	3	1	2	7	7
Ga	19.9								
Cu	248	250	9	4	20	14	16	13	14
Zn	109	107	54	49	83	78	68	76	91
Co	23								
Ba	1078	388	479	658	502	473	750	465	625
La	23								
Ce	52								
U	1.3								
Th	6.6								
Sc	21	26.3	8.9	10	10.8	9.1	9.9	9.2	8.4
Pb	15								

Sample ID	CH1-1324	CH1-1344	CH1-1414	CH1-1422	CH1-1438	CH1-1450	CH1-1459
Rock Unit/Location	Middle Bonanza	Middle Bonanza	Upper Bonanza	Upper Bonanza	Upper Bonanza	Upper Bonanza	Upper Bonanza
SiO <sub>2</sub>	55.55	55.96	48.09	50.58	53.10	44.32	48.77
TiO <sub>2</sub>	0.49	0.50	0.63	1.02	1.10	0.87	0.95
Al <sub>2</sub> O <sub>3</sub>	17.13	17.81	19.36	16.11	16.42	19.45	18.05
Fe <sub>2</sub> O <sub>3</sub> *	5.73	6.08	8.06	11.30	11.43	8.93	10.97
MnO	0.22	0.16	0.13	0.18	0.19	0.15	0.16
MgO	1.28	1.88	2.09	3.08	3.77	2.90	4.44
CaO	6.55	6.94	11.00	8.66	7.66	11.31	10.99
Na <sub>2</sub> O	2.35	3.40	2.83	2.87	3.36	2.64	2.50
K <sub>2</sub> O	1.99	1.56	0.28	0.25	0.70	0.27	0.44
P <sub>2</sub> O <sub>5</sub>	0.27	0.32	0.21	0.21	0.26	0.17	0.17
Total	91.56	94.62	92.68	94.27	97.99	91.02	97.44
LOI	7.782878	5.34222	6.287992	5.864722	1.771144	8.158787	2.383564
Rb	78	59	45				6
Sr	449	944	522	574	475	596	489
Y	24.8	24.2	22.6	27.4	31.7	21.4	23.6
Zr	126	124	71	80	98	61	64
V	121	136	154	244	246	252	350
Ni	9	9	21	3		15	23
Cr			42			14	8
Nb	3	4	6	1	6	1	1
Ga							
Cu	5	10	70	57	80	24	36
Zn	63	92	79	90	98	76	101
Co							
Ba	721	451	181	163	224	95	157
La							
Ce							
U							
Th							
Sc	9.3	8.3	23	31.3	34	26.1	34
Pb							

## Appendix D - XRF precision and accuracy

Precision and Accuracy of standard and replicate geochemical data from this study via XRF at  
Franklin and Marshall College.

Chemical	BHVO-2									
	SiO <sub>2</sub>	TiO <sub>2</sub>	Al <sub>2</sub> O <sub>3</sub>	Fe <sub>2</sub> O <sub>3</sub> *	MnO	MgO	CaO	Na <sub>2</sub> O	K <sub>2</sub> O	P <sub>2</sub> O <sub>5</sub>
<b>USGS accepted concentration Units</b>	49.9 Wt%	2.73 Wt%	13.5 Wt%	12.3 Wt%	0.17 Wt%	7.23 Wt%	11 Wt%	2.22 Wt%	0.5 Wt%	0.27 Wt%
<b>Replicate 1</b>	49.9	2.72	13.63	12.43	0.17	7.3	11	2.196	0.5	0.27
<b>Replicate 2</b>	50	2.73	13.66	12.45	0.17	7.29	11	2.19	0.5	0.27
<b>Replicate 3</b>	50	2.73	13.66	12.41	0.17	7.29	11	2.197	0.5	0.27
<b>Replicate 4</b>	49.9	2.72	13.65	12.42	0.17	7.29	11	2.2	0.5	0.27
<b>Replicate 5</b>	49.8	2.72	13.61	12.4	0.17	7.29	11	2.202	0.5	0.27
<b>Replicate 6</b>	50	2.73	13.62	12.43	0.17	7.31	12	2.191	0.5	0.27
<b>Replicate 7</b>	50	2.73	13.65	12.42	0.16	7.3	11	2.19	0.5	0.27
<b>Replicate 8</b>	49.9	2.73	13.62	12.42	0.17	7.29	11	2.199	0.5	0.27
<b>Replicate 9</b>	50	2.73	13.64	12.43	0.17	7.29	11	2.192	0.5	0.27
<b>Replicate 10</b>	50	2.72	13.66	12.43	0.17	7.29	11	2.197	0.5	0.27
<b>Mean</b>	49.9	2.73	13.64	12.424	0.17	7.29	11	2.195	0.5	0.27
<b>Standard Deviation</b>	0.05	0.01	0.019	0.0135	0	0.01	0	0.004	0	0
<b>LOD - t value 2.764</b>	0.14	0.01	0.052	0.0373	0	0.02	0	0.012	0	0
<b>LOQ</b>	0.51	0.05	0.189	0.135	0	0.07	0.1	0.044	0	0.01
<b>mean % recovery</b>	1	1	1.01	1.0101	0.97	1.01	1	0.989	1	0.99
<b>(+/-)</b>	0.14	0.01	0.052	0.0373	0	0.02	0	0.012	0	0

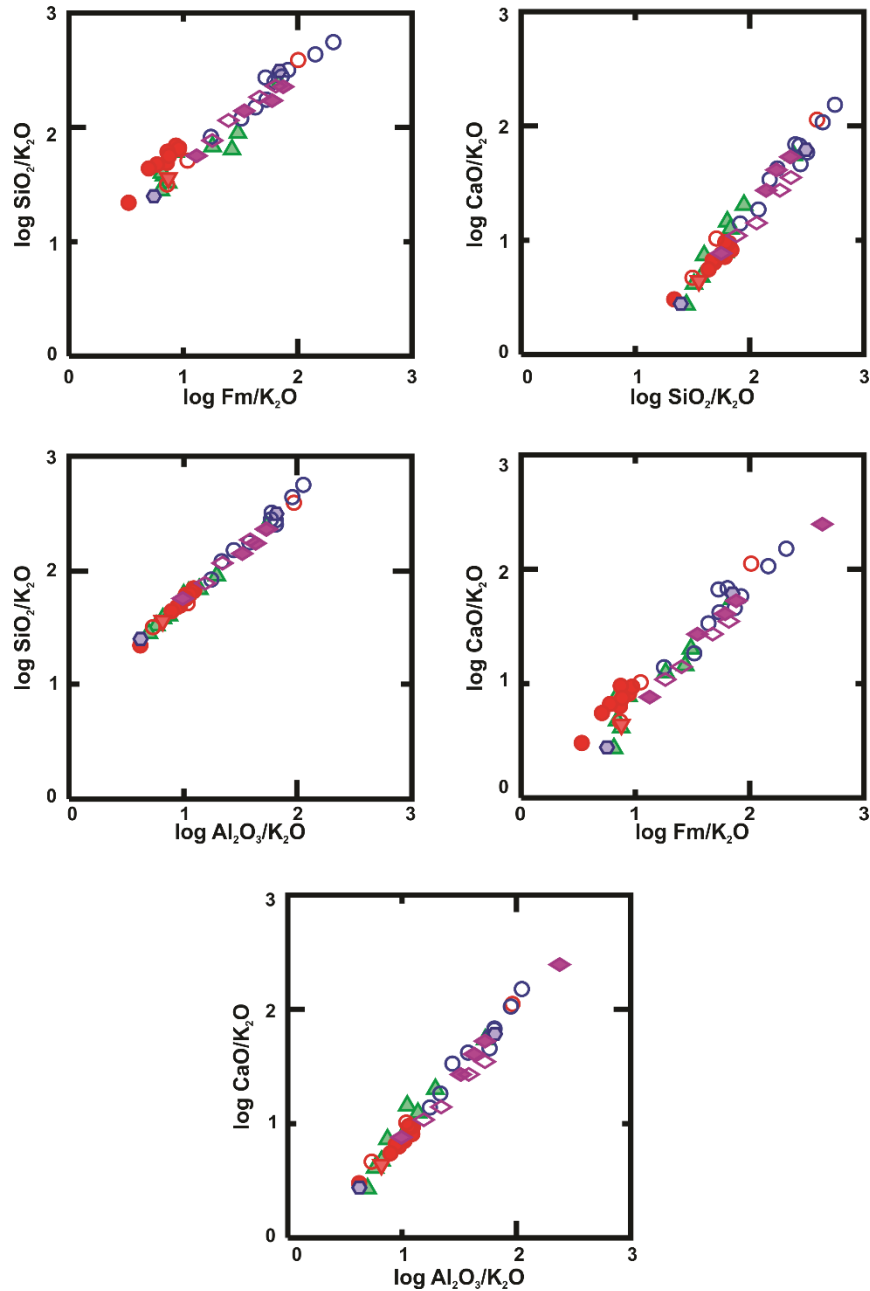
## Appendix E - CIPW data

CIPW norm data calculated for basaltic rocks.

sample	Q	Or	Ab	An	Lc	Ne	Di	Hy	OI	Mt	Il	Ap
CH1-1450	0.00	1.81	24.68	44.70	0.00	0.00	13.36	8.30	0.62	4.26	1.83	0.44
CH1-1414	5.05	1.78	25.99	42.67	0.00	0.00	12.53	6.13	0.00	4.01	1.30	0.53
CH1-1459	2.75	2.68	21.90	37.93	0.00	0.00	14.25	13.04	0.00	5.18	1.86	0.41
Klein 1	0.00	8.58	31.28	29.85	0.00	0.15	13.87	0.00	6.06	5.31	2.75	2.14
Barker 1	1.18	5.18	22.94	35.00	0.00	0.00	12.13	12.18	0.00	8.40	1.91	1.08
Chisana	0.00	6.13	25.29	33.06	0.00	0.00	17.86	2.93	7.63	4.56	1.76	0.78
PM18-22	0.00	2.61	23.51	42.40	0.00	0.00	8.29	9.71	6.63	5.06	1.44	0.34
JT23LA	0.00	5.17	24.43	35.31	0.00	0.00	12.21	12.71	2.50	5.36	1.62	0.69
JT22LA	0.00	7.23	24.69	23.56	0.00	0.00	20.90	6.03	8.70	5.33	2.51	1.04
Barker 2	0.00	2.11	19.10	30.04	0.00	0.00	18.31	20.14	1.52	6.69	1.64	0.45
Barker 3	4.11	0.88	17.16	38.74	0.00	0.00	20.22	9.90	0.00	7.24	1.36	0.40
Barker 4	4.38	2.18	21.59	43.47	0.00	0.00	13.17	5.81	0.00	7.14	1.81	0.45
Barker 5	4.47	0.47	12.81	41.34	0.00	0.00	19.71	14.75	0.00	4.89	1.25	0.31
Barker 6	4.45	1.42	17.17	50.45	0.00	0.00	10.52	11.10	0.00	3.37	1.21	0.31
Barker 7	4.61	1.42	17.50	49.99	0.00	0.00	10.87	10.28	0.00	3.82	1.19	0.31
CH1-1422	9.68	1.58	26.00	32.42	0.00	0.00	10.02	11.99	0.00	5.74	2.05	0.53
JT01LA	1.99	1.96	26.28	37.81	0.00	0.00	11.79	13.27	0.00	4.75	1.60	0.55

## Appendix F - Alteration Filter from Beswick and Soucie

Geochemical samples from this study that passed the alteration filter proposed by Beswick and Soucie (1978). Samples show relatively little variation from a near-linear array when plotted on plots after Beswick and Soucie (1978).



## Appendix G - Sr/Y Calculations

The following calculations from Profeta et al (2015) were performed for all low-magnesium (between 0 and 6 wt. %) calc alkaline samples between 55 and 68 wt. % SiO<sub>2</sub>:

$$Sr/Y = 0.9d_m - 7.25, \quad \text{or} \quad d_m = 1.11 Sr/Y + 8.05$$

Where  $d_m$  represents crustal thickness. For samples from Barker (1994) which have La/Yb data, La/Yb calculations, after those outlined in Profeta et al. (2015), were performed on low-magnesium (between 0 and 6 wt. %) calc alkaline samples between 55 and 68 wt. % SiO<sub>2</sub>:

$$La/Yb_n = 0.98e^{0.047 dm} \quad \text{or} \quad d_m = 21.277 \ln (1.0204 La/Yb_n)$$

Where  $La/Yb_n$  implies that the ratio was normalized to chondritic values of McDonough and Sun (1995). Error calculations are made based on calculations from Zhu et al. (2017):

$$Error = 2.29Ln(La/Yb_n) + 4.32$$

Values and calculations are presented in the following table:

Sample	Sr	Y	Sr/Y	dm (Km)	La	Yb	La n	Yb n	La/Yb	dm	error
CH1-1109	759	24.8	30.6	42.0	-	-	-	-	-	-	-
CH1-1130	966	19.2	50.3	63.9	-	-	-	-	-	-	-
CH1-1191	875	20	43.8	56.6	-	-	-	-	-	-	-
CH1-1232	962	25	38.5	50.8	-	-	-	-	-	-	-
CH1-1291	695	24	29.0	40.2	-	-	-	-	-	-	-
CH1-1299	660	24.8	26.6	37.6	-	-	-	-	-	-	-
CH1-1324	449	24.8	18.1	28.1	-	-	-	-	-	-	-
CH1-1344	944	24.2	39.0	51.3	-	-	-	-	-	-	-
Jacksina-01	1295	22.7	57.0	71.4	-	-	-	-	-	-	-
Jacksina-02	905	26	34.8	46.7	-	-	-	-	-	-	-
JT02LA	478	40.6	11.8	21.1	-	-	-	-	-	-	-
JT07LA	629	42.2	14.9	24.6	-	-	-	-	-	-	-
JT08LA	651	19	34.3	46.1	-	-	-	-	-	-	-
JT09LA	634	19.1	33.2	44.9	-	-	-	-	-	-	-
JT15LA	763	31.3	24.4	35.1	-	-	-	-	-	-	-
PM18-12	430	30.1	14.3	23.9	-	-	-	-	-	-	-
PM18-13	701	23.9	29.3	40.6	-	-	-	-	-	-	-
PM18-15	671	24	28.0	39.1	-	-	-	-	-	-	-
PM18-18	595	16.7	35.6	47.6	-	-	-	-	-	-	-
PM18-2	540	29.8	18.1	28.2	-	-	-	-	-	-	-
PM18-20	991	24.5	40.4	52.9	-	-	-	-	-	-	-
PM18-4	600	37	16.2	26.1	-	-	-	-	-	-	-
PM18-5	537	39	13.8	23.3	-	-	-	-	-	-	-
PM18-8	591	25.7	23.0	33.6	-	-	-	-	-	-	-
Barker 14	960	20	48.0	61.3	22	2.5	92.8	15.5	6.0	38.5	8.4
Barker 15	1130	22	51.4	65.1	22	2	92.8	12.4	7.5	43.2	8.9
Barker 16	761	18	42.3	55.0	25	2.1	105.5	13.0	8.1	44.9	9.1
Barker 17	788	22	35.8	47.8	22	2.2	92.8	13.7	6.8	41.2	8.7
<b>Average</b>	<b>748.6</b>	<b>25.7</b>	<b>31.5</b>	<b>43.0</b>							